Solar Augmentation of Process Steam Boilers for Cogeneration

Prepared by:

Onekai Adeliade Rwezuva

RWZONE001

Department of Mechanical Engineering

University of Cape Town

Supervisor:

A/Prof. Wim Fuls

December 2020

Submitted to the Department of Mechanical Engineering at the University of Cape Town in partial fulfilment of the academic requirements for a Master of Science degree in Mechanical Engineering

Key Words: Solar assisted power generation, Heat exchanger sizing

Abstract

In this study, the techno-economic feasibility of converting an existing process steam plant into a combined heat and power plant, using an external solar thermal field as the additional heat source was studied. Technical feasibility entailed designing a suitable heat exchanger, which uses hot oil from the solar field to raise the steam conditions from dry saturated to superheated. The solar field was sized to heat a selected heat transfer fluid to its maximum attainable temperature. A suitable turbine-alternator was chosen which can meet the required plant power demand. For this to be a success, the processes which require process steam were analysed and a MathCAD model was created to design the heat exchanger and check turbine output using the equations adapted from various thermodynamics and power plant engineering texts, together with the Standards for the Tubular Exchanger Manufacturer's Association. The U.S. National Renewable Energy Laboratory system advisor model was used to size the suitable solar field.

A financial model was developed in Excel to check the economic feasibility of the project, using discounted payback period as the economic indicator. It was found out that amongst loan interest rates, variation of system output and the electricity output, the profitability of the project was largely influenced by the electricity tariff. An optimum size for the heat exchanger of 30ft was established from the sensitivity analysis and it was concluded that the project is currently not economically viable on an independent investor financing model, unless either the electricity tariff improves or the solar thermal energy and turbine technology costs decrease.

Declaration

I, Onekai Adeliade Rwezuva, hereby declare the work contained in this dissertation to be my own. All information that has been gained from various journal articles, textbooks or other sources has been referenced accordingly. I have not allowed and will not allow anyone to copy my work to pass it off as their own work or part thereof.

Onekai A Rwezuva _____ 05/03/2021

Name Date

Acknowledgements

To my parents, for being my pillar of strength and believing in me. Thank you… 😊

Firstly, I would like to thank my supervisor A/Prof. Wim Fuls whose assistance in my research I cannot put a price tag on. It was not an easy journey but your emphasis on going down to fundamentals and in-depth knowledge in power plant systems has been a unique resource I could not do without. I am very grateful.

Secondly, I very much acknowledge Prof. T. Harms from the Solar Thermal Energy Research Group from the University of Stellenbosch for his assistance in the solar design aspect of my research. You came through and answered my questions like I was part of the STERG family. I appreciate.

I would also like to thank the Mandela Rhodes Foundation for financing my studies and I hope I will take with me the vision of the foundation and put my education to good use for the betterment of the continent.

Many thanks go to the staff at John Thompson Boilers, Tongaat Hulett Triangle, African Distillers and Kadoma Paper Mills for providing the vital information which formed the basis of this study. Special mention goes to my friends and family who have always been supportive of my endeavours, and the postgraduate community at the University of Cape Town, particularly the AtPROM research unit. You made it bearable to be in a new environment, thank you.

Above all, I thank the Lord Almighty for his guidance and grace. Most certainly, the skills I acquired whilst working on this research will help me grow, both personally and professionally.

Table of Contents

List of Figures

List of Tables

List of Nomenclature

General symbols

$\dot{m}$	mass flow rate	x	steam quality
P	power, pressure	s	specific entropy
Q	heat	k	thermal conductivity
T	temperature	w	specific work
C	heat capacity	A	area
$\overline{c_p}$	mean specific heat capacity at constant pressure	h	specific enthalpy, heat transfer coefficient

Greek symbols

θ	angle, temperature	ε	effectiveness
Δ	change	η	efficiency
μ	kinematic viscosity	ρ	density

Acronyms and Abbreviations

CAPEX	Capital Expenditure
CSP	Concentrated Solar Plant
ESKOM	Electricity Supply Commission of South Africa
HX	Heat exchanger
HTF	Heat Transfer Fluid
IPH	Industrial Process Heat
NERSA	National Energy Regulator of South Africa
NREL	United States Department of Energy National Renewable Energy Laboratory
OPEX	Operating Expenditure
REFIT	Renewable Energy Feed in Tariff
SAM	System Advisor Model
SAPG	Solar Assisted Power Generation

SOP	Sent Out Power
STHE	Shell & Tube Heat Exchanger
STTC	Steam Turbine Topping Cycle
tph	tonnes per hour
w.r.t	with respect to
ZAR	South African Rand
ZESA	Zimbabwe Electricity Supply Authority
ZERA	Zimbabwe Energy Regulatory Authority

1. Introduction

In this research, the techno-economic feasibility of converting a conventional process steam plant into a combined heat and power plant using an external solar field as the additional source of process heat was investigated. This chapter provides an overview of the framework of the research project, with an emphasis on the background to the study, statement of the problem, objectives of the study, and a brief outline of the method which will be adopted in the execution of the project.

1.1 Background to the problem

Africa has a huge energy deficit, evidenced by massive load shedding during peak hours in most African countries. In Zimbabwe, during the period 2014 – 2015, there was a peak demand deficit of 900MW which saw most industries and households going for more than six hours without electricity per day. Of late South Africa has started experiencing load shedding, and although its problems are different to the Zimbabwean problem, there is a need to provide alternative power generation sources to kick in in the event of a failure of the main energy source to provide the much-needed electricity to drive various industries.

In addition, Africa's cost of energy is very high, pegged at a weighted average of US$0.14/ kWhr in Sub-Saharan Africa compared to US$0.04 – 0.08/kWhr for the rest of the world [1]. With energy being the key driver of all sectors of the economy, this explains why Africa is still behind the rest of the world as far as techno-economic advancement is concerned. To partly address the energy deficit, existing process steam plants can be used to generate electricity for that plant's needs and export the excess to the grid. Food processing plants like breweries use saturated steam to drive a lot of their processes e.g., distillation, cleaning of product lines, packaging, and bottling. The steam used in such process plants is usually in a saturated state, and by superheating this steam, it could also be used for power generation.

1.2 Project aim

The project will study the feasibility to convert an existing process steam plant to be able to co-generate electricity, without negatively impacting the process needs. The additional heat source required to superheat the steam to the point of useful turbine inlet conditions will be provided by an external solar field, thus no additional fuel cost is required. A detailed techno-economic feasibility study of the solar field will not be included, rather, the focus will be placed on the process requirements and equipment on the steam side.

1.3 Project scope and limitation

In this study, the major focus will be designing the system which will raise the steam conditions from dry saturated to superheated steam. Site visits will include:

- A fire-tube boiler manufacturing company to understand the boiler design,
- An existing Cogeneration process plant to understand how the system was designed and operates,
- Current steam-only process plants to identify potential sites to carry out the research.

Following the site visits and selection of a suitable plant for demonstration, the design of the superheater section will be done. Mathcad models, Microsoft Excel worksheets and the SAM solar design software will be used to aid in the design and performance evaluation.

Some limiting constraints are placed on the design:

i. The industrial process should still receive the same steam conditions.
ii. The boiler maximum operating pressure will be the maximum pressure in the combined cycle.
iii. The boiler firing rate or steam production cannot be changed.
iv. No thermal storage of excess solar heat.
v. The minimum design electrical energy output from the cogeneration will be the process plant maximum electricity demand.

1.4 Research outline

The research was executed in the manner shown in the flow chart below:

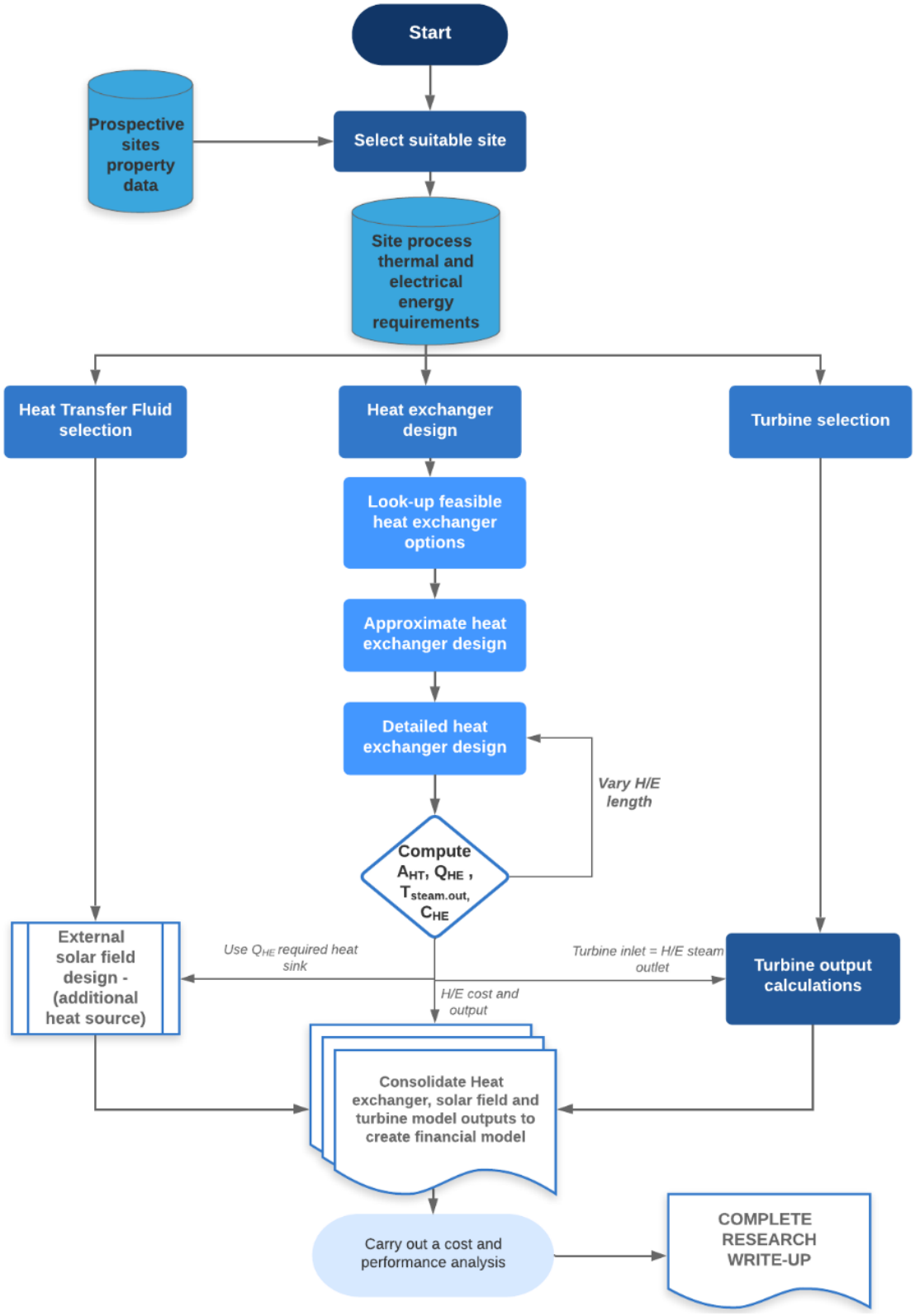

Fig 1: Research Outline flow diagram

1.5 Expected outcomes

At the end of this research, **the following will be produced**:

- A framework for the integration of process steam boilers with steam turbine generator sets for power generation whilst meeting process thermal load requirements.
- A heat exchanger design to raise the steam conditions from dry saturated to superheated.
- An indication of financial feasibility and typical costs associated with the uptake of such a project.

1.6 Disclaimer

Techno-economic studies can be highly site, industry and country specific. This project does not claim to be a comprehensive feasibility of the chosen site. Rather, it is meant to identify and highlight certain aspects that could make solar augmentation of an existing process steam plant potentially viable, or completely non-viable.

2. Literature Review

Literature pertinent to this study will be reviewed in this chapter. The chapter begins by looking at the existing process steam plants and their operating thermodynamic cycle, the Rankine cycle. Following that, the concept of cogeneration will be presented, focusing on what has been put forward to date, its relevance to this study and how a process steam plant can be converted into a combined heat and power plant. Solar thermal systems, heat exchangers, steam plants and steam plant economics will be explored subsequently as they are important in this study.

2.1 Process steam plant and the Rankine cycle

A steam plant is a system that utilizes a high-pressure boiler to generate steam for heating and or power generation. Traditional process steam plants produce steam at mostly dry saturated conditions and use it as a heat source for thermal processes. The Rankine cycle on the other hand is a heat engine cycle, which uses water as the working fluid to convert heat energy to mechanical work whilst the working fluid goes through phase changes [2]. The mechanical work is predominantly further converted to electrical energy. Described first in 1859 by William Rankine, thermal power plants worldwide utilize the cycle for power generation. It has four physically different processes, which use different equipment joined by pipework to make a closed cycle (Figure 2).

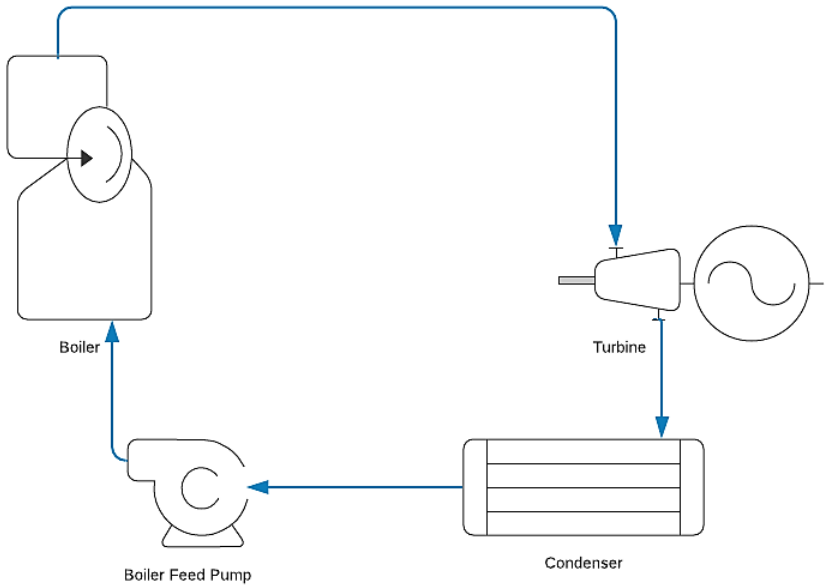

Figure 2: Rankine cycle basic flow diagram

The simple ideal cycle, with superheat consists of the following stages [3];

- 3 - 4: Isentropic compression in the boiler feed pump,
- 4 - 1: Constant pressure heat addition in the boiler,
    - 4 – 5: Subcooled liquid heat addition to boiling point,
    - 5 – 6: Latent heat addition to change state from liquid to gas,
    - 6 – 1: Superheating to increase thermal state at turbine inlet,
- 1 - 2: Isentropic expansion in the turbine,
- 2 - 3: Constant pressure two-phase heat rejection in the condenser.

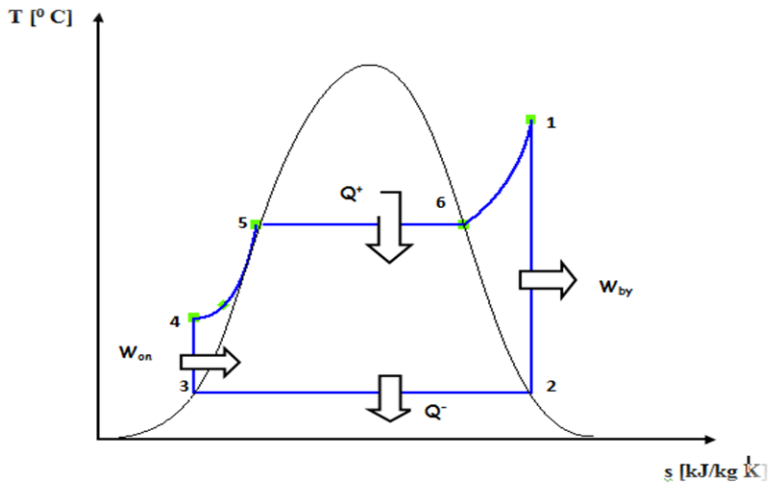

Figure 3: Ideal Rankine cycle T-s diagram

Several enhancements to the simple cycle have been made to improve the cycle efficiency by either increasing the thermal state of the high-pressure steam at the turbine inlet or reducing the thermal state of the low-pressure steam at the condenser outlet. This can be realized in one of these ways:

- Increasing boiler pressure,
- Increasing boiler exit temperature,
- Decreasing condenser pressure,
- Feedwater heating – (Increasing the enthalpy of the working fluid at boiler inlet),
- Reheating – (increasing the enthalpy of the high-pressure turbine stage exhaust, before feeding it into the intermediate/ low pressure turbine stage).

In this study, the objective is to increase the thermal state after boiler heat addition to superheated steam, which allows the steam to be first expanded in a turbine for power generation, and then use the turbine exhaust for process heating applications. Given that the original steam plant layout is only for saturated process steam, the introduction of superheating will enable the simultaneous production of heat and power, which is widely known as Cogeneration.

2.2 Cogeneration

Cogeneration is the production of two usable sources of energy, usually heat and electricity, from the same fuel [4] leading to considerable fuel cost savings. Practical use of the technology dates to the earliest commercial Edison coal- fired power plants in the late 1800s [5]. The OPEC crisis of 1973 led to the use of renewables to augment supply, giving birth to the world's first independent power producers tied to the national grid and formulation of the Public Utility Regulated Policy Act widely known as PURPA. This law paved the way for large scale cogeneration and independent power production [5].

According to the International Energy Agency [4], cogeneration coupled with renewables leads to a supply of low carbon electricity and heat which is vital to the realization of a sustainable future. It is also a vector of energy efficiency, as the production of the heat and power occurs at the place of consumption, minimizing transmission line losses. Classification of cogeneration systems is based on the sequence of energy use, being either topping or bottoming cycles. Topping cycles (the most common ones) produce electricity first and use the waste heat for industrial or district heating. Bottoming cycles on the other hand produce useful heat first for high-temperature thermal processes (glass and steel industries) then use the waste heat for power generation in heat recovery steam generators.

Today, many process steam plants employ cogeneration, mainly steam turbine topping cycles to provide electricity to meet plant demand and the turbine exhaust for process thermal load. The researcher visited a few process steam plants in Zimbabwe to get an in-depth knowledge on how the cogeneration systems are set up, and the findings are given in detail in the next chapter. However, a point to note in this literature survey is that the process steam plants with cogeneration were designed with cogeneration in mind from the onset, hence use utility water tube boilers for steam generation. The process steam plants under investigation in this study use fire tube boilers, which produce only dry saturated steam which is not adequate for power generation. A steam turbine topping cycle (STTC) will be employed, generating the electricity from the superheater outlet, and then using the turbine exhaust as the process steam. A steam turbine topping cycle (with a back-pressure turbine) is shown in the figure below:

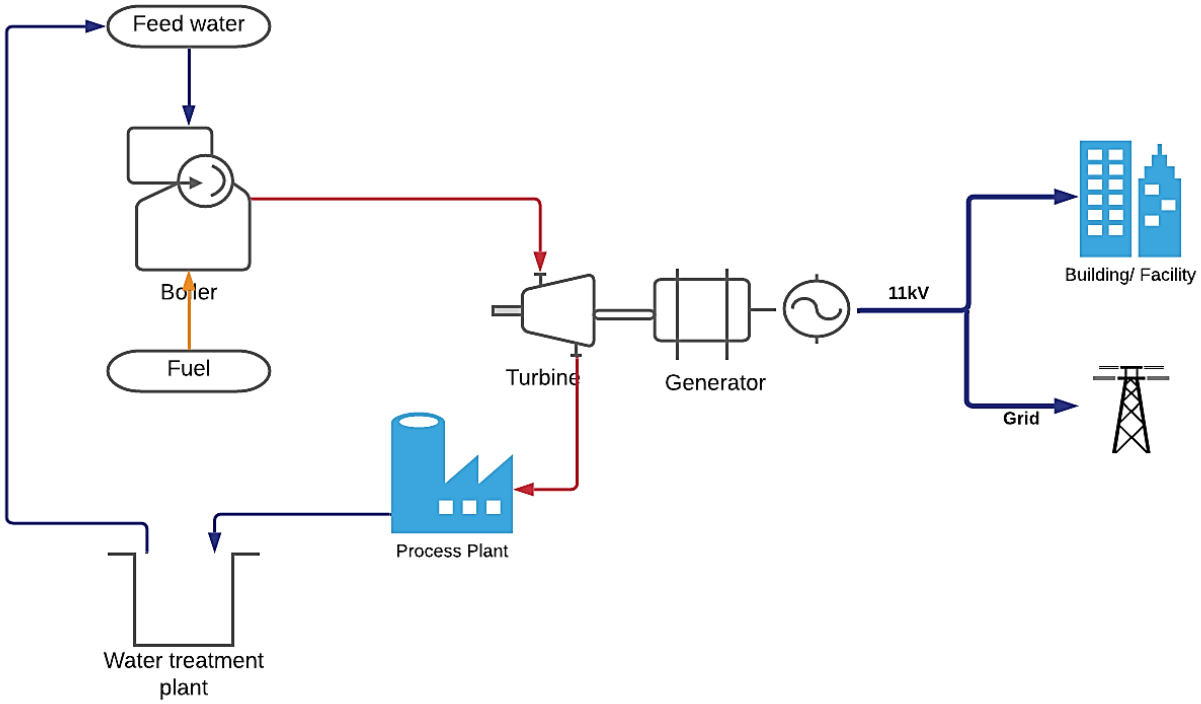

Figure 4: Cogeneration – Back Pressure Steam turbine topping cycle

The turbine options in a STTC are either a back pressure (shown above) or extraction-condensing type. In the back-pressure turbine STTC, the steam is exhausted from the turbine at a pressure above atmospheric which is equal to the process steam pressure requirement. Also note that there is no condenser in the back-pressure steam turbine topping cycle because the process plant "acts as the condenser". The advantages of the backpressure STTC are the simple configuration, lower capital costs as no condenser is required (low or no need of cooling water as the turbine exhausts to the process plant which acts as the condenser) and a higher thermal efficiency as all the heat added in the boiler is fully utilized in both the turbine and process plant. The downside of a backpressure STTC is that there is little or no flexibility in matching the electrical power output to the demand as the thermal load controls the turbine output.

The second option, the extraction-condensing STTC uses an extraction-condensing/pass-out turbine which partly bleeds steam to the process and partly condenses the remaining steam (detailed explanation on the differences between the two turbine types is outlined in Section 2.5 below). The advantage of the extraction-condensing turbine is that the electrical power output control is independent of the thermal load requirement, thus the cogeneration plant can match the electrical demand to the turbine output. The disadvantage however of this set-up is that the thermal efficiency is lower as heat is lost to the surroundings in the condenser and higher capital costs as there is need for a condenser and cooling water supply.

2.3 Solar thermal systems

The conversion of solar energy to mechanical and electrical energy is as old as 1872 when a steam powered press was exhibited at the Paris Exposition [6]. The system used concentrating collectors to supply heat to the heat engines and from that other solar thermal-mechanical systems were developed for small-scale applications, mostly solar water pumping.

Basic energy conversion in solar thermal systems is shown in the picture below:

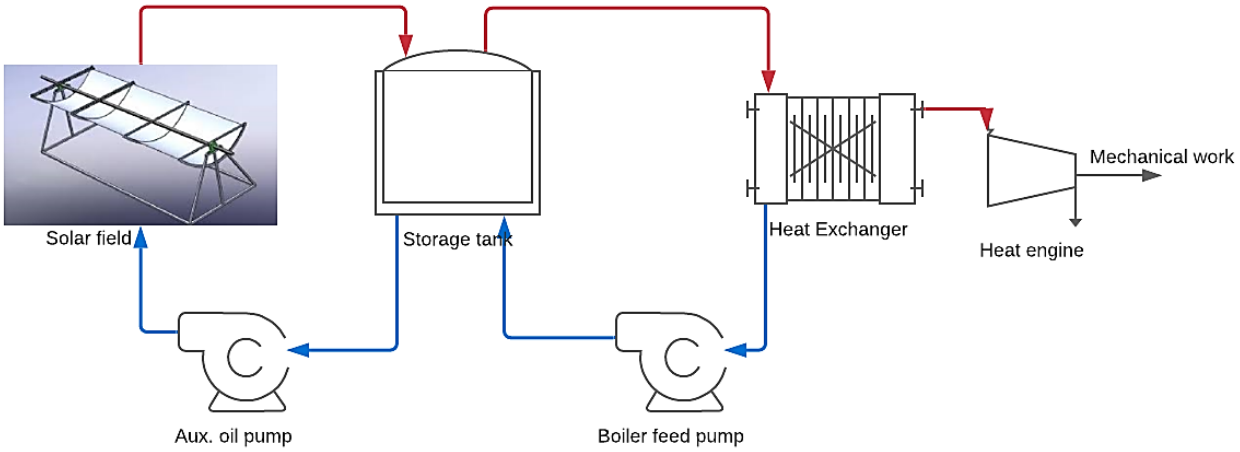

Figure 5: Solar thermal system basic layout

The energy conversion process consists of:

- Solar energy collection by either a flat plate or concentrating collector (parabolic trough shown above),
- Storage, in indirect integration solar systems, which usually use molten salts as thermal storage heat transfer fluid,
- Heat addition in the heat exchanger,
- Conversion of heat energy to useful work in the heat engine.

Flat plate thermal collectors are usually utilized in small-scale solar thermal systems like home water heating systems. Large scale solar thermal systems like solar power plants, use various kinds of focus systems for concentrating the heat with a higher efficiency despite being more expensive and complex to construct. The four main concentrated solar collector types are: parabolic trough systems, linear Fresnel systems, power towers also known as central receiver systems and parabolic dishes. Present day commercial Concentrated Solar Power (CSP) projects employ parabolic troughs as they are the most developed CSP technologies with measured optical efficiencies as high as 78% in the SkyFuel trough systems [7]. Power towers, though being more efficient and offering better energy storage options are less developed than the trough system.

Solar thermal technologies in power plants can be utilized in one of two ways: stand-alone solar thermal power plants (STPPs) or solar assisted power generation (SAPG). SAPG is a synergy of solar and fossil fuels which combines the environmental benefits of the solar energy and scale, reliability and efficiency of traditional fossil fuel plants [8] . According to Pierce [8], a SAPG plant is 25% more efficient and 1.8 times more cost effective than a STPP of equal size of parabolic trough solar technology. Other authors, Petrov et al [9]; Yang et al [10] and Hu et al [11] have also shown that SAPG utilizes solar thermal energy better than stand-alone STPPs.

SAPG systems are employed in countries with a rich fossil fuel resource base and high solar insolation, which makes it relevant for Zimbabwe as it has an abundance of both the coal resource and solar resource (annual average of 2100 peak sunshine hours per annum [12]). In utility high scale systems, solar thermal energy is integrated for: production of main steam (superheating), or production of intermediate steam (reheating) or preheating of feedwater. There are two options of augmentation: direct and indirect integration. In direct integration, the steam is directly heated in the solar field whereas in indirect heating, an additional heat exchanger with a separate solar loop is employed. According to Petrov et al [13], the feedwater heating is the most effective in large utility scale projects [13].

The world's first true solar-coal hybrid project was located at Cameo Generating station in Colorado, USA [14] (shown in the figure below):

Figure 6: Cameo Generating Station SAPG system [15]

The system used parabolic troughs to heat mineral oil heat transfer fluid to $\sim 300℃$, which was used to preheat feedwater for one of the 49-MW plant's coal fired units. Commissioned in 2010, the plant underwent a 7-month demonstration programme and showed positive results with an increase in overall plant efficiency $> 1\%$ and reduction in coal demand and emissions. It was decommissioned after the 7-month pilot project. Another notable feedwater heating project was the New South Wales Novatec Solar, Liddell power station solar boost. The 9.3MWth plant commissioned in 2012, cut annual CO_2 emissions by ~ 5000 tonnes but was closed down in 2016 due to technical and contractual issues [16].

Kogan Creek A Power station solar boost project was a SAPG project which produced main steam to add 44MW to the 750MW Kogan Creek Power Station during peak solar conditions in Queensland, Australia [17]. The system, the largest in the capacity for SAPG to be ever developed commercially, used compact linear Fresnel reflector technology. Construction began in 2012 but the project was never completed due to technical and contractual issues. In 2016, the project was discontinued as it could not be deployed commercially without a further substantial capital investment. Findings from the project showed that location selection for a solar thermal addition plays a pivotal role given that solar projects favour high insolation areas (arid and semi-arid areas). These high insolation areas usually do not coincide with existing standalone utility coal fired plants which are in areas with

an abundant supply of cooling water. Another key issue was the use of technology, which was in early stages of development.

The figure below shows a typical solar parabolic trough system, with thermal storage and a power cycle:

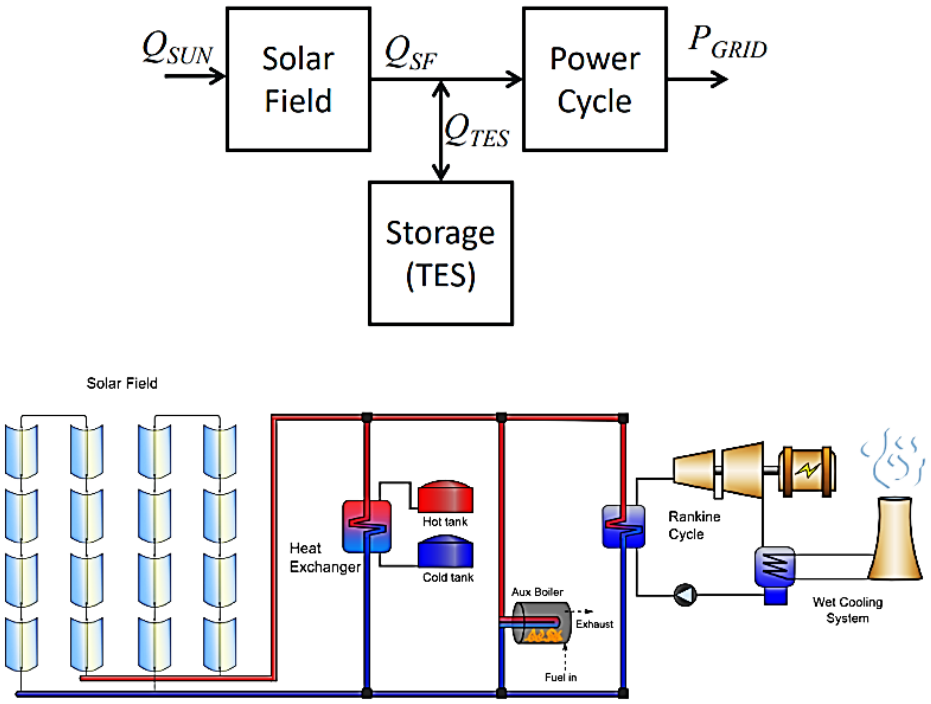

Figure 7: Concentrated Solar Power Parabolic Trough system adapted from the US Department of Energy [18]

The physical trough model is one of the US National Renewable Energy Laboratory (NREL) open-source System Advisor Model (SAM) software's models, which is designed for power generation applications. SAM is a performance and financial model used to help renewable energy industry researchers, technology developers, project managers and engineers make informed decisions when sizing and designing solar projects [18].

Another model in the SAM NREL software package, which is similar to the CSP physical trough is the industrial process heat parabolic trough (IPH), which instead of the power block assumes that the heat from the solar field is used for thermal applications rather than driving a power cycle. In this study, the IPH model will be used in the solar field design because the heat from the field is used to heat up dry saturated steam to superheated steam. No thermal storage will be employed as it is beyond the scope of this study and will escalate the capital costs, despite being the most effective way of harnessing the solar resource. Given that indirect integration will be employed, a suitable heat exchanger will be designed to superheat the steam.

2.4 Heat exchanger design

Heat exchangers are process industry work horses, widely employed in thermal applications where there is need for heat transfer between two or more process fluids. The heat transfer process (heating or cooling) and the process fluids determine the type of heat exchanger to be used. Most applications have several alternative designs and final selection must be done based on different performance and cost factors [19] for example:

- For small duties, annular heat exchangers are the most feasible option as they are cheaper to manufacture.
- For heavier duties where sealing gaskets do not give rise to operational difficulties, plate and frame heat exchangers are the heat exchanger of choice. However, where pressure and temperature of process fluids exceed 40bar and 350˚C [20], sealing becomes a problem and the plate and frame heat exchanger becomes uneconomical to use.
- For heavier duties with high process pressures and temperatures, the shell and tube heat exchangers become the cheaper option.
- Where space is limited, compact exchangers like the plate-fin, tube fin and rotary regenerators are employed. However, plate-fin and tube fin exchangers can only be considered if the working fluid does not pose significant fouling characteristics. Fouling significantly increases the heat exchanger maintenance costs and diminishes the heat exchanger long term performance.
- Where hygienic demands are high and it is desired to ensure no cross contamination between the hot and cold fluid, plate heat exchangers are used.

Given the above considerations, and the process and heat transfer fluids' operating temperature and pressure, the shell and tube heat exchanger (STHE) is the most feasible option and the subsequent sub-sections will focus on the thermal design of shell and tube heat exchangers.

2.4.1 STHE Basics

The basic layout for a shell and tube heat exchanger, with one tube pass and multiple shell passes is shown below:

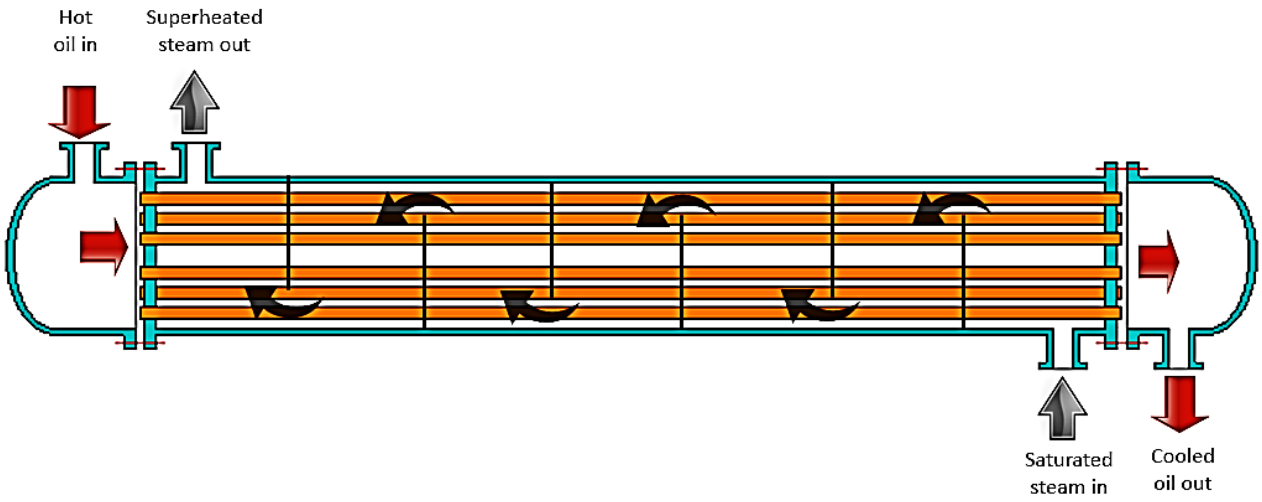

Figure 8: Shell and Tube Heat Exchanger layout

Various tubes are arranged into a bundle, kept in place by a tube sheet on each end of the entire tube length. The tube bundle is then welded into the shell, which is usually a steel pipe of required shell material. However, only shell diameters up to 24" are fabricated from steel pipes [21]. Above that, steel plates are rolled into the desired shell diameter. Baffles are used to both direct the shell fluid into multiple passes and support the tubes (maximum unsupported span of the tubes is specified in Tables R-4.41 and CB-4.41 of the TEMA standards [21]). The ends of the shell are designed based on the fluid operating pressures and the whole component can be simplified into a schematic diagram showing the flow of the hot and cold fluid streams as shown below:

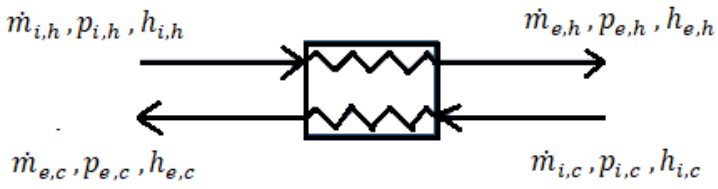

Figure 9: Heat Exchanger Schematic

where the subscripts $i,h; i,c; e,h \; and \; e,c$ denote the hot fluid inlet, cold fluid inlet, hot fluid exit and cold fluid exit respectively. The fundamental heat transfer equation states that:

$$\dot{Q} = UA\Delta T_{LMTD} \tag{2.1}$$

Where $\dot{Q}$ is the heat transfer rate, U is the overall heat transfer coefficient, A is the heat transfer area and ΔT_{LMTD} is the logarithmic mean temperature difference, calculated as shown in (2.2) below for a pure counter flow arrangement:

$$\Delta T_{LMTD} = \frac{(T_{i,h} - T_{e.c}) - (T_{i,c} - T_{e,h})}{\ln\left(\frac{T_{i,h} - T_{e.c}}{T_{i,c} - T_{e,h}}\right)} \tag{2.2}$$

The logarithmic mean temperature difference (LMTD) can also be expressed as follows:

$$\Delta T_{LMTD} = \frac{\Delta T_1 - \Delta T_2}{\ln\left(\frac{\Delta T_1}{\Delta T_2}\right)} \tag{2.3}$$

Where ΔT_1 and ΔT_2 are the temperature differences between flows on the left-hand side and right hand side of the graphs shown in Figure 10 below:

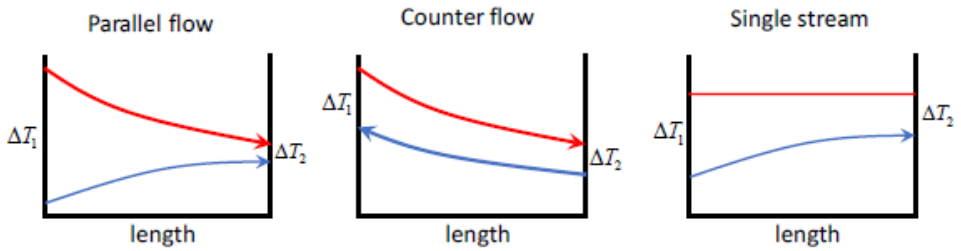

Figure 10:Temperature differences for different heat exchanger flow arrangements

where the flow deviates from pure counter flow or parallel flow, a flow correction factor, F_T, is multiplied to ΔT_{LMTD} to give the true temperature difference as follows:

$$\Delta T_{true} = F_T \cdot \Delta T_{LMTD} \tag{2.4}$$

The flow correction factor is a function of the fluid temperatures and the number of shell and tube passes [22] and is determined graphically, from graphs developed by Kern and other researchers using a correlation of two dimensionless constants, R and S defined below:

$$R = \frac{T_{i,h} - T_{e,h}}{T_{e,c} - T_{i,c}} \qquad S = \frac{T_{e,c} - T_{i,c}}{T_{i,h} - T_{i,c}}$$

The overall heat transfer coefficient is a measure of how well heat is transferred between the different heat transfer media. In this instance, heat is transferred by convection from the fluids to the wall surface, and conduction through the tube wall separating the hot and cold fluids. The overall heat transfer equation, assuming clean conditions is calculated as follows [19, p. 264]:

$$U = \left(\frac{1}{h_i} + \frac{D_o \cdot \ln D_o / D_i}{2k} + \frac{1}{h_o} \cdot \frac{D_o}{D_i} \right) \tag{2.5}$$

Where, h_o, h_i, k, D_o and D_i are the shell-side fluid convective heat transfer coefficient, tube-side fluid convective heat transfer coefficient, tube wall thermal conductivity, tube outer and inner diameter respectively. The convective heat transfer coefficient is defined as the rate at which heat is transferred between a fluid and a solid surface per unit surface area of heat transfer per unit temperature difference. It is a function of the fluid properties, Nusselt number and thermal conductivity and the heat transfer surface dimensions (the diameter if it is a cylindrical section).

The first law of thermodynamics must be satisfied in any heat exchanger design, both at macro and micro level [23] thus by principle of conservation of energy;

$$\dot{Q}_h + \dot{Q}_c = 0 \tag{2.6}$$

i.e., the heat gained by the cold stream equals the heat lost by the hot stream where,

$$\dot{Q}_h = \dot{m}_h \left(h_{e,h} - h_{i,h} \right) \tag{2.7}$$

And

$$\dot{Q}_c = \dot{m}_c \left(h_{e,c} - h_{i,c} \right) \tag{2.8}$$

Which reduces to

$$\dot{Q} = UA\Delta T_{true} = \dot{m}_h c_{ph} \left(T_{e,h} - T_{i,h} \right) = -\dot{m}_c c_{pc} \left(T_{e,c} - T_{i,c} \right) \tag{2.9}$$

if the heat transfer process occurs at constant pressure and c_p is the specific heat capacity at constant pressure.

Another heat exchanger heat transfer analysis method which is widely used is the effectiveness method, popularly known as the ε-NTU method, where ε and NTU denote the effectiveness and the Number of Transfer Units of the heat exchanger respectively. This method was formally introduced in 1942 by London and Seban [23] and relates the heat transfer rate to the fluid flow rates, effectiveness and temperature as follows:

$$\dot{Q} = \varepsilon \cdot \dot{Q}_{\max} \tag{2.10}$$

$\dot{Q}_{\max}$ is the theoretical maximum possible heat transfer rate which would be obtained if the heat exchanger had a pure counterflow arrangement, infinite surface area and no heat losses to the surroundings. It is calculated as follows:

$$\dot{Q}_{\max} = C_{\min} (T_{i,h} - T_{i,c}) \tag{2.11}$$

and,

$$C_{\min} = \min(\dot{m}_h \cdot c_{p,h}; \dot{m}_c \cdot c_{p,c}) \tag{2.12}$$

The effectiveness, ε, is a measure of how the heat exchanger performs and relates the actual heat transferred by the heat exchanger to its maximum possible theoretical value. It is a dimensionless factor, with a range of values between zero and 1

$$\varepsilon = f(NTU; C_r)$$

Where C_r is the heat capacity ratio:

$$C_r = \frac{C_{\min}}{C_{\max}} = \frac{(\dot{m} \cdot c_p)_{\min}}{(\dot{m} \cdot c_p)_{\max}} \tag{2.13}$$

The number of transfer units (NTU) designate the non-dimensional "heat transfer size/ thermal size" of the heat exchanger [23], calculated as the ratio of the overall conductance and minimum heat capacity rate as follows:

$$NTU = \frac{UA}{C_{\min}} = \frac{1}{C_{\min}} \int_A U dA \tag{2.14}$$

Various analytical equations exist relating NTU and ε, and is a function of the specific flow arrangement and fluid conditions. In the case where there is one shell pass, the ε-NTU correlation is as shown in equation (2.15) below [24]:

$$\varepsilon_1 = 2\left\{1 + C_r + \sqrt{\left(1 + C_r^{\,2}\right)} \times \frac{1 + e^{\left(-NTU_1 \cdot \sqrt{\left(1+C_r^{\,2}\right)}\right)}}{1 - e^{\left(-NTU_1 \cdot \sqrt{\left(1+C_r^{\,2}\right)}\right)}}\right\}^{-1} \tag{2.15}$$

where the subscript 1 denotes values for the single pass shell. For multiple shell passes and multiple tube passes (n shell passes and 2n, 4n… tube passes), the effectiveness-NTU correlation is a function of the single shell, multi-tube pass effectiveness and is calculated as follows [24]:

$$\varepsilon = \left[\left(\frac{1 - \varepsilon_1 \cdot C_r}{1 - \varepsilon_1}\right)^n - 1\right] \cdot \left[\left(\frac{1 - \varepsilon_1 \cdot C_r}{1 - \varepsilon_1}\right)^n - C_r\right]^{-1} \tag{2.16}$$

where all symbols have their usual meanings. Given that the baffles direct the shell fluid, the chosen baffle type plays a pivotal role in the direction of shell fluid flow (parallel for longitudinal baffles, cross-flow for transverse baffles or mixed flow). The flow direction also has a bearing on the shell-side heat transfer coefficient with flow parallel to the heat exchanger achieving pure counterflow and having the highest possible heat transfer. In shells where transverse baffles are employed, flow ceases to be pure counter-flow, but a mixture of cross and parallel flow. Although transverse baffles

increase turbulence of the shell fluid [23], increasing the shell-side velocity, their heat transfer rate is less than that of a pure counterflow heat exchanger of the same length due to losses in the baffle clearances and window zones. However, according to Cayglan and Buthod [25], where the number of transverse baffles are greater than ten, the heat exchanger is assumed to be a pure-counterflow heat exchanger. Where the flow is pure counter-flow and the heat capacity ratio is less than 1, the NTU equation is given as:

$$\varepsilon = \frac{1-e^{-NTU(1-C_r)}}{1-C_r \cdot e^{-NTU(1-C_r)}} \tag{2.17}$$

And where the hot and cold fluid heat capacities are the same, i.e. $C_r = 1$,

$$\varepsilon = \frac{NTU}{NTU+1} \tag{2.18}$$

2.4.2 Design Considerations

The objective in heat exchanger design is to ensure that it performs its thermal duty at the lowest cost whilst still maintaining in-service reliability [26]. There is always a trade-off between heat exchanger size, cost and pressure drop.

The general inputs in shell and tube heat exchanger thermal design are hot and cold fluid properties (pressure, temperature) and flow rates. Design of a new heat exchanger means selection of a heat exchanger construction type, flow arrangement, tube and shell material and physical size to meet the specified heat transfer and pressure drop requirements [23]. The common heat exchanger design problems are rating and sizing problems. In a rating problem, the performance evaluation (determination of heat transfer rate, outlet fluid temperatures and pressure drop) of an existing or already sized heat exchanger is done. The sizing problem determines the physical size (length, width, height, and surface area) of a heat exchanger for a given duty [23].

Whether it is a rating or sizing problem, all designs of STHEs have two aspects, namely thermal and mechanical design. Thermal design focuses on the determination of the heat transfer area, tube and shell layout and fluid pressure drops. The designer then must check if the mechanical parts can withstand the operational conditions without failure of components in the mechanical design. Optimum design of STHEs involves the consideration of the following design parameters [22]:

Process considerations

i. Fluid flow arrangements and properties.
ii. Shell and tube side pressure drop limits.
iii. Shell and tube side velocity limits.

Mechanical considerations

i. Heat exchanger Tubular Exchanger Manufacturers Association (TEMA) layout.
ii. Tube specifications such as size, layout, pitch, and material.
iii. Setting design limits on tube length.
iv. Shell specifications - material, baffle cut, baffle spacing and clearances.
v. Setting design limits on shell diameter.
vi. Thermal cycles for fatigue prediction.
vii. Thermal gradients during transients which influence the design of thick-walled components like the tube sheet and shell attachments.

Heat exchangers with shell inside diameters up to 100” and max design pressure of 3000psi [21] are manufactured to the standards set out by the Tubular Exchangers Manufacturers Association (TEMA). The above limits are enforced to limit the shell wall thickness to 76mm for ease of manufacturing, and the 9th Edition of the standard will be referenced throughout this design.

2.4.3 TEMA Heat Exchanger types

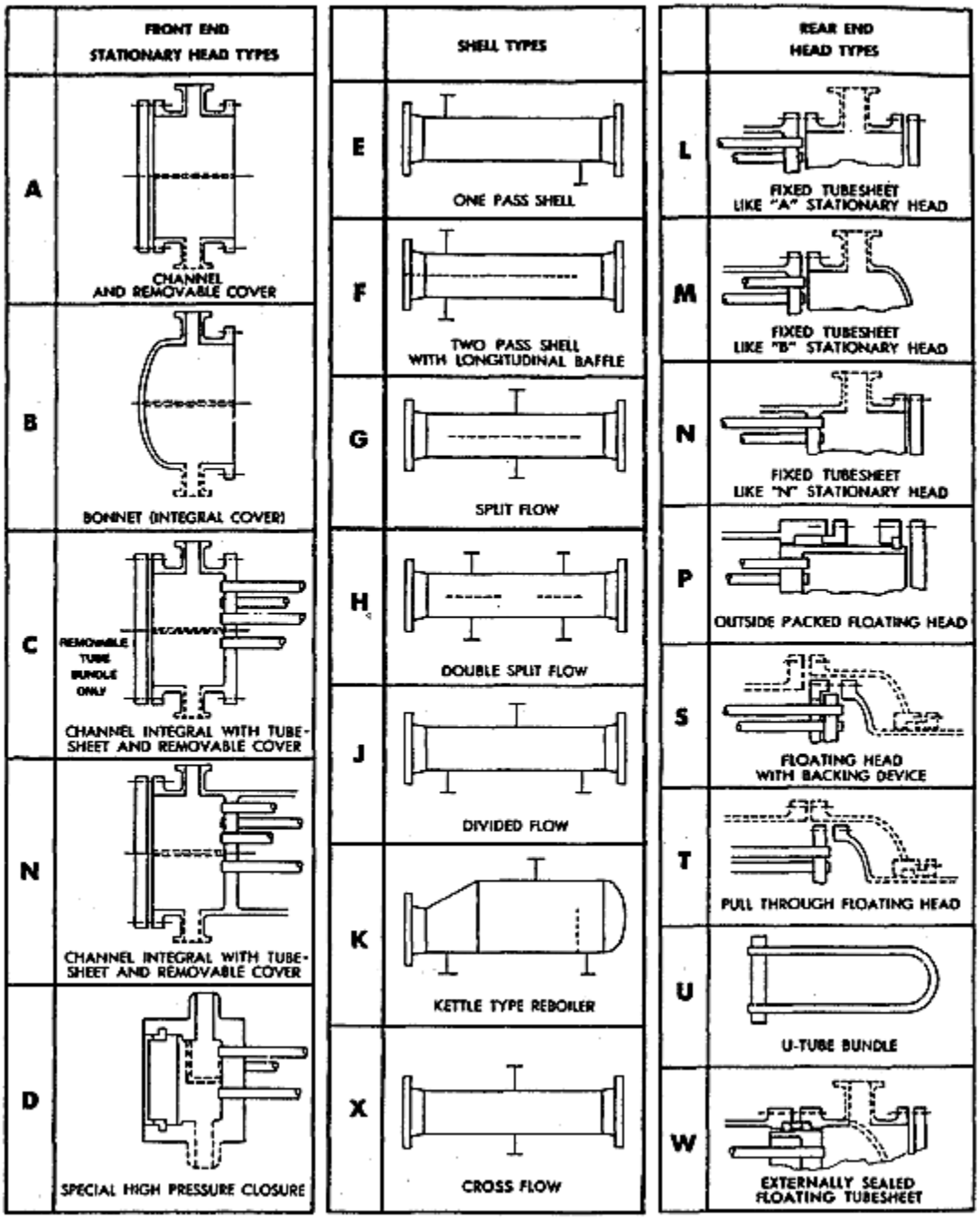

Figure 11:TEMA Exchanger types adapted from Standards of the Tubular Exchanger Manufacturers Association, 9th Edition [21]

TEMA type designation, shown in Figure 11 above, is by letters describing the front end, shell type, rear end in that order, followed by the size which has the nominal shell diameter (inside shell

diameter rounded in inches) and nominal length of tubes in inches, followed by the metric size in brackets. A typical example for a TEMA heat exchanger designation is:

SIZE 19-84 (483-2134) TYPE BGU

meaning a U-tube exchanger with bonnet type stationary head, a split flow shell, 19" (483mm) shell inside diameter and straight tube length of 84" (2134mm).

The right shell choice leads to an optimized heat transfer rate [27]. TEMA standardized 7 types of shells, described in detail below.

The type E, single pass shell is the most common for single phase shell fluid applications due to its simplicity, ease of manufacture and subsequent low cost. Tubes can be single or multiple pass and are supported by transverse baffles which also act as shell fluid multi-pass compartments. The most effective heat exchanger is the type E shell with a single tube pass arrangement as it approaches a pure counterflow arrangement.

Where a process requires a larger heat transfer area, such that more than one tube pass is used, or if there is a temperature cross in the type E shell, the F shell is used to achieve a counter-current flow and achieve effectiveness values as close to the 1-1 pass arrangement. It has a longitudinal baffle separating the type E shell into two distinct sections. However, the disadvantage of the F shell is baffle leakage and conduction heat losses to the baffle which reduces the shell side heat transfer coefficient.

TEMA G (spilt flow) and H (double split flow) shells are employed where the pressure drop is supposed to be kept at the minimum. The G shell has no baffles, just a single support in the middle and fluid enters in the middle section and divides into two, hence the term split flow. Where the tube lengths are longer, the H shell is employed which is like two G shells combined into one.

The J-shell is used where the pressure drop in the shell is too large for the E shell to handle [27] which can lead to tube vibration. The shell side velocity in this shell is half that of the type E shell, which implies that the pressure drop will be almost a quarter of that of the E shell. Fluid enters at the centre, splits into two streams and leaves through two separate outlets which can be recombined outside the shell.

The X shell is used for pure cross flow design where it is desired to have little or no pressure drop in the shell. Fluid enters from one side and leaves at the direct opposite end of the inlet nozzle. The final shell type is the K shell used for partially vaporizing the shell fluid in kettle reboilers. Almost like the X shell, the K type has an enlarged shell to allow for vapor disengagement and minimize carryover.

2.4.4 Fluid Flow Allocations

Fluid flow allocation to either the shell side or tube side has a huge impact on the heat exchanger effectiveness, maintenance requirements, initial cost and cost of replacement parts [28]. Practical guidelines state that the flow arrangements for optimum operation should be as follows:

- Higher pressure (HP) fluid in the tubes as they have smaller diameters and nominal wall thickness, making the design cheaper than having the fluid in the shell which will then call for a thicker shell to withstand the pressure. However, if the HP fluid can only be put in the shell, it is necessary to make the shell smaller in diameter and long length to minimize costs.
- Higher fouling fluid in the tubes as they are easier to clean using mechanical methods compared to the shell.
- Lower heat transfer coefficient fluid in the shell.
- If all properties are almost similar, the corrosive fluid in the tubes as it is less expensive to use special alloys for corrosion resistance in the tubes than the shell alloys.
- Lower velocity fluid in the tubes as the lower the fluid flow velocity, the higher the fouling rates. Acceptable tube side velocity varies with the fluid, with most liquids ranging from 0.9-1.52m/s and gases ranging from 15-30m/s.

2.4.5 Heat transfer model selection

Heat transfer model selection depends on the heat transfer process (sensible, boiling or condensing); surface geometry of both the tube and shell side; fluid flow regime (laminar, turbulent or mixed) and surface orientation (horizontal or vertical) [22]. In this study, the heat transfer process is for sensible heat transfer and only the sensible heat transfer models in turbulent flow will be discussed for both the shell and the tube -side.

Shell-side film coefficient methods

Stream analysis

In this method, usually employed in computer thermohydraulic programs for heat exchanger design, the pressure drop across the baffles is balanced for each possible flow path, including leakage flow areas [22].

Kern Method [29, p. 137]

The original Kern method was an adaption of the Nusselt equations to suit evaluation of fluid conditions at film temperature for streamline flows with Reynolds numbers in the range of 1800 – 2100. The Colburn method on the other hand, is applicable to turbulent flow in industrial heat exchangers using standard tube pitch designs. Using existing experimental techniques and different

heat transfer fluids, Kern was able to show that for sensible heat transfer with turbulent flow in segmented baffle shells:

$$Nu_s = 0.36 \cdot \mathrm{Re}_s^{0.55} \cdot \mathrm{Pr}_s^{1/3} \cdot \left(\frac{\mu_t}{\mu_{wall}}\right)^{0.14} \tag{2.19}$$

where the subscripts s and t denote the shell and tube side fluids respectively and the Reynolds and Prandtl numbers are calculated as follows:

$$\mathrm{Re}_s = \frac{G_s \cdot D_e}{\mu_s} \text{ and } \mathrm{Pr}_s = \frac{c_{p.s} \cdot \mu_s}{k_{.s}}$$

where G_S is the shell-side mass velocity and D_e is the equivalent shell diameter, calculated as shown in (2.29). This Nusselt correlation by Kern strongly agrees with the Colburn and Short methods [29].

Bell-Delaware Method [19, pp. 275-277]

The Bell-Delaware method is an improvement of the Kern method and corrects for heat transfer coefficient reduction due to leakage flows by accounting for the losses due to leakages through the tube holes and baffle clearances, by-pass flows and effect of baffle configuration on the shell-side fluid flow pattern. In this method, the ideal shell side heat transfer coefficient is first calculated using the Kern method, then correction factors for the leakage flows are calculated and factored in the ideal heat transfer coefficient to give the corrected actual heat transfer coefficient.

Tube-side film coefficient methods

Dittus-Boelter Equation [19, p. 105]

This is the most popular correlation used to calculate the average Nusselt number for fully developed (both thermally and hydrodynamically) turbulent flows in liquids and gases with a range of Reynolds numbers, Re>10000; Prandtl number 0.7<Pr<150 and length to diameter ratio of tubes greater than 10. It states that:

$$Nu_D = 0.023 \cdot \mathrm{Re}_D^{0.8} \cdot \mathrm{Pr}^n \tag{2.20}$$

where the coefficient n is either 0.3 when the tube-side fluid is being cooled or 0.4 when the tube-side fluid is being heated. However, the Dittus-Boelter equation is less accurate for rough tubes and flows characterized by large temperature variations.

Sieder-Tate Equation [29, p. 103]

The Sieder-Tate equation was developed to account for the effect of variation of fluid viscosity with temperature, particularly in instances where the difference between the fluid and surface temperatures is very large. It states that:

$$Nu_D = 0.027 \cdot \mathrm{Re}_D^{0.8} \cdot \mathrm{Pr}^{0.33} \cdot \frac{\mu_{fluid}}{\mu_{wall}}^{0.14} \tag{2.21}$$

for flows in horizontal and vertical pipes involving inorganic liquids, aqueous solutions and gases with a range of Reynolds numbers, Re>10000; Prandtl number 0.7<Pr<700 and length to diameter ratio of tubes greater than 60.

Gnielinski Equation [24, p. 515]

Although equations (2.20) and (2.21) are easily applied and satisfactory for many heat transfer applications, they result in errors as large as 25% [24] and a more recent correlation, the Gnielinski correlation can be used. It is valid for a wide range of Reynolds numbers, including the transition region and reduces the error to less than 10%. It states that:

$$Nu_D = \frac{\left(f/8\right)\left(\mathrm{Re}_D - 1000\right) \cdot \mathrm{Pr}}{1 + 12.7\left(f/8\right)^{1/2}\left(\mathrm{Pr}^{2/3} - 1\right)} \tag{2.22}$$

Where f is the Darcy friction factor, which accounts for the frictional losses in the pipe or duct, obtained from the Moody diagram.

The VDI-Mean Nusselt method [19, pp. 73-79]

In this method, the average heat transfer coefficient of the whole tube bank is evaluated, as opposed to a single tube in cross-flow [22] and bases the Reynolds number calculation on the maximum flow velocity, rather than upstream velocity. It states that:

$$Nu_m = a \cdot \mathrm{Re}^m \cdot \mathrm{Pr}^{0.34} \cdot F_1 \cdot F_2 \tag{2.23}$$

Where a and m are correlation constants and F_1 and F_2 are correction factors for surface to bulk physical property variations [22].

A number of computer thermohydraulic design programs have been developed to aid in the design and optimization of heat exchangers like CC-Therm and CHEMCAD [30], and automatically select

the applicable heat transfer model for a given set of boundary conditions. In this study, an iterative optimum sizing will be done using a MathCAD analytical calculation, developed for this purpose.

2.4.6 Tube design

Tube diameter and material

Standard tube sizes are available from $^1/_4$" to 2" outer diameter, OD, with the common sizes being ODs of $^3/_4$" and 1". The tube wall thickness is defined by the Birmingham wire gauge and standard tube sizes are specified in Table RCB-2.21 of the TEMA standard. Tube materials are copper, steel and alloy steel like aluminium-bronze, copper-nickel and admiralty, with other application specific materials, diameters and gages still being acceptable.

Tube length and count

Straight and U-tube exchangers have common standard lengths of 12, 15, 18, 20 and 30ft. Other sizes can also be used. Tube length determines the heat transfer area, but very long unsupported lengths pose threats of in-service vibration and shell side distribution problems [22].

Tube count refers to the number of tubes in the tube bundle and dictates the velocity of fluid inside the tubes. Acceptable tube side velocity varies with the fluid, with most liquids ranging from 0.9-1.52m/s and gases ranging from 15-30m/s [19]. These values are however very dependent on the type of fluid and fluid properties like viscosity, with Therminol VP-1, a thermal oil having acceptable velocity ranges of 0.36 – 4.97m/s according to its manufacturer [31]. The minimum tube side velocity is set to avoid settling of the fluid particle which increases fouling and the maximum to avoid too much turbulence which leads to tube erosion. The desired flow velocity determines the tube count. The bundle layout is determined by geometric factors, dimensions and clearances, removal of scavenger air, etc., with the tube layout and tube pitch being the critical deciding factors [32]. Table 11-3 of Perry's Chemical Engineers' Handbook sets out standard tube count data.

The tube count is calculated by dividing the shell circle area by the projected area of the tube layout [33]. Figure 12 below shows typical baffle and bundle geometries useful in calculating the tube count:

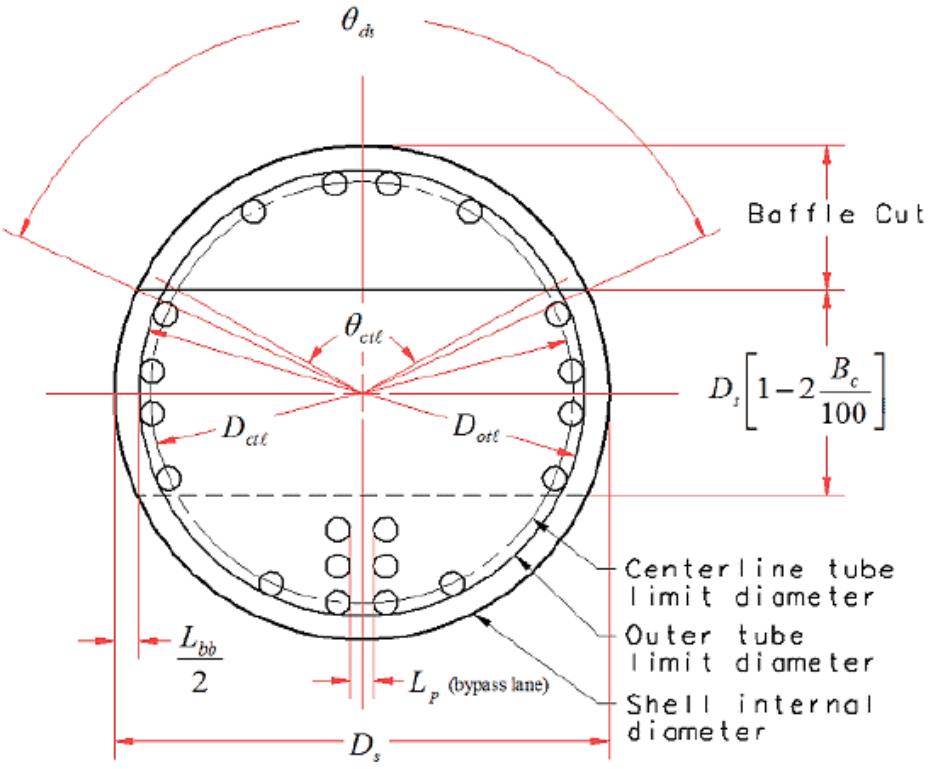

Figure 12: Baffle and tube bundle geometries [32]

According to Taborek, a simple estimation formula can be used for fixed tube sheets with a single tube pass and no tubes removed at the entrance and exit areas as follows [32, pp. 3-8]:

$$N_t = \frac{0.7854 \cdot D_{ctl}^{\ 2}}{CL \cdot L_{tp}^{\ 2}} \tag{2.24}$$

where, D_{ctl} is the centreline tube limit diameter, calculated as the difference between the outer limit tube diameter and the tube outside diameter; CL is the tube layout constant and L_{tp} is the tube pitch. On the other hand, defining the tube count from first principles reduces the expression to [33, p. 76]:

$$N_t = \frac{\pi \cdot CTP \cdot D_S^{\ 2}}{4 \cdot CL \cdot PR^2 \cdot D_o^{\ 2}} \tag{2.25}$$

Where CTP is a constant for tube passes defined as 0.93, 0.9 and 0.85 for one, two and three tube passes respectively, D_S is the shell inside diameter and PR is the ratio of the tube pitch to the tube outside diameter. Knowing that the tubes have a limit of how far they go as far as the shell inside diameter is concerned (which is accounted for in Taborek's equation by using the centreline limit diameter) and also to account for different tube pass arrangements in the analytical modelling of the heat exchanger, the researcher combined aspects of equations (2.24) and (2.25) to calculate the tube count as follows:

$$N_t = \frac{\pi \cdot CTP \cdot D_{ctl}^{\ 2}}{4 \cdot CL \cdot L_{tp}^{\ 2}} \tag{2.26}$$

Tube clearance, pitch and layout

Too small a distance between two adjacent tube holes weakens the tube sheet and thus a considerable amount of space should be left between tube holes to maintain tube sheet structural integrity [29]. Tube clearance is the shortest distance between two adjacent tube holes and tube pitch is the shortest centre to centre distance between adjacent tubes [29]. The tube pitch is calculated as follows:

$$L_{tp} = D_o + C \tag{2.27}$$

Where L_{tp} is the tube pitch in the transverse direction, D_o is the tube outer diameter and C is the tube clearance. The pitch is also dependant on the tube layout with the common layouts being outlined below:

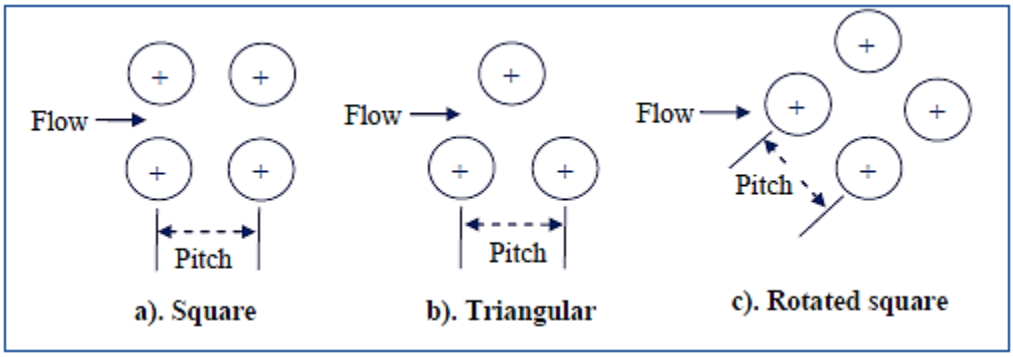

Figure 13:Tube layouts adapted from NPTEL Chemical Engineering Design Module I [33]

The square pitch is most widely used because the tubes are accessible for external cleaning and it also has a lower pressure drop if the shell fluid flows in the direction shown above. Triangular pattern provides a more robust tube sheet construction [22] but should not be used where mechanical cleaning methods are used to clean the shell. According to TEMA, the minimum tube pitch should be 1.25 times D_o .

Tube sheet

Tubes are fixed to the tube sheet, which also acts as the barrier between shell-side and tube -side fluids. Because the tube sheet is exposed to the most adverse of the operating conditions (varying temperatures and pressures from shell and tube-sides), care must be taken in its design to avoid either shear or bending failures in-service. TEMA specifies the minimum tube sheet thickness as

greater than 75% of D_o . Detailed design of the tube sheet is specified in Appendix A of the TEMA Standard.

2.4.7 Shell design

The objective in shell design is to specify a shell which fits the tube bundle, at the same time performing its thermal duty in the allowable range of fluid pressure drop. The method which will be discussed in this section is the Taborek modification of the Bell-Delaware method as it gives a more accurate result.

Shell diameter

The shell diameters are not standardized according to TEMA, but the selection of a shell inside diameter should be such that the tube count is within limits for that size. Pipe and plate shells are governed in accordance to ASTM/ASME pipe specifications [21]. The minimum shell thickness is selected such that the whole shell withstands the pressure differential exerted on it, as well as accounting for a corrosion allowance set in the TEMA standard.

The flow area in the shell is a function of the shell diameter. However, because of the presence of the tube bundle in the shell, the shell flow area becomes non uniform necessitating the need of finding a *shell-side equivalent diameter,* an approximate diameter which accounts for the non-uniform fluid flow in the shell. It is a function of the hydraulic radius, which is the ratio of the cross-sectional area of a non-circular flow conduit to its wetted perimeter. According to Kern [29], the direction of flow in the shell is partly along and partly across the length of the tubes, the flow area is variable from tube row to row. Because the hydraulic radius based upon the flow area across any one row could not distinguish between square and triangular pitch [29], this led to the formulation of the equivalent shell diameter which combines both the size and pitch of the tubes and their type of pitch by considering the flow along (instead of across) the tube length to be four times the hydraulic radius. The shell equivalent diameter is calculated as [29]:

$$D_e = \frac{4 \cdot FreeArea}{Wettedperimeter} \quad [1] \tag{2.28}$$

Which reduces to:

$$D_e = \frac{4\left[L_{tp}{}^2 - \frac{\pi}{4} \cdot D_o{}^2 \right]}{\pi \cdot D_o} \tag{2.29}$$

[1] Kern uses free area to avoid confusion with free-flow area, an actual entity in the hydarulic radius [29]

For a design with square pitch tube arrangement.

Shell geometry

A typical TEMA type E shell with segmental cut baffles is shown below:

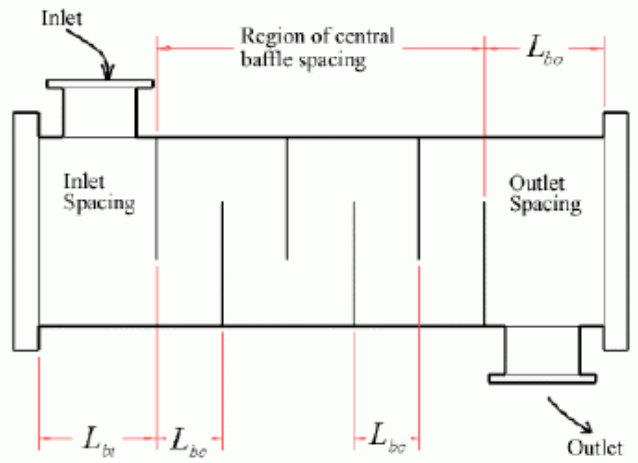

Figure 14: Single segmental shell and tube type E shell showing baffle spacings [32]

The inlet, central and outlet baffle spacings are as shown above. It is the baffles which introduce leakages in the system. Because of the presence of baffles, the E shell is divided into cells which resemble multi-shell cells, as shown in Figure 14, and the fluid will seek a path of least resistance from the inlet to the outlet of the exchanger which results in "leaks". This deviates the shell fluid flow from pure counter-flow into part counter and part crossflow. The first investigator to systematically analyse this multi-pass phenomenon in the TEMA E exchanger was Nagle in 1933 and provided correction factors for the mean temperature difference in a n-2n[2] STHE.

After Nagle, several other researchers further investigated this phenomenon and added to the literature which is now widely used in the design of STHE shells [34]. It was from this research that Cayglan and Buthod proposed that for any number of baffles greater than 10, the 1-1 TEMA E exchanger is approximated into a pure counter-flow heat exchanger [25]. In 1977, Gardener and Taborek also analysed the same phenomenon considering the fluid in the tubes to be perfectly mixed and drew the same conclusions as Cayglan and Buthod. Present day literature states that for all number of baffles greater than six, the shell can be assumed to be pure counterflow [34].

Baffles

Baffles are used to support the tube bundle, maintain tube spacing and direct the shell fluid, along or across the tube bundle [23]. They are either normal or parallel to the tubes, with transverse baffles directing the shell fluid at right angles to the tube bundles, increasing the turbulence of the

[2] Where n is the shell passes and 2n denotes the tube passes

shell side fluid, which in turn increases the shell-side heat transfer coefficient. Longitudinal baffles on the other hand are parallel to the tube bundle and are used to control the flow of the shell side fluid, particularly in the F, G and H shells [23].

According to TEMA, the segmental or multi-segmental type baffle is standard. The baffle cut is the segment opening height expressed as a percentage of the shell inside diameter. The figure below shows the stream analysis of shell side flow parts, divided into individual streams with letter designations as described by Tinker [32] :

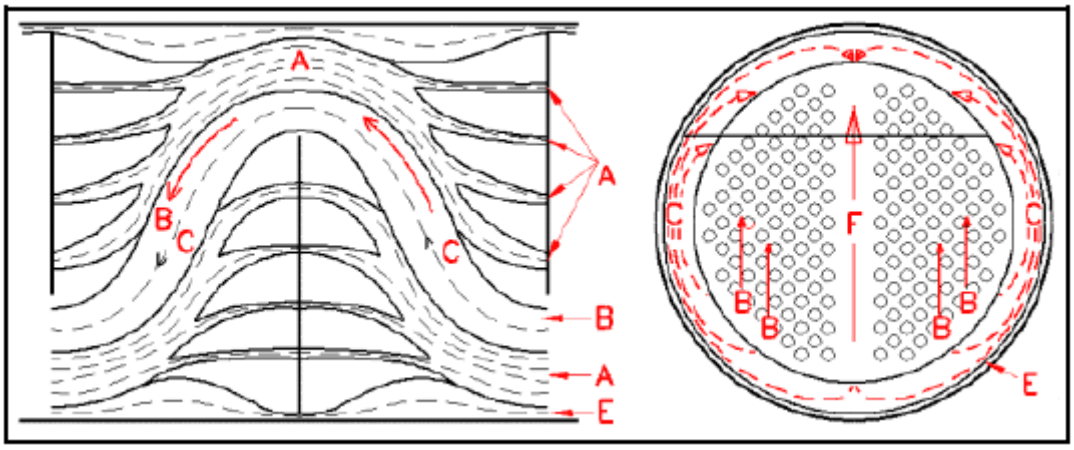

Figure 15: Shell-side flow paths in a segmental baffled heat exchanger [32]

Stream A: Leakage through the tube hole.

Stream B: Idealized crossflow stream.

Stream C: Bundle by-pass stream which flows through the annular opening between the outside of the tube bundle and the inner shell wall.

Stream E: Shell-baffle by-pass stream which flows between the inner shell wall and the baffle edge.

Stream F: The pass partition by-pass which flows through the spaces where there are pass partition plates.

The above streams give rise to the various correction factors (leakage, baffle cut, bundle by-pass, unequal baffle spacing correction factors) which are factored in the ideal (if the flow was pure parallel) shell side heat transfer coefficient to get the actual heat transfer coefficient as:

$$h_{steam.actual} = J_B J_R J_S J_L J_C \cdot h_{steam.ideal}$$

Where $J_B, J_R, J_S, J_L \& J_C$ are the bundle by-pass, laminar flow, unequal spacing, baffle leakage and baffle cut correction factors respectively[3].

2.4.8 Detailed heat exchanger design process flow model

The detailed design of STHEs is briefly described in the flow chart below. The design process begins with an approximate design which arrives at a tentative heat transfer area and physical design from estimating the heat load and outlet temperatures. The most widely accepted approximate design method is Bell's Method [23]. After, that a more detailed design follows which takes into consideration TEMA design guidelines and tolerances. Tube side design is quite standard as it involves consideration of the tube side fluid, allowable tube-side pressure drops and then selecting a suitable material to withstand the operating conditions of the tube side fluid.

Shell side design and performance on the other hand is quite rigorous due to the presence of shell side constructional clearances (in the baffles and tube sheets) which cause fluid leakages, distorting the perfect streamline flow of fluid [23] which has the net effect of reduction in heat exchanger thermal effectiveness. Various methods have been put forward to determine shell side performance, with the first flow distribution pattern being proposed by Tinker and later modified by Palen et al [23]. This physical flow pattern was then used in the widely known and accepted Bell-Delaware method for shell side performance [32] and then later modified by Taborek to account for the shell-side heat transfer loss and additional pressure drops due to various leakages in the shell.

[3] The equations for the stream leakage flow correction factors will be outlined in the mathematical model in Appendix B of this report.

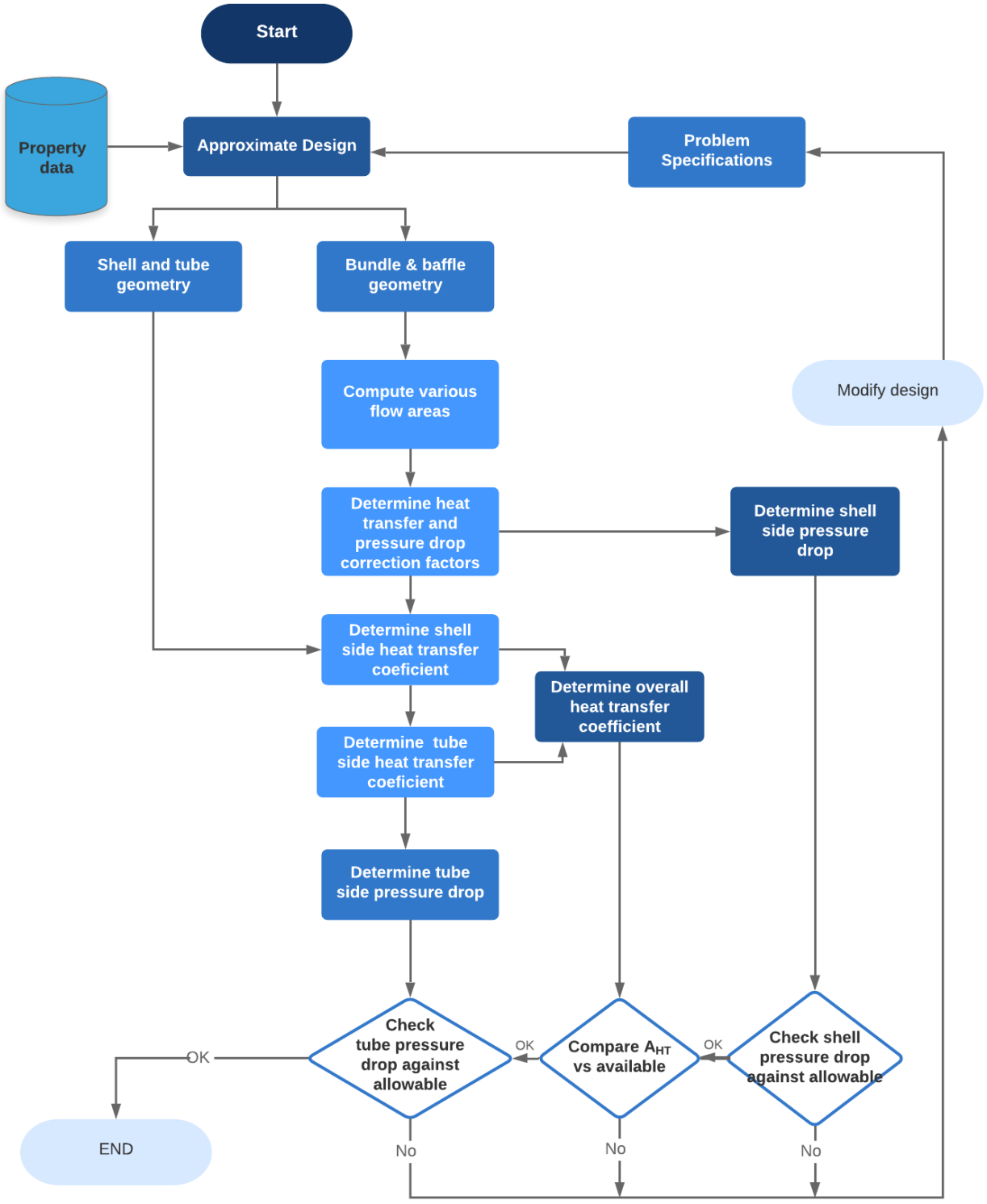

Figure 16: Shell & Tube heat exchanger design flow chart adapted from Heat Exchanger Design Handbook [23]

2.5 Shell and tube-side pressure drops

After all the critical mechanical design parameters are calculated, the final step is checking if the shell and tube-side pressure drops conform to the set design limits. The tube-side pressure drop

affects the pumping power requirement which in turn affects the auxiliary energy consumption. According to the Indian Central Electricity Regulations Council, the allowable aux. power consumptions for combined cycle thermal generating stations should be in the order of 2 – 5% for thermal efficiency improvement [35].

Shell-side pressure drops, in this case has additional pressure drops due to cross flow, window zone flow leakages, and end zone and nozzle inlet and exit losses, which will be calculated for the shell side and added to the ideal pressure drop. The shell side pressure drop had to be kept as low as possible to ensure the highest possible state at turbine inlet.

2.6 Feedwater heater structural design

An efficiency improvement to the basic Rankine cycle, shown in Figure 2 is using the low pressure turbine steam (either exhaust steam or steam extracted after high pressure turbine expansion) to preheat the feedwater, before it enters the economizer section of the boiler. In power plants, there are two types of feedwater heaters: high pressure (HP) feedwater heaters situated after the feedwater pump, and low pressure (LP) feedwater heaters located between the condenser and feedwater tank [36]. In the HP feedwater heaters, the feedwater and the steam are not mixed, with the normal construction being a shell and tube heat exchanger, with steam flowing in the shell and feedwater in the tubes. For this reason HP feedwater heaters are also called closed feedwater heaters. LP feedwater heaters can be closed or open, with the feedwater tank acting as an open feedwater heater, responsible for both feedwater heating and removal of oxygen and carbon dioxide gases (in the deaerator) which is necessary in feedwater chemistry control.

In the open feedwater heater, there is direct contact between the hot and cold fluids, with the feedwater being sprayed into the tank and the LP steam bubbled from the bottom of the feedwater tank, mixing with the feedwater and exchanging heat until thermal equilibrium is reached. The HP heaters after the feedwater tank are also closed feedwater heaters, with large power plants typically employing 3-4 LP feedwater heaters and 3 -5 HP feedwater heaters [36]. Optimum placement of the HP feedwater heaters begins by defining the enthalpy difference between the feedwater pump and the economizer inlet, then dividing it by the number of HP feedwater heaters, giving the enthalpy rise in each HP feedwater heater stage [36].

2.7 Steam turbines and application to small steam plants

The steam turbine is a heat engine which transforms thermal energy from pressurized steam to kinetic energy by flow through nozzles, which is then converted to a force doing work on rings of blading mounted on a shaft [37]. It is used for various industrial operations, mostly power

generation and providing mechanical work to drive process equipment like pumps and fans. The first practical turbine was made by C. Parsons in 1884 and the usual turbine consists of four fundamental parts:

- Rotor – shaft which carries the blades or buckets,
- Stator – also known as the cylinder or casing within which the rotor turns and where the nozzles are fixed,
- Nozzles – which direct the steam on the rotor blades,
- Frame/ base – for supporting the turbine assembly.

The energy conversion process in the steam turbine is from potential (high pressure) and thermal (temperature) energy in the steam, to kinetic energy (acceleration in the nozzle) and then rotational energy (torque and speed) in the rotor shaft.

Classification of steam turbines is done in various ways [37]:

i. w.r.t form of blade passage – impulse, reaction or combination impulse and reaction turbine.
ii. w.r.t internal design and flow sequence - single flow, double flow, divided flow, compound flow etc.
iii. w.r.t direction of steam flow relative to plane of rotation – axial, radial or tangential flow.
iv. w.r.t rotational speed – for 60 cycle or 25 cycle generators and for geared units without special speed requirements.
v. w.r.t conditions of use – reheat, extraction, back pressure, regenerative or mixed pressure turbines.
vi. w.r.t passes of steam flow through blades – single pass or re-entry turbines.

In this section, more literature will be covered on classification of steam turbines with respect to conditions of use to enable the selection of a suitable turbine for the operating conditions required.

2.7.1 Classification of steam turbines w.r.t conditions of use

This classification places emphasis on the boundary conditions of the steam at both turbine inlet and exit, focusing on:

- Inlet pressure – high, intermediate, or low-pressure turbine.
- Exhaust condition – condensing, non-condensing or back pressure, extraction-condensing turbine.
- Steam mass flow through the turbine – extraction, regenerative or reheat turbine.

Condensing turbine

The condensing turbine exhausts steam at below atmospheric pressure to allow it to be condensed to liquid water in the condenser. It is employed in power plants where the requirement is power only and thus all the steam which enters the turbine is exhausted at the exit stage (assuming no leaks or extractions).

Non-condensing/ Back-pressure turbine

In the non-condensing turbine, the steam is exhausted at low pressure but above atmospheric, usually between 1-12bar. It is mostly employed in process plant industries where there is both a power and process steam requirement. In this set-up, the condenser is removed, and the process plant acts as the "condenser" whilst utilizing the heat in the exhaust steam for process heating.

Extraction- condensing turbine

In this turbine, part of the steam is bled/ extracted at the process pressure requirements and the remaining steam is further expanded in the low-pressure turbine stages and finally condensed in the condenser.

High pressure (HP) turbine

Usually employed in utility power plants, where operating pressures are high and receive high pressure, high temperature steam (main steam) from the boiler. The HP turbine can be condensing or non-condensing. High pressure condensing turbines exhaust at below atmospheric pressure and large volume [37] thus are designed to have short blading at the HP end and long blading at the low pressure (LP) end.

High pressure non-condensing turbines on the other end exhaust steam at moderate steam conditions for use in factory processing or heating applications. They are also used in instances where cooling water for condensing is unavailable and are built in small or moderate sizes [37].

Intermediate pressure (IP)/ Reheat turbine

The intermediate pressure turbine is usually placed between the high- and low-pressure turbines. It receives the HP turbine exhaust as its input steam and exhausts to the LP turbine inlet. It is however mostly known as the reheat turbine, because the turbine does not receive the HP exhaust

directly from the HP turbine, but from the boiler reheaters. After expansion in the HP turbine, the HP exhaust is sent to the boiler reheater tubes located usually between the platen and pendant superheaters, at HP exhaust pressure and reheated to the main steam temperature. After that, the steam is then returned to the IP turbine to complete its expansion before subsequent exhaustion into the LP turbine. Such arrangements are generally only found in power generation plants.

Low pressure (LP)/ Exhaust turbine

The low-pressure turbines are usually the last stages of expansion before condensing. They are employed in applications where large power output (hence large mass flow) is required in a single machine [37]. In order to control the length of the turbine and avoid turbine vibrations, the HP and LP stages are divided into separate casing, having a separate LP turbine. There are also very often more than one LP turbine running in parallel for a single HP turbine due to the large volume flow requirement at the exhaust. The LP turbine is designed to handle high volume, low pressure, and lower quality steam at the final stages.

Mixed pressure turbine

The mixed pressure turbine is designed to handle two different steam pressures. It can be HP-LP/ IP-LP combination, or two different LP inlets and the low-pressure inlet is usually from another heat engine or turbine e.g., gas turbine combined cycle plants. This turbine is thus more employed in applications where it is desirable to recover waste heat from other heat engines for power generation. The LP steam joins the HP steam after it has been expanded down to the pressure at which LP steam is usually received at.

Regenerative or bleeder turbines

The regenerative turbine receives HP steam at inlet, and at one or more stages before the steam has been exhausted to its final low pressure, it is bled / withdrawn at intermediate pressures for feedwater heating [37]. The feedwater is heated in stages with the last feedwater heating occurring at the highest temperature bled steam. Regenerative turbines are almost similar in principle as the extraction-condensing turbine except the extraction turbine steam goes to the process not feed water heaters.

In this study, the maximum pressure is 950kPa, and the steam is required to be exhausted at 400kPa to meet process plant demands. The suitable turbine for this operation is thus a back-pressure turbine which can operate in the low-pressure ranges. Important to note, in addition to knowing

the turbine operating conditions it is important to know how the steam changes state from turbine inlet to exhaust. This is done on the Mollier diagram, using a turbine expansion line.

2.7.2 Turbine Expansion Line

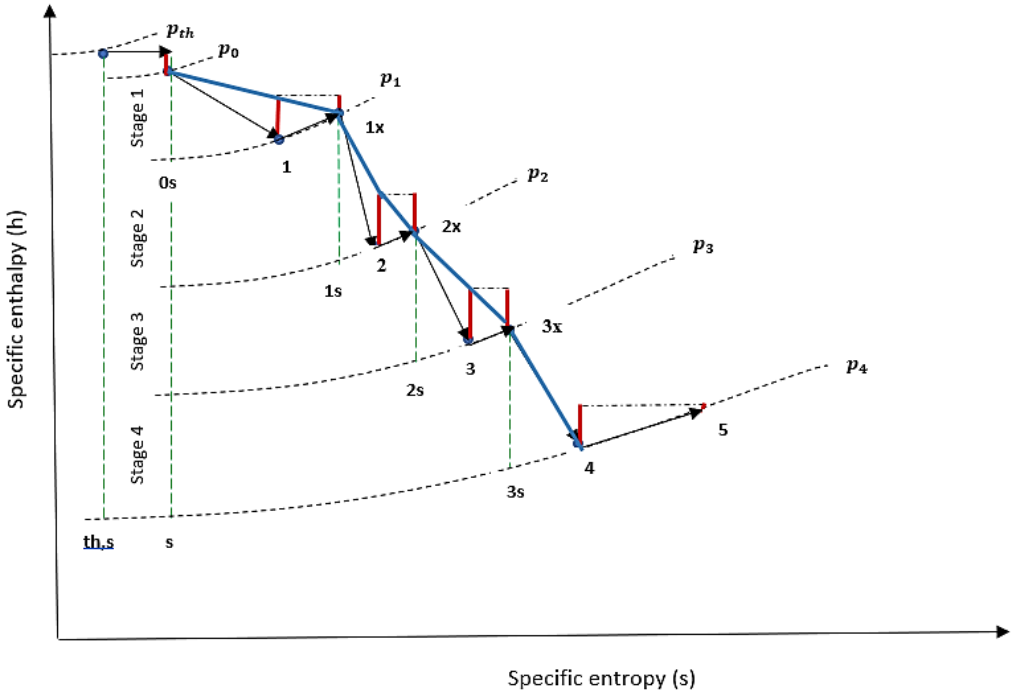

Figure 17: Typical turbine condition line

Also known as the condition line, the turbine expansion line (shown above), depicts the thermal state of the steam as it expands through the turbine. Steam enters the governing valve at state point *th*, where the pressure is reduced due to valve losses to point *0*. From point *0 – 1*, the flow is accelerated in the nozzle but due to nozzle losses, the flow is shifted from the ideal lossless exit enthalpy at *0s* to state point *1*. In each turbine stage, the rotating blades extract a portion of the flow's kinetic energy (depicted as the red vertical bars), and the remainder moves on to the next stage. At entry to the next stage, some kinetic energy is lost due to carryover losses. This further shifts the steam state to point *1x* where it has lower inlet velocity at entry to stage *2*.

The carryover losses, also known as leaving-velocity losses occur between stages because of the difference in the stage diameters or when there is a huge axial space between adjacent stages. It is high in the governing and the exhaust stages because of the formation of eddies between the nozzle and moving blades and also since there is no further device to extract kinetic energy after the last stage. This heat loss which is not extracted as useful work, but raises the total heat and entropy of the steam from point *1* to point *1x* is also known as reheat as it appears like more heat has been added to the steam between stages which can be seen in Figure 17 above. The more the number of stages, the more these "inter-stage reheats" are, which increases the turbine's reheat factor.

However, for any specified initial steam conditions, final pressure and stage efficiency, there is a limiting value of the reheat factor which corresponds to an infinite number of stages and for any finite number of stages, the reheat factor will be less [37].

At point *4*, all the unused kinetic energy is lost at outlet to point *5*. The enthalpy at point *4* and *5* is known as the expansion line end point (ELEP) and used energy end point (UEEP) enthalpy respectively. The blue line is the condition line of the turbine.

2.7.3 Turbine efficiency

Turbine efficiency is a measure of how well the turbine converts the input heat into mechanical work. It is determined by considering the actual work output to the maximum possible work which could be extracted by the turbine. The maximum work is only realized when there are no losses, which is represented by the ideal isentropic line (*0* - *s*) between the inlet and outlet on Figure 17 above. The actual turbine work is depicted by the condition line from the turbine inlet to the UEEP and thus the efficiency is calculated as:

$$\eta_{turbine} = \frac{h_0 - h_5}{h_0 - h_s} \tag{2.30}$$

A Siemens SST-060 turbine alternator was selected as the suitable turbine to convert the thermal energy in the superheated steam from the heat exchanger, to mechanical work and electrical energy. This decision was arrived at basing on information acquired from previous research done by the researcher in an undergraduate project.

2.7.4 Siemens SST-060 Turbo-Alternator set

Siemens Turbomachinery Equipment (STE) has a range of small-scale turbine technologies, with four distinct product lines: the SST-050 (up to 750kW), the SST-060 (up to 5000kW), the SST-110 (up to 7 000kW and the SST-120 (up to 10 000kW) with basic technical values as follows:

- Live steam pressure: 3 - 131bar (absolute),
- Live steam temperature: Dry saturated – 530˚C,
- Exhaust steam pressure: 0.08 – 29bar,
- Speed: 500 – 23000rpm,
- Power: Up to 10 000kW.

Through consultation with the Siemens team, the SST-060 was recommended as the most applicable set for this duty.

Figure 18: Siemens SST-060 Turbo-alternator set

Previously known as the "Dampfturbine", the SST-060 (shown above) was originally designed and manufactured by Kuhnle, Kopp & Kausch AG, a company established in 1899 which was later acquired by Siemens in 2007. The turbine range has a modular design which allows it to be connected in different combinations, making it very flexible and able to meet a wide range of customer specifications [38].

It is a predesigned radial inflow impulse turbine, which has many applications and can be ordered as a standalone unit (without generator) for use in mechanical drivetrains or as a turbo-alternator for power generation in cogeneration, biomass, waste-to-energy, and heat recovery generator projects [39]. The turbo-alternator can be used as both a backpressure or condensing turbine, with an integral cooling system. It can operate smoothly through its range of operating speeds up to overspeed. The figure below shows the detailed specifications of the SST-060 unit.

SIEMENS

Turbine series

Turbine series SST-060 (AFR / CFR – type)

General

Integral gear design
Overhung design

Technical Data (max)

• Power	5,0 MW
• Live steam pressure	65 bar a
• Live steam temperature	480 °C
• Saturated steam	
• Speed	up to 24 900 rpm
• Exhaust steam pressure	up to 17 bar a
• Turbine wheel diameter	300 / 500 mm
• 5 different gearing sizes	

Typical dimensions

Length 1,5 m
Width 2,5 m
Height 2,5 m
Weight: Turbine inkl. oil reservoir and coupling: up to 12 t

Characteristics

- Exhaust steam pressure type
- Package unit design
- Flexible rotor
- Oil unit integrated in base frame
- Quick start without pre-heating
- Custom made
- Short delivery times

Scope of supply

- Turbine package
- Oil unit
- Electrical scope of supply
- Generator
- Short delivery times

Figure 19: SST-060 Specifications [39]

The researcher used the Siemens option as it was the only manufacturer with easily accessible literature on the small-scale turbines and has been referenced in many cogeneration webinars like the International Energy Agency Bioenergy Task 32 and 33 [39]. Siemens is a well-known turbine manufacturer with years of providing quality and reliable turbines. Another factor which made the SST-060 a turbine of choice, is the fact that it is suitable for quick start without preheating, making it ideal for a SAPG system which has an intermittent heat supply source for the main steam.

2.8 Steam plant economics

One of the most important aspect of project evaluation is assessment of profitability or cost effectiveness. Power plant projects are mostly must-have capital intensive investments [40], whose investment appraisal focuses on minimizing costs (least cost approach) rather than maximizing profit. Where the power plant project is state-owned, the economic viability is measured based on levelized cost of energy rather than payback period. Capital for these projects is government sourced, and the investment is paid back from tax revenue, unlike in independent power producer

scenarios where the projects are private investor owned and the narrative shifts from just minimizing costs but ensuring a positive return on investment in the shortest possible time.

In this research, the researcher adopted the discounted payback period to check the profitability of the project. Despite there being other widely used and accepted methods of evaluating project profitability (net present value or internal rate of return), the discounted payback method was selected because for an already operational food and beverage processing industry whose key objective is food processing, focus is on how soon the CAPEX can be recouped than other profitability indicators like the net present value. The important factor to consider in this augmentation is at what cost and how long it takes to recoup the initial investment rather than cost of energy. The total capital investment was calculated based on the procedure outlined below.

2.8.1 Primary equipment

The capital investment of the project is largely influenced by the turbine capital costs, size of solar field required to meet the thermal heat addition and heat exchanger cost. The turbine costs were obtained from the manufacturer in 2016, shown in Appendix D of this research. Efforts to obtain a more recent quote did not yield any positive results as manufacturers only release accurate cost data to customers with orders. However, the initial quote was in Euros and the variation in exchange rate of the Euro:US$ in the past 5 years is not that big and will be accounted for in the sensitivity analysis rather than trying to refine cost estimates which is beyond the scope of this study.

Solar system costs will be done using the SAM NREL system advisor model costing template which is based on actual United States Department of Energy's National Renewable Energy Laboratory (NREL) past project's cost data. The SAM financial model is also based in US$ and variations in the exchange rate between the US$ and the ZAR will be used in the sensitivity analysis to account for the time value of money.

2.8.2 Heat exchanger costs

Critical in this study is designing a heat exchanger to superheat the saturated steam of the boiler, thus estimation of the manufacturing cost of the optimum design is a major concern. Cost optimization of heat exchangers, particularly shell and tube heat exchangers has been an ongoing process, with parametric methods or variant based costing being the most popular [41]. The parametric costing models rely on heat transfer area as the base factor to calculate total heat exchanger cost and uses an exponential equation to calculate direct manufacturing cost, such as the

formulation of Hall [42]. To increase the accuracy of the result, application (pressure factor) and structural (length of tubes) coefficients are also included.

However, the parametric estimates are based on a specific heat exchanger configuration, provide a purchasing cost which is affected by market situations and limited to a range of heat exchanger sizes (e.g., Hall's formulations are limited to heat transfer areas below 140m^2) [41]. This has led to the development of generative cost models which allow for up-to-date cost estimates, which reflect the effect of design variations on the manufacturing costs. The equations used to calculate the heat exchanger cost were adapted from the works of Caputo et al. [42] and will be presented below.

Direct manufacturing cost of a heat exchanger is the sum of materials and manufacturing processes cost:

$$C_{m,x} = C_{mat,x} + \sum_{k=1}^{n} C_{op,k} \tag{2.31}$$

where $C_{m,x}$ is the manufacturing cost of the xth component of the heat exchanger; $C_{mat,x}$ is the material cost, *n* is the number of processes needed for each component of the heat exchanger and $C_{op,k}$ is the cost of the kth operation on the xth component .

The material cost of the xth component:

$$C_{mat,x} = V_x \rho_x C_{mat} \tag{2.32}$$

where V is volume in m^3, ρ_x is the density in $^{kg}/_{m^3}$ and C_{mat} is the material cost in ZAR.

The cost of the kth operation on the xth component:

$$C_{op,k} = \left(\frac{L_k}{v_k} \right) C_{H,k} \tag{2.33}$$

Where L is the manufacturing process length, v is the operation speed and C_H is the hourly rate. However, the detailed cost of processing includes summing up the labour, consumables and equipment amortization which is beyond the scope of this research. For simplicity's sake, the manufacturing cost was estimated as 50% of the total material cost and would be included in the sensitivity analysis if it was found to play a major role in the overall costing. The eventual component cost equation therefore reduced to:

$$C_{m,x} = 1.5 \cdot V_x \rho_x C_{mat} \tag{2.34}$$

2.8.3 Total capital investment

Total capital investment is the amount of money required to install the system. It includes the total heat exchanger cost, steam turbine cost and solar system capital costs. This will be the loan amount which will be used to calculate of the discounted payback period, using the energy savings obtained by operating the power generating system when the solar resource is available during the day.

$$Loan = C_{turb} + C_{sf} + C_{H/E} \tag{2.35}$$

Where C_{turb}, C_{sf} and $C_{H/E}$ are the turbine, solar field and heat exchanger capital costs respectively. The cost of process control e.g. isolation valves, control valves, safety valves, modulators, instrumentation and distributed control system integration could potentially cost as much as the HX but due to scope of this study will not be included. Impact of HX cost variation will be studied in the sensitivity analysis.

2.8.4 Payback period

Payback period is the time required to recover the costs incurred in an investment. The ordinary payback period is calculated by dividing the initial capital outlay with the estimated periodical net cash flows. Where the time value of money is considered, by considering loan interest rates, it is called the discounted payback period. This is particularly of interest to the investor as it gives an insight on how long it will take to recoup the initial capital investment of the project. In this study, the annuity equation was used to derive the discounted payback period formula. The annuity equation states that:

$$A = \frac{Loan \cdot r}{1-(1+r)^{n}} \tag{2.36}$$

Where A is the yearly / monthly fixed instalment to be paid back to recoup the initial loan investment over a predetermined period n and r is the interest rate per period. It is however advisable to pay back the instalments in the shortest possible time as each instalment reduces the balance on the capital, subsequently reducing the interest payable. By making n the subject of the formula, the discounted payback period can be calculated as shown in (2.37) below:

$$DPP_{months} = \ln\left(1 - \frac{Loan \times \frac{r}{12}}{\frac{CF}{12}}\right) \div \ln\left(1 + \frac{r}{12}\right) \quad (2.37)$$

Where DPP_{months} is the discounted payback period in months, r is the interest rate per annum and CF is the annual cash savings made by producing energy at the site, calculated as:

$$CF = (E_{annual,produced} \times Tariff) - C_{OPEX} \quad (2.38)$$

Where $E_{annual,produced}$ is the electrical energy produced per annum and C_{OPEX} is the annual operating and maintenance costs of the system.

2.9 Conclusion

The literature reviewed in this chapter will be the backbone for the model development and system design that form part of this thesis. The first section looked at the process steam plant basics, focusing on the process steam plant thermodynamic cycle and how it is related to the conventional power plant cycle. The next section looked at cogeneration and how a basic steam plant can be retrofitted to enable the generation of both heat and power by adding additional heat into the system. Section 2.3 looked at solar thermal plants, which will be used to provide additional heat to superheat the steam from the boiler and the next section focused on the design of the superheater. Steam turbines were briefly discussed as they are the heat engines responsible for converting the thermal energy to mechanical work. The last section looked at steam plant economics as this gives the measure of economic viability of undertaking such a project to both the researcher and potential investors.

3. Methodology

3.1 Model Investigation

In this section of the report, the findings of the qualitative component of this research which were used in the development of ideas for the quantitative research are presented. A number of site visits were done to food and beverage processing industries with the capacity to install combined heat and power systems, as well as those which already have such systems in place, to gather information on how their current systems are working. In addition to that, the researcher visited a local steam boiler manufacturing company to learn more about steam boiler design.

3.1.1 Research Questions

The research questions were broken down into three distinct groups: questions on boiler design, questions on process plants with the potential to adopt Cogeneration, and those for plants with Cogeneration already in place. Outlined below are the different research questions:

3.1.2 Boiler Design Questions

- Can an existing fire-tube (package) boiler be retrofitted to produce superheated steam?
- What are the design considerations to be made when retrofitting a package boiler?
- What is the effect of exceeding the maximum continuous rating of a boiler, especially on the steam release rate?

3.1.3 Process Steam plants

- What is the maximum plant electricity demand?
- What is the capacity of the existing process plant?
- Which processes require process steam in the operation and at what temperature and pressure?

3.1.4 Existing Combined Heat & Power Plants

- How is the cogeneration system currently working?
- What is the plant process thermal load requirement?
- Is power generation driven by the thermal load or electrical load?
- How are fluctuating demands, in terms of both thermal and or electrical load managed?
- Was the system originally designed for Cogeneration or was it upgraded to one? If yes, what were the considerations made in the upgrade?

After drawing down the relevant questions for each section of the research, document analyses, interviews, and observations were used to provide answers to the questions at the sites which were visited. The data obtained provided the basis of the quantitative aspect of the research.

3.2 Site visit reports

3.2.1 John Thompson Boilers

John Thompson boilers, a division of ACTOM Private Limited manufactures electro-mechanical equipment (package boilers, water-tube boilers, utility boilers) largely used in the steam plant industries. The visit to John Thompson was meant to answer questions on the design considerations to be made when retrofitting a package boiler to produce superheated steam and effects on boiler operation.

Package Boiler Retrofit

It is possible to convert an existing package boiler to superheat steam for power generation. However, the design of Fire-tube boilers is governed by BS EN 12953:3 which outlines specific tolerances and design standards. At John Thompson, the superheater is fitted on the smoke box and boilers in service can be sent back for the retro fitment. Boiler energy efficiency can be analysed on three different levels:

- Boiler thermal efficiency - how well the boiler transfers heat?
- Combustion efficiency - ability of the burner to completely use the energy in the fuel without generating carbon monoxide or leaving hydrocarbons unburned.
- Fuel-steam ratio.

When making any changes to the boiler, one should take into cognizance that the pressure rating cannot be changed as it is proportional to material thickness and composition. The boiler is approved by a third party and certified by the department of labor based on the pressure, steaming rate and fuel fired. If any of these parameters change, the boiler will have to be re-certified.

In addition to that, further questions came up from this visit:

- How does preheating the feedwater with an external energy source affect the boiler firing rate and flue gas flows?

It was noted that preheating the feedwater with an external thermal energy source like solar power will reduce the mass flow rate of coal, lowering the flue gas fumes. This reduces the boiler's carbon footprint.

3.2.2 Kadoma Paper Mills

Kadoma Paper Mills manufactures tissue and craft products from recycled wastepaper. The recycled paper is sorted, graded, and pulped to manufacture different grades of paper (enhanced white tissue, hand towelling tissue, tinted tissue and craft paper).

Existing Steam Plant Specifications

Kadoma Paper Mills has four fire-tube boilers: three rated at 4.5 tonnes per hour (tph) and one rated at 3.5tph used for process steam generation. The steam is generated at between 10 and 12bar and used mainly on their M.G. Cylinder (tissue making machine) for paper drying, pulping, and preheating processes around the plant. Currently, one 4.5tph boiler is enough to run the whole plant as their second section which was the largest was decommissioned following the economic decline in Zimbabwe. The current maximum electrical power demand is 741kW.

Thermal Load Specifications

The table below outlines the process steam requirements at Kadoma Paper Mills:

Table 1: Kadoma Paper Mills Process Steam Requirements

Process	**Temperature [T - ˚ C]**	**Pressure** $\left[P - kPA\right]$	**Dependence**
Paper drying	110-150 (Off-take) 140 (Boiling)	540 500	**T, P**
Pulping	50	300	**P**

3.2.3 Tongaat Hulett Triangle Zimbabwe

Triangle Limited is an Agri-based industry that produces a variety of sugar products (raw, brown, and white sugar) from sugarcane. The diagram below shows the process flow at Tongaat Hulett:

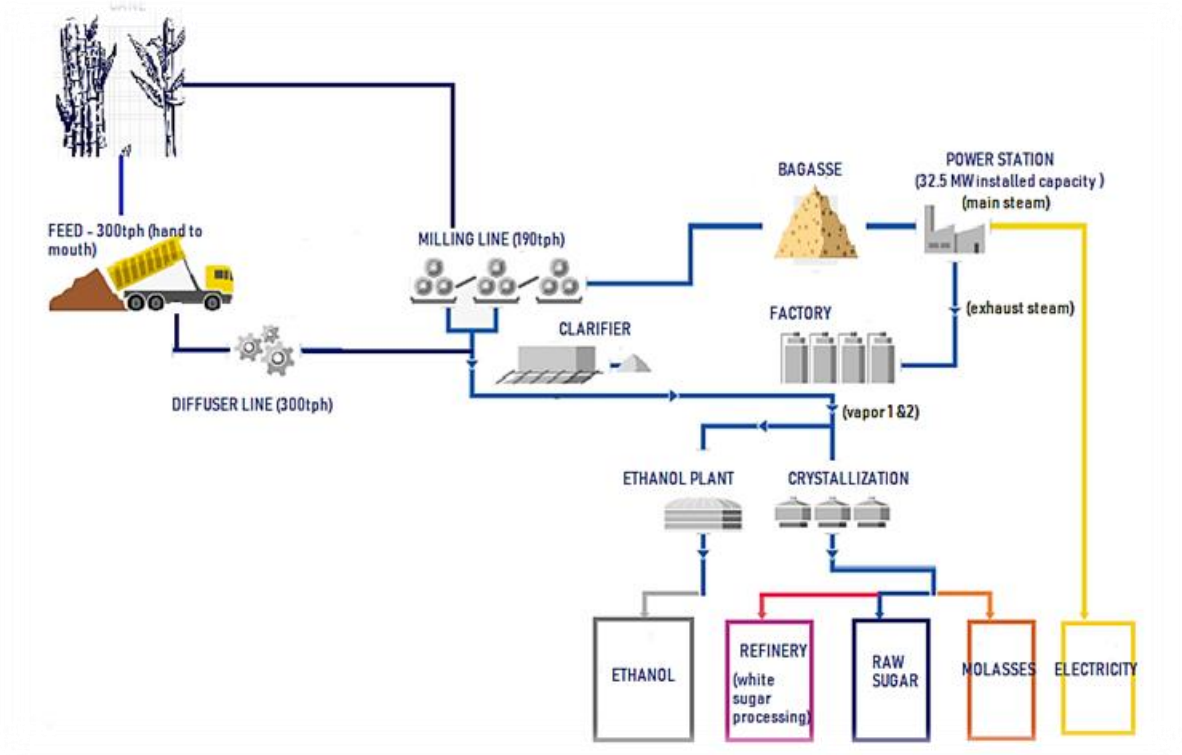

Figure 20: Tongaat Hulett Triangle Process Flow Diagram

The process inputs are cane, which is processed to produce cane juice and waste known as bagasse. All the plant electrical power needs are met with a steam turbine topping power plant, which uses the waste bagasse as the fuel source.

Existing Steam Plant Specifications

Tongaat Hulett began operations in 1931 when the first sugar plantation was planted. Processing was done much later in 1939 and old mills from their sister company in South Africa were used. In the late 1960s, as the business grew, it was decided to relocate to where the current mill house is and that is when the power plant was also set up to meet the demands of their large equipment (the shredder alone is rated at 1.8MW). Steam turbines and auxiliary equipment were bought from Hwange Power Station as they were upgrading their plant and the boilers from John Thompson. From the look of the current setup, the plant was designed for Cogeneration from the onset to provide for both the process plant steam needs and plant power demand.

Currently four boilers are in operation: Boiler 7 & 8 rated 45tph each, Boiler 9 rated 100tph and Boiler 10 rated 150tph. Steam is generated in the boilers at 3.2MPa and at 370˚C when using coal as fuel and 390˚C when using bagasse as fuel. The main fuel source is bagasse which is obtained from the cane extraction plant at 50% moisture. Coal is mainly used as a supplement during start-ups, breakdowns, and routine maintenance in the extraction plant. The maximum plant steam

demand is 250tph and varies as the cane fed varies. Main steam is sent to the steam turbines for power generation.

The total installed capacity is 32.5MW, with five back pressure and one condensing steam turbine (TA2). All turbines are impulse type axial flow steam turbines rated as follows: TA1 - 6MW, TA2 – 3MW, TA3 – 2MW, TA4 – 6MW, TA5 - 8MW and TA6 -7.5MW. The backpressure turbines exhausts at 130 ± 10 kPa and 120 ± 5˚C, and the exhaust steam is sent to the factory for heating and drying purposes. Below is a steam and condensate flow diagram detailing how the steam flows in the system:

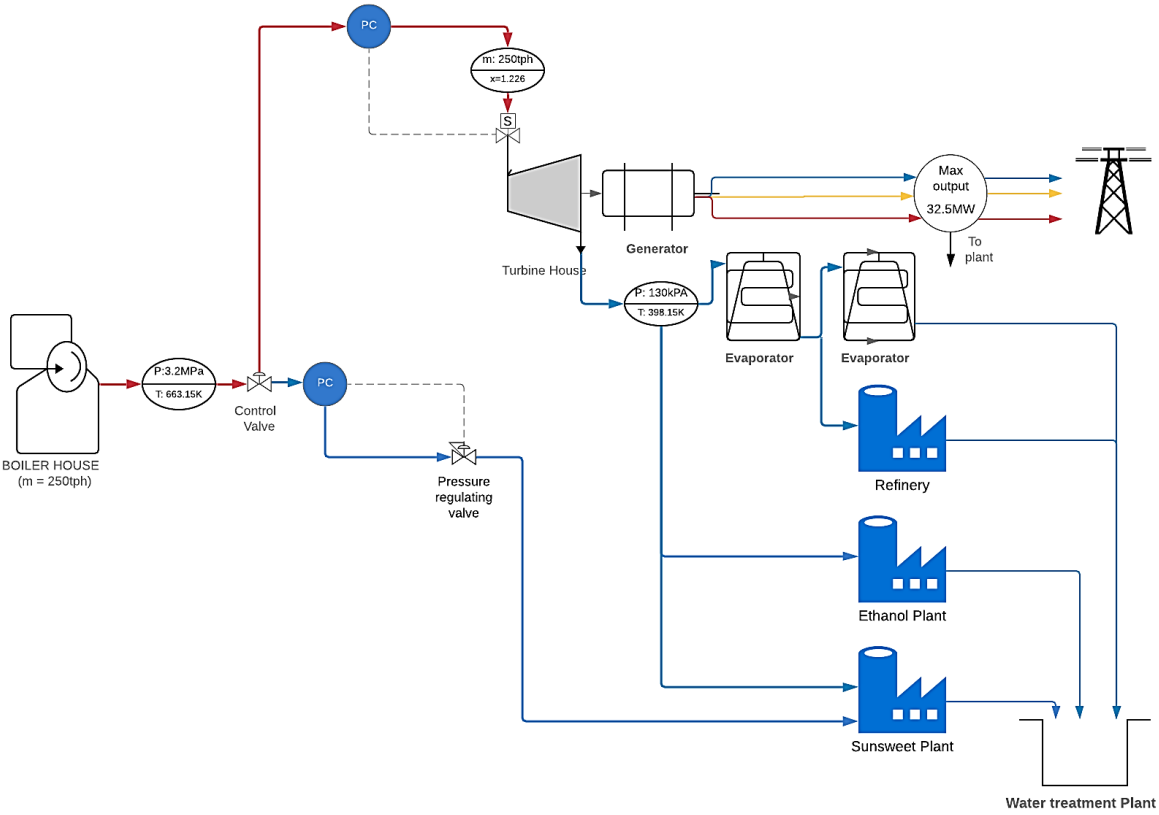

Figure 21: Tongaat Hulett Triangle Steam & Condensate Flow Diagram

The condensing turbine was left out of the flow diagram as only one turbine was made representative of the four back-pressure units. It is only used momemtarily when the steam flow is more than the process thermal load requirement. The ideal operating scenario is to ensure that the mass flow into the turbine matches the process plant steam requirement. Where the mass flow into the turbines exceeds the process plant requirement, some of the steam is condensed whilst decreasing the boiler firing rate to match thermal load requirement. This will be explained further in the System manipulation section.

System Manipulation

In-order to manage fluctuations in both the thermal load and plant power demand, the following is done:

If the thermal load increases beyond the capacity of the steam coming from the turbine exhaust, live steam is bled from the boilers and passed through pressure reduction drag valves where the pressure is reduced to 150kPa and sent to the process. When the thermal load falls below what the turbines are producing, the exhaust steam is condensed and at the same time the boiler firing rate is reduced to match turbine exhaust with the process steam requirements. Excess bagasse is stockpiled for use when the thermal load spikes up.

When the electrical load increases above the power generated when operating in island mode (off-grid), the system is synchronized with the 6.6kV busbar and set to import from Zimbabwe Electricity Supply Authority (ZESA). On the other hand, when the turbine-alternators produce more than the plant electrical demand when operating in island mode, the turbine-alternators are synchronized with the 6.6kV bus bars and export to the grid momentarily whilst the boiler feed rate is lowered to match generation with plant electricity demand. Tongaat Triangle, unlike Tongaat Hulett Hippo Valley Estates does not have a contract with ZESA to sell its excess to the Power Distribution Utility. In that case, any energy exported by Triangle Limited is free of charge thus the ideal operation scenario is to just produce electricity enough to meet their own needs.

3.2.4 African Distillers

African Distillers manufactures, distributes, and markets under license, branded wines, spirits, and ciders for both the local market and beyond. Situated in Mt Hampden, about 30km west of Harare's central business district, African Distillers (AFDIS) has six depots in Harare, Bulawayo, Kwekwe, Mutare, Victoria Falls, and Masvingo, supplemented by customer collection depots countrywide.

Existing Steam Plant Specifications

AFDIS has three coal fired fire-tube boilers: two 4.5 tph boilers and one 2.5 tph boiler, which are currently used for process steam generation. The steam is generated at between 600 and 850kPa and used in the blending and bottling departments for distillation, pasteurization, cleaning in place (CIP), bottle washing, and bottle warming. Plant maximum electrical power demand is 621.28kW.

Thermal Load Specifications

Table 2: African Distillers Process Steam Requirements

Process	**Temperature [T - ˚ C]**	**Pressure** $[P - kPA]$	**Dependence**
Distillation	*75-78 (Off-take)* *95-98 (Boiling)*	*350*	***T, P***
Pasteurization	*72.3-80*	*400*	***T, P***
Cleaning In Place (CIP)	*80*	*400*	***T, P***
Bottle Washing	*90*	-	***T***
Bottle Warmer	*28-30*	-	***T***

The location for conducting the research was largely selected based on the available infrastructure for setting up a combined heat and power plant, ease of access to plant data and scale of production from the three sites visited by the researcher namely Kadoma Paper Mills, African Distillers and Tongaat Hulett Triangle Limited. Tongaat Hulett was ruled out as it already has Cogeneration in place and based on the criteria, the best site for the project was identified as African Distillers (AFDIS) Private Limited.

3.3 Model development

The next step after site selection was coming up with a feasible process layout for the new system, considering different arrangements and design considerations. The design concepts are briefly described in the subsequent section.

3.3.1 Design concepts

Concept 1: Solar thermal feedwater heating and boiler modification for superheating

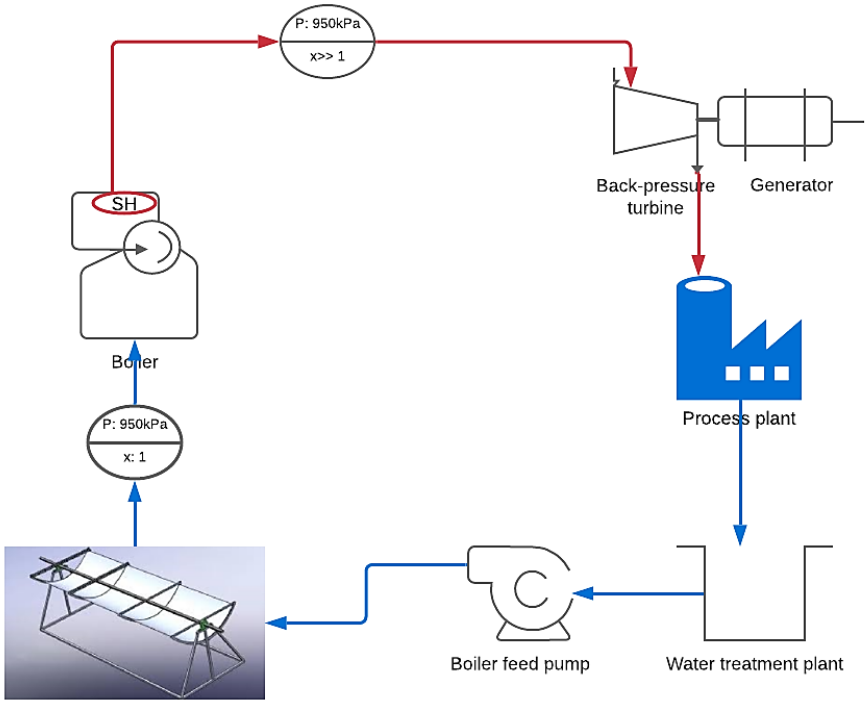

Figure 22: Solar thermal feedwater heating and boiler modification for superheating

In this scenario, the solar resource would be used to preheat the feedwater and then a superheater section would be retrofitted in the smoke box of the boiler (current way of retrofitting fire-tube boilers to enable superheating at John Thompson boilers). The major advantage of such a set-up is a smaller solar field required to preheat the feedwater compared to superheating and there is direct solar thermal integration, which means lower CAPEX and OPEX requirement.

The downside however is that for the boiler to be retrofitted to enable superheating, it must be taken out of service and be shipped back to John Thompson for modification, a process which takes months to complete with the whole plant offline. This defies the limiting condition of augmenting the plant without affecting the original process plant requirements. Also because the solar resource is intermittent, the feedwater can only be heated when there is beam radiation available, decreasing the system's capacity utilization.

Concept 2: Direct solar thermal integration with super-heating

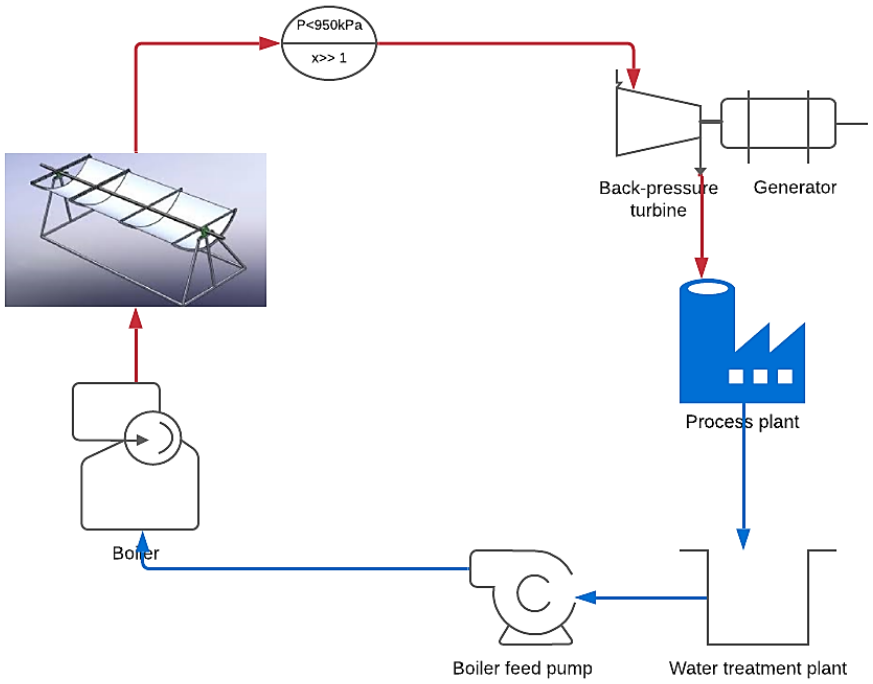

Figure 23: Direct solar integration for superheating

Direct integration of the solar thermal system with the existing process plant involves feeding the boiler exit saturated steam into the solar thermal field as shown in Figure 23 above. In this system, less solar field system components are required as direct superheating of steam can be done, which also lowers the CAPEX and OPEX requirement. The major disadvantage however is that due to the daily variation of the solar resource there are instances when the system, instead of adding heat to the dry saturated steam from the boiler, will be extracting heat from it, lowering system efficiency. In addition to that this might imply frequent turbine trips, when the steam quality at turbine inlet does not meet the turbine boundary conditions, and poor process temperature control.

Concept 3: Indirect solar thermal integration with super-heating

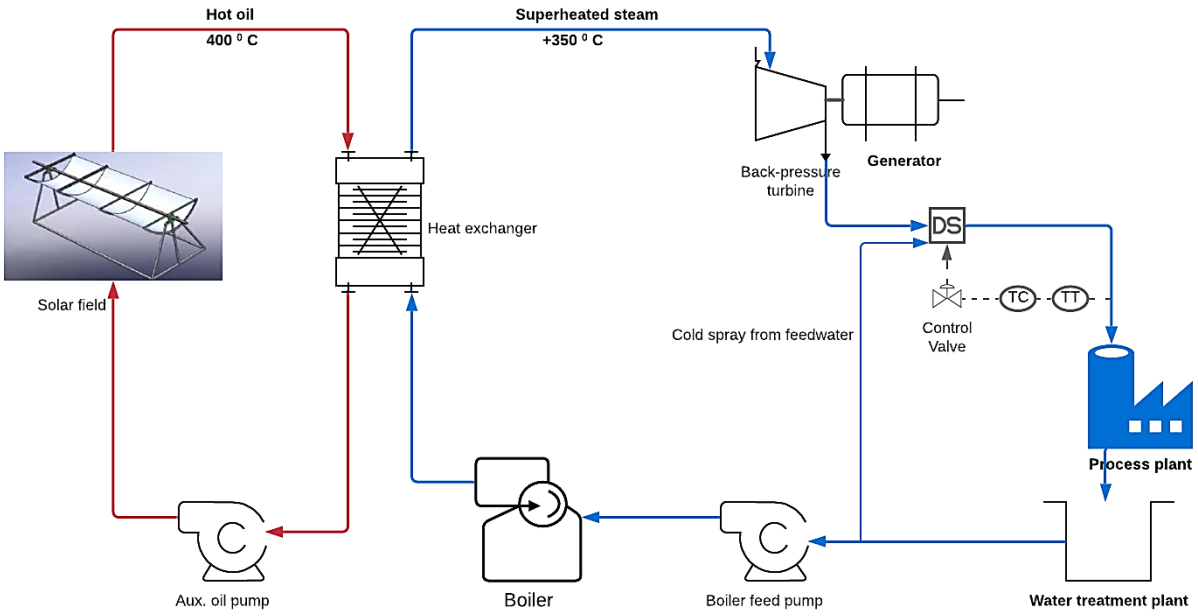

Figure 24: Indirect solar thermal integration with superheat

For better temperature and pressure control, which is of critical importance at the turbine inlet, indirect integration becomes a better option as a separate heat exchanger is used to heat the steam using the solar thermal energy. The downside however for this set-up is increased capital and operating costs as there are more system components. In addition to that, exhausting at the process pressure implies superheated steam is exhausted at the turbine exhaust stage because of the low operating pressure of the turbine. This calls for the use of a de-superheating mechanism like the direct spray type shown above. The desuperheater introduces cold feedwater to the exhaust steam and it cools it down to dry saturated state before it is piped to the process.

Concept 4: Indirect solar thermal integration with super-heating and feedwater heating

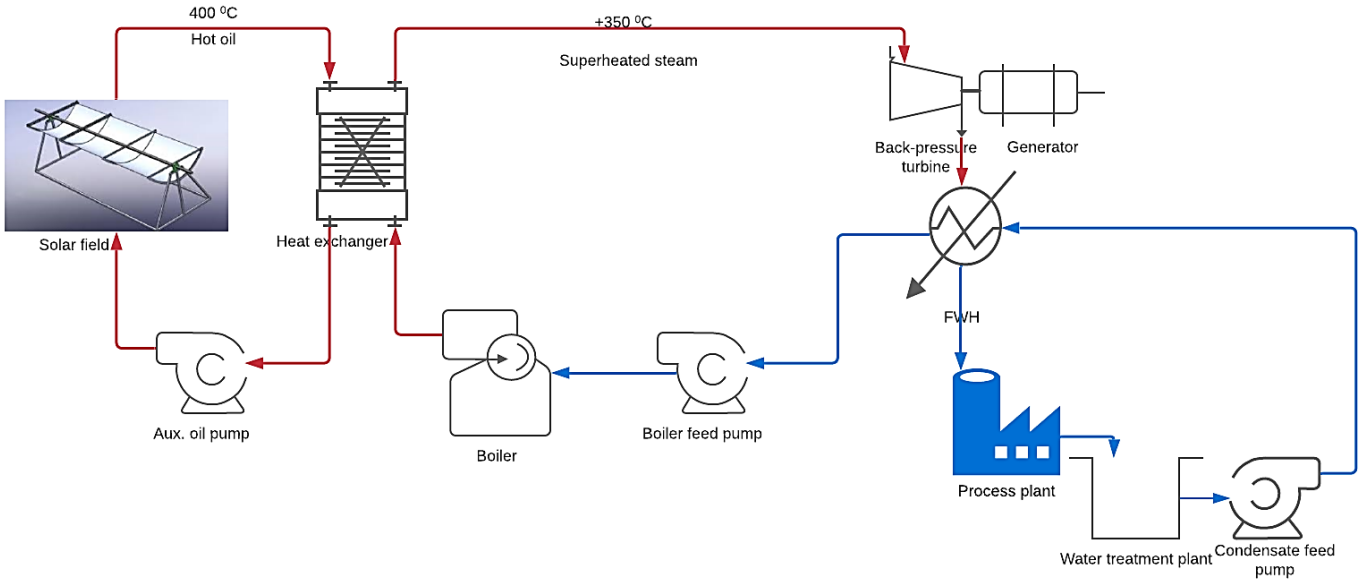

Figure 25: Indirect solar thermal integration with superheat and feedwater heating

This concept is a thermal efficiency improvement of Concept 3. Because of the moderately low steam inlet conditions to the turbine, the steam at the exit at 400kPa will still be superheated, whilst the process requires dry saturated steam. Instead of using a spray desuperheater, an efficient way of de-superheating the turbine exhaust is introducing a second heat exchanger for feedwater heating before piping the exhaust to the process.

This concept will improve the boiler fuel efficiency at the expense of additional capital investment. Since the same amount of coal is used in both Figure 24 and Figure 25, there is actually a fuel cost saving. This concept will however not be considered in the system design but offered as a system improvement in the recommendations section.

From the above considerations, Concept 3 was selected as the best possible concept which can meet the system requirements, whilst adhering to the limiting conditions.

3.3.2 Solar radiation resource

AFDIS is located at latitude $17.7135°S$ and longitude $30.895°E$. Solar radiation and temperature values for a typical year was obtained from the European Commission Photovoltaic Geographic Information System's website [43] and plotted using the System Advisor Model from the U.S. National Renewable Energy Laboratory [44].

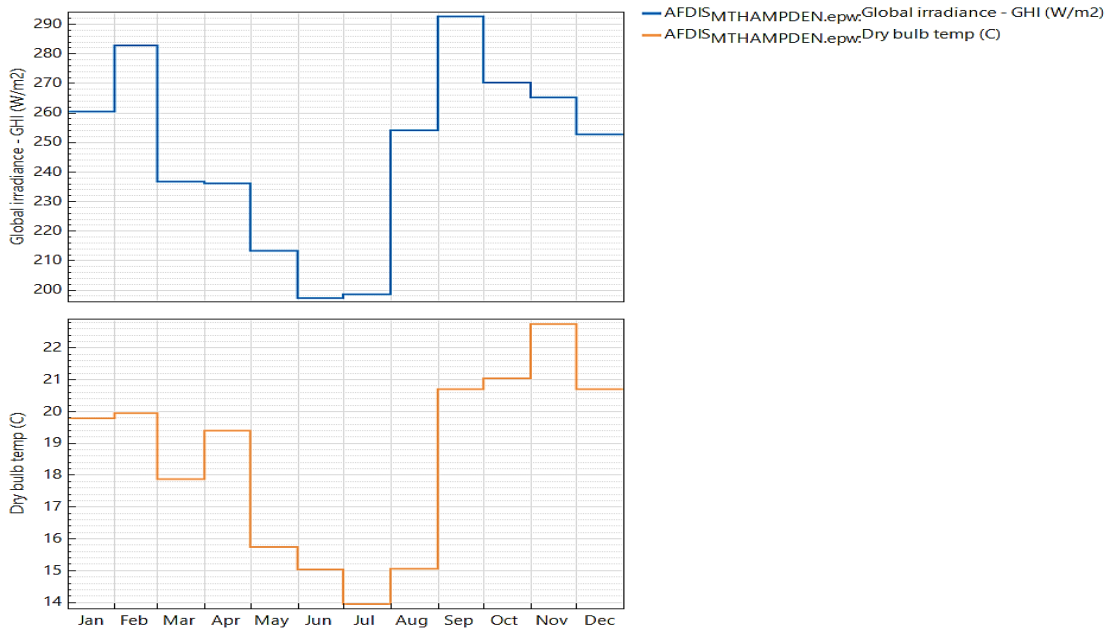

Figure 26: AFDIS GHI and dry bulb temperature annual variations from SAM NREL

The global horizontal irradiance (GHI) is the total solar radiation incident on a surface. It is the sum of the direct and diffuse component of radiation incident on a surface and is a measure of the total available solar thermal energy which can be harnessed. In CSP projects, the important component is the beam radiation (direct normal irradiance). The design point DNI for the site is $920\,{}^{W}/_{m^2}$. Temperature data is the dry bulb temperature and is very important to consider when selecting the solar heat transfer fluid which is best suited for the site's weather conditions.

3.3.3 System Design Inputs

System boundary conditions are the boiler outlet steam properties (which will be the cold fluid inlet conditions in the heat exchanger) and the process thermal load requirements (which will be the turbine exhaust conditions). Additional data is the plant power demand which will dictate the size of superheater. The heat input need not exceed the power requirement. However, it is possible that due to other limitations, it may not be possible to achieve the total required heat input. The actual heat exchanger thermal load will be an input to the external solar field sizing, as the field need only be as big as the heat that can be transferred in the heat exchanger. The table below summarizes the key system design inputs:

Table 3: System Boundary Conditions

Parameter	Value
Steam mass flow	2.5 kg/s
Boiler outlet	950 kPa, x=1.0
Turbine exit	400 kPa
Electrical load	622 kW
Process input	100 °C, 350 kPa

3.3.4 Heat Transfer Fluid Selection for the Solar Field

The key decision factors in selecting the suitable heat transfer fluid for the solar field are briefly discussed below.

- *Heat capacity:* Temperature change is inversely proportional to the heat capacity. Fluids with a higher heat capacity need a lot of heat to be added before a significant temperature change is noted and vice versa. An ideal heat transfer fluid should have a high heat capacity to be able to store as much heat energy as possible.
- *Thermal stability:* Certain oil based HTFs can significantly degenerate at elevated temperatures thus the operating temperature range should be below the temperature the HTF degenerates.
- *Solidification temperature:* The ideal heat transfer fluid should have a freezing point lower than the site's minimum temperature to avoid in service solidification which leads to blocked piping.
- *Evaporation temperature*: This is the thermal stability limitation. The HTF should have a high evaporation temperature at low pressure to avoid flashing in service.
- *Thermal conductivity:* High thermal conductivity to ensure the receiver temperature is as close as possible to the heat transfer fluid temperature.
- *Viscosity:* The higher the HTF viscosity, the greater the pumping power required to pump the fluid in the system. Ideal HTF should have low viscosity to minimize plant auxiliary power requirement.
- *Density:* The HTF should have a high density to enable its use as a storage medium.
- *Toxicity and environmental hazards:* Easy to dispose and non-toxic heat transfer fluids are preferred to avoid damaging the environment and posing health risks to plant personnel.

- *Corrosivity:* A corrosive fluid leads to higher operational costs due to frequent heat exchanger piping replacement. An ideal fluid should be non-corrosive.
- *Explosivity:* For safety of both plant and personnel, the ideal HTF should be non-explosive.

The table below shows the key thermophysical properties used in the selection of the heat transfer fluid:

Table 4: Heat Transfer Fluid selection decision table [31], [45]

HEAT TRANSFER FLUID	**Specific heat capacity** $\left(\frac{kJ}{kgK}\right)$	**Max temp** $\left(^0C\right)$	**Min temp** $\left(^0C\right)$	**Kinematic viscosity @ 100˚ C** $\left(\frac{mm^2}{s}\right)$	**Market popularity**
Therminol VP-1	2.889	400	12	0.99	Popularly used
Dowtherm^{TM} A	2.4093	400	15	0.91	Popularly used
Hitec Salt	1.56	538	149	-	Still in the developmental phases

- The heat capacity of a fluid is its ability to absorb heat relative to its change in temperature.
- Maximum operating temperature is the maximum attainable temperature of the HTF and the higher the maximum temperature, the more favourable the HTF for use in the heat exchanger.
- Minimum temperature is the limit the HTF can operate without change in state or physical properties. The lower the minimum temperature, the lower the freeze point and the more favourable the HTF for low ambient temperature conditions
- Viscosity is the measure a fluid's resistance to flow, the more viscous the fluid, the difficult it is to flow. An ideal HTF should have less resistance to flow to avoid clogging and fouling of the heat exchanger.
- The more popular a HTF is on the market, the ease of availability of both the HTF and all the necessary in-service data.

Therminol VP-1 was selected as the final heat transfer fluid because of its higher heat capacity and popularity in the market as a HTF. Although the molten salt has more favourable properties, its use in the solar thermal systems is still in the development phase.

3.3.5 Heat exchanger approximate design

The detail calculations for the approximate design can be found in Appendix A. The flowchart below outlines the process and is followed by a brief explanation of the steps.

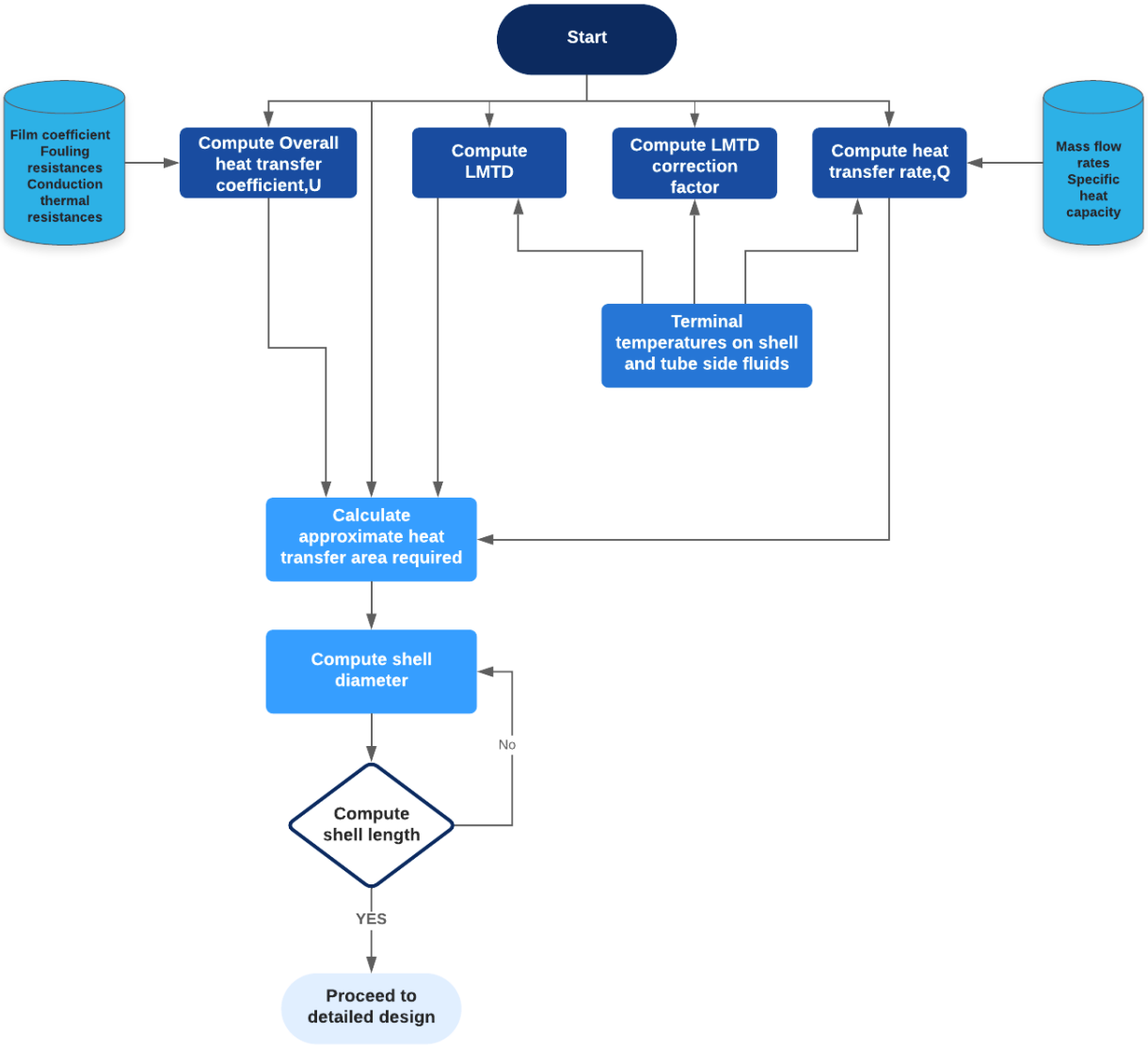

Figure 27: Heat exchanger approximate design flow chart [23]

Step 1: Fluid flow allocation and fluid boundary condition properties calculation

For the heat exchanger design, the heat transfer fluid, being the higher fouling fluid was placed in the tube-side and the steam in the shell. Using the Therminol Fluid properties calculator [31], the heat transfer fluid inlet conditions were calculated, assuming the solar field heats the fluid to its maximum attainable temperature of 400˚C. Steam inlet properties were calculated using formulae

developed by The International Association for the Properties of Water and Steam [46] which were programmed in MathCAD. The hot fluid (Therminol-VP1 oil) and cold fluid (saturated steam) velocity were assumed to be 1m/s and 20m/s respectively to simplify the design. It was assumed that the oil mass flow is 8 times more than the steam mass flow. This was chosen to arrive at a moderately sized heater. A smaller number results in fewer tubes in parallel for the chosen oil velocity, and a very long shell.

Step 2: Calculation of the heater UA value

The heat exchanger terminal temperature difference was assumed to be TTD = 5°C, which allows one to calculate the steam outlet temperature:

$$T_{steam.out} = T_{oil.inlet} - TTD$$

Using the calculated steam outlet temperature and equation (2.9) the heat gained by the steam was calculated and subsequently used to calculate the oil outlet temperature.

After calculating all the temperature values, the LMTD of the heat exchanger was calculated using equation (2.2). Since the heater can be approximated as pure counterflow, no LMTD correction factor was needed. From equation (2.1) desired heater UA was calculated using the calculated values of the LMTD and heat exchanger heat load.

Step 3: Tube-side heat transfer coefficient calculation

Stainless Steel tubes with inside diameter $^{3}/_{4}$ " , schedule 40 and a square pitch of 1.25 were initially selected as HX tubes. Using the Sieder-Tate equation (2.21), as the most appropriate heat transfer model for an inorganic liquid in a horizontal pipe, the oil heat transfer coefficient, h_{oil} was calculated to be about 1345W/m^{2}K. For simplification, the effect of the tube wall was ignored, as well as the change in viscosity due to temperature between the bulk fluid and wall.

Step 4: Shell-side ideal heat transfer coefficient calculation

Using the Kern Method for sensible heat transfer in turbulent flow and equation (2.19), the shell side heat transfer coefficient was calculated to be 440 W/m^{2}K. Once again, the change in viscosity between the bulk and wall was ignored, as well as changes in fluid properties as the steam is superheated.

Step 5: Calculation of overall heat transfer coefficient and required heat transfer area

Using the afore-calculated tube side and shell-side heat transfer coefficients and assuming no fouling resistance or tube wall resistance, the overall heat transfer coefficient,

$$U = \left(\frac{1}{h_{steam}} + \frac{1}{h_{oil}} \right)^{-1} = 331.7 \, W/m^2 \cdot K$$

The required heat transfer area was calculated to be about 70 m^2.

Step 6: Approximate size

Given the chosen oil mass flow and tube diameter, about 100 tubes in parallel are required, and to achieve the total heat transfer area, the heater must be 11m (37ft) long. Using the equation (2.24) the tube bundle diameter is 270mm, hence a shell size of 12in or more should be sufficient.

3.3.6 Shell diameter deciding factors

Following the approximate design, an initial standard shell diameter of 13.25in was selected and the following limiting conditions checked in the detailed design to see if the given shell diameter and length met the requirements below:

i. Shell side pressure drop – because the heated fluid is in the shell, the pressure drop of importance in this design is the shell side pressure drop. The higher the shell side pressure drop, the lower the thermal state of the superheated steam at turbine inlet hence the pressure drop in this design was set to be at most 5% of the boiler exit pressure.
ii. Oil flow velocity – According to Eastman Inc, the velocity limits for Therminol VP-1 are 0.36m/s - 4.97m/s to avoid tube fouling and erosion respectively.
iii. Tubesheet thickness -According to TEMA, the calculated tubesheet thickness should be at least 75% of the tube outer diameter to avoid warping and bending failure in service.

Initial tube diameter of 19.05mm, shell inner diameter of 13.25in and effective length of 37ft were used and manually scaled up until the shell side pressure drop, oil flow velocity and tube sheet thickness were within limits.

3.3.7 Detailed heat exchanger design

As outlined in Figure 16, the heat exchanger detailed design was performed using the Taborek version of the Bell- Delaware method. The TEMA E shell, with one tube pass and multi-segmented

baffles was selected as it gives an almost pure counter-flow arrangement, which has the highest effectiveness. The detail design is shown in Appendix B of this report. In this section a summary of the important steps and results will be described in the way the design process progressed.

Step 1: System inputs and assignment of variable inputs

The system inputs, like the approximate design inputs, were defined. The only exception was the assignment of variable inputs which could influence the heat exchanger size (the shell inside diameter, tube length and an oil scale factor).

The steam and oil inlet conditions, as well as steam mass flow defines the system boundary conditions. Only three other parameters are set as variable inputs to the model, namely:

- Shell diameter
- Tube length
- Oil mass flow scale factor

The diameters of both the shell and the tubes were based on the initial sizing and varied between the values[4] shown in Table 5 below:

[4] The shell diameters are the lower and upper limits respectively, the shell diameter was increased gradually from 13.25" to 39" (using standard shell diameters), taking note of the changes in shell side pressure drop, oil flow velocity and tubesheet thickness.

Table 5: Variation of shell diameter and tube dimensions with critical design parameters.

	UoM	**Value**				**Limiting value**
Shell diameter	*in*	**13.25**	**13.25**	**39**	**39**	
Tube nominal size	*in*	$^3/_8$	$^3/_4$	$^3/_8$	$^3/_4$	
Number of baffles	*ea*	55	55	19	19	
Effectiveness	*%*	52.6	85.3	88.4	99.6	
Shell side pressure drop	*kPa*	13.5	85.6	0.3	3.7	As low as possible for higher thermal state at turbine inlet
Steam outlet temperature	*˚C*	294	366.5	373.3	398.0	
Oil velocity	*m/s*	3.5	1.4	0.4	0.1	Value should be between 0.36 and 4.97m/s
Tubesheet thickness	*mm*	8.4	8.4	18.8	18.8	Min should be greater than 0.75D
Hx cost	*ZAR (millions)*	1.3	1.3	1.2	1.2	
Heat transfer area	*sqm*	32.5	47.4	317.8	483.9	

For the 13.25” shell, the shell side pressure drop was excessively high for the $^3/_4$” pipe (nominal pipe size -NPS), with a tube sheet thickness way below the minimum required value. To decrease the pressure drop, the tubes were reduced to a NPS of $^3/_8$”, which came with a decrease in effectiveness and steam outlet temperature.

The shell diameter was manually varied from the 13.25” shell, using standard shell diameter increments until it was fixed to 39”, while the tube length was varied as part of the cost optimization. Since the diameter was fixed, the number of tubes in parallel is also somewhat fixed, which means the oil mass flow rate must be chosen such that the velocity is within the prescribed range as identified in section 2.4.6. The result is that the oil mass flow scale factor was kept constant at 8.

Step 2: Shell and tube geometry selection

Tube size was selected as stainless steel (material recommended by HTF manufacturer) with a nominal pipe size (NPS)[5] of $3/8"$, schedule 40 and square pitch of 1.25". TEMA standards were used to select the tube hole diameters and standard tolerances.

25% segmental cut baffles were chosen, and with the fixed diameter, the actual baffle cut height, baffle spacing, outer tube limit diameter and centre-line tube limit diameter were calculated.

Step 3: Tube sheet layout

Critical in HX design is ensuring that the calculated number of tubes fit inside the given shell diameter. The number of tubes in the shell was calculated using equation (2.26) and the tube count was then checked against the allowable count for that specific shell inside diameter [29, p. 841].

Step 4: Calculation of the shell leakage areas and correction factors for shell leakages

Equations from the Wolverine Tube, Inc Engineering Data Book III [32] were used to calculate the baffle cut, baffle leakage, bundle by-pass and bundle spacing correction factors.

Step 5: Calculation of shell side heat transfer coefficient

An initial guess of the steam bulk fluid temperature and wall temperature was made. The ideal shell side heat transfer coefficient was then calculated using equation (2.19), using the mean steam temperature to calculate fluid properties and the actual heat transfer coefficient was calculated by applying the adjustments as described in section 2.4.7.

Step 6: Calculation of tube side heat transfer coefficient

The oil flow rate was calculated by scaling the steam mass flow with the chosen scale factor. Using the calculated oil flow rate, tube dimensions and oil viscosity, the Reynolds number was calculated, including the effect of the tube count:

[5] NB: Nominal Pipe size is not the actual pipe diameter, actual pipe dimensions were obtained from the ANSI 836.10 standard except in Table D-1 of the TEMA standard [21]

$$\mathrm{Re}_{oil} = \frac{4 \cdot \dot{m}_{oil} \cdot \frac{n_p}{n_t}}{\pi \cdot (D_o - 2 \cdot t_{tube}) \cdot \mu_{oil}}$$

The oil velocity was checked to confirm that it is within the suggested limits for the oil. The heat transfer coefficient was then calculated using equation (2.21).

Step 7: Determination of overall heat transfer coefficient and HX outlet temperatures

The overall heat transfer coefficient was calculated, factoring in the corrected shell side heat transfer coefficient and conduction wall resistance in the tube pipes. Using the calculated U value and heat transfer area from tube count and geometry, the heater number transfer units were calculated. The effectiveness was calculated using equation (2.17).

The pure counterflow heat exchanger assumption was employed as the calculated number of baffles was greater than 10 for all the different scenarios under investigation. From the effectiveness, the steam outlet temperature was calculated and checked to agree with the guessed mean bulk shell fluid temperature. Using the energy balance equation, the oil outlet temperature was also calculated, together with true temperature difference and the heat load of the heat exchanger. The heat load will be used to calculate the size of the solar field, which is crucial in the costing and performance evaluation section of the project. Lastly, the wall temperature was calculated and compared to the initial guess.

Step 8: Determination of shell and tube side pressure drops

Tube-side pressure drops affect the pumping power required to pump the HTF. The tube-side pressure drop was set to be at most 5% of the total turbine generated power. As outlined before in section 2.4.7 above2.52.5 above, the detailed shell-side additional pressure drop calculations due to the shell geometry are detailed in Appendix B of this report. The ideal shell diameter and tube-geometry combination was the one with the lowest shell side pressure drop, in order to ensure the highest possible thermal state at turbine inlet.

Step 9: Material cost

A tube sheet design was performed using the guidelines set out in Appendix A of the TEMA standard, and the end heads were designed according to [47, pp. 815-823], using thick cylinder theory. Total material cost was calculated as set out in Section 2.6 above. Material costs were obtained from Euro

Steel and AVENG Trident steel [48] and the calculated heat exchanger cost was used as input in the cost analysis.

3.3.8 Solar field sizing

Sizing of the solar field required to heat the heat transfer fluid to 400˚C and meet the thermal load requirements was done using the SAM NREL industrial process trough (IPH) model [49]. Outlined below are the steps taken in the solar field sizing:

Step 1: Input of location and solar resource data.

The site data inputs as mentioned in section 3.3.2 were entered into the system. The site weather and radiation data for use in the sizing process were downloaded as a typical meteorological year data file from the European Commission Photovoltaic Geographical Information System [43]. The weather file has DNI, ambient temperature, wind speed, and other hourly data that SAM uses during simulation to calculate hourly energy output based on the solar resource and meteorological conditions [50].

Step 2: System design.

System design inputs include solar field data, heat sink requirements and system availability and curtailment (a default SAM NREL IPH model constant loss factor of 4% was used). The heat sink power was obtained from the heat exchanger model, and the SAM default values are based on tried and tested projects undertaken by the NREL in their many solar systems research projects and are typical values for IPH projects.

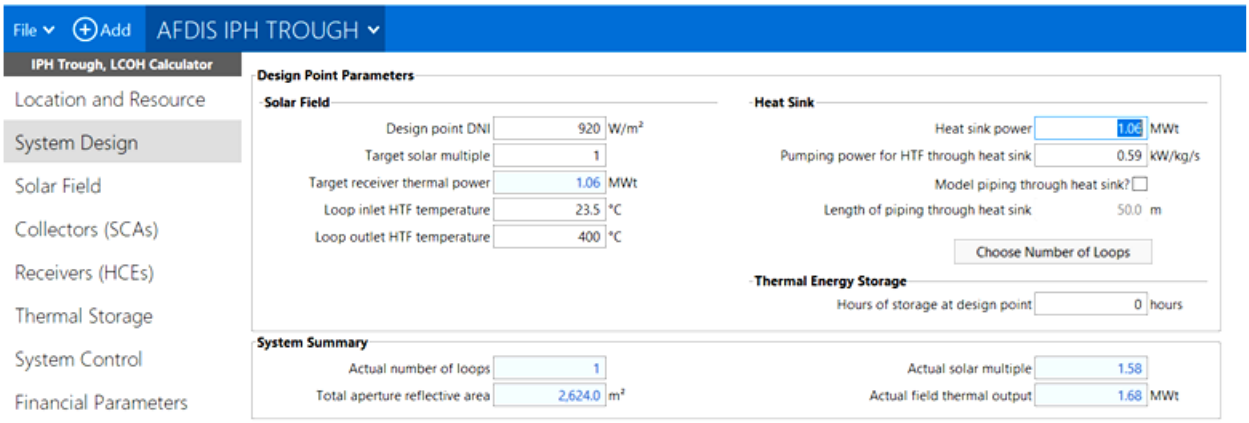

Figure 28: Solar field system design inputs

Step 3: Selection of the solar collector and receiver.

After design specifications, the next critical step was selection of the collector and the receiver. The selected solar collectors were SkyFuel trough collectors as they are the most developed to date in the parabolic trough systems, with efficiencies as high as 75% and the Schott PTR 80 receiver because it is the largest on the market [7].

Step 4: Specification on the HTF and thermal storage requirements.

Since no thermal storage is required, only specifications for the heat transfer fluid, freeze protection temperatures and flow rates were needed. The selected HTF was Therminol VP-1, using the HTF specified operational limits as previously discussed.

Step 5: Results and running a parametric simulation for different heat loads.

For each different length of heat exchanger, a different heat load is calculated. A parametric simulation was done for the different heat exchanger sizes by changing the Heat sink power input in the model. This produced the required solar field size, capital costs, annual operational and fixed maintenance costs and the annual thermal energy output.

3.3.9 Turbine Calculations

Based on the heat exchanger outlet steam temperature and required process plant thermal load boundary conditions, the turbine work was calculated as follows:

Step 1: Determination of required turbine power to meet plant demand.

The SST-060 comes with a name-plate efficiency of 86% for the turbo-alternator and 95% for the generator. Using those efficiency values, the turbine efficiency was calculated as 90.5%. Given that the plant maximum demand is 621.68kW, the required generator input power was calculated as:

$$P_{gen.in} = \frac{P_{\max.demand}}{\eta_{generator}}$$

Using the turbine efficiency, the required turbine power was calculated as:

$$P_{turb.required} = \frac{P_{gen.in}}{\eta_{turbine}}$$

This is the required input power to the turbine if it were to fully meet the plant power demand.

Step 2: Calculation of turbine boundary conditions.

The turbine exhaust conditions are governed by the process steam plant requirements of 400kPa and 100˚C and the heat exchanger steam outlet feeds into the turbine. Assuming a 5% pressure drop in all the steam lines and governing valve, the turbine exhaust pressure was scaled up by 5% to cater for steam line losses.

The turbine inlet pressure was calculated as the boiler pressure, minus the shell side pressure drop and the 5% line and valve losses. The inlet enthalpy to the turbine is the heat exchanger steam exit enthalpy.

Step 3: Calculation of actual turbine power.

The actual turbine exit enthalpy is calculated from the turbine efficiency equation, (2.30), and the inlet and exit boundary conditions used to calculate the inlet enthalpy, ideal lossless turbine exit enthalpy and turbine efficiency. From the actual exit enthalpy, the actual turbine power, steam exit temperature and quality were calculated.

Step 4: Auxiliary power requirements and import power calculation.

Knowing the actual turbine power output, and the oil pump power requirement from the Heat Exchanger Design analytical calculation, the auxiliary power requirement was checked to see if it was in the 5% range of total power output (if too large, some changes to the shell diameter and oil mass flow would be needed). The Sent-Out Power was then calculated as the difference between the actual turbine output power and auxiliary oil pump power requirement, and power was compared with the plant demand to calculate the imports required if any. The detailed turbine calculation is attached in Appendix C of this report.

3.3.10 Project costing and optimization

The project capital costs were calculated as set out in section 2.8 and the heat exchanger length varied to calculate the optimum heat exchanger size for this application. The heat exchanger length determines the heat transfer area and by increasing or decreasing it, the actual work/heat load of the heat exchanger is altered. This affects the thermal uptake of the system and subsequently the solar field size requirement, which in turn increases or reduces the CAPEX of the project.

It is therefore desirable to find that point where the size of the heat exchanger serves its purpose in a cost-effective manner. Above that point, the extra cost does not give any substantial energy saving benefit and below that point, the system does not offer the real value for money. Base assumptions in the inputs were used for the interest rate, electricity tariff and then varied in the sensitivity analysis to evaluate profitability of the project. The figure below shows the current feed-in tariff (REFIT) in South Africa for various renewable technology options. Currently the REFIT system in Zimbabwe only has rates for solar photovoltaic technologies and none on solar thermal technologies, so the default to not pay for the electricity produced (i.e., as-if being paid the same rate as the import rate of R1.50/kWhr – assumed average South African industrial tariff).

Table 6: NERSA Phase renewable energy feed-in tariff (REFIT) table adapted from Energypedia

	Technology	**Tariff (Rand/kWh)**	**Tariff (€/kWh)**
Phase I	Landfill gas power plant	0.90	0.09
	Small hydro power plant (less than 10MW)	0.94	0.10
	Wind power plant	1.25	0.13
	Concentrating solar power (CSP) with storage	2.10	0.21
Phase II	Concentrating solar power (CSP) without storage	3.14	0.32
	Biomass solid	1.18	0.12
	Biogas	0.96	0.10
	Photovoltaic systems (Large ground or roof mounted)	3.94	0.40
	Concentrating solar power (CSP) central tower with storage capacity of 6 hours	2.31	0.23

The results and findings of the design process will be outlined in detail in the next chapter.

4. Results and Discussion

4.1 System Model

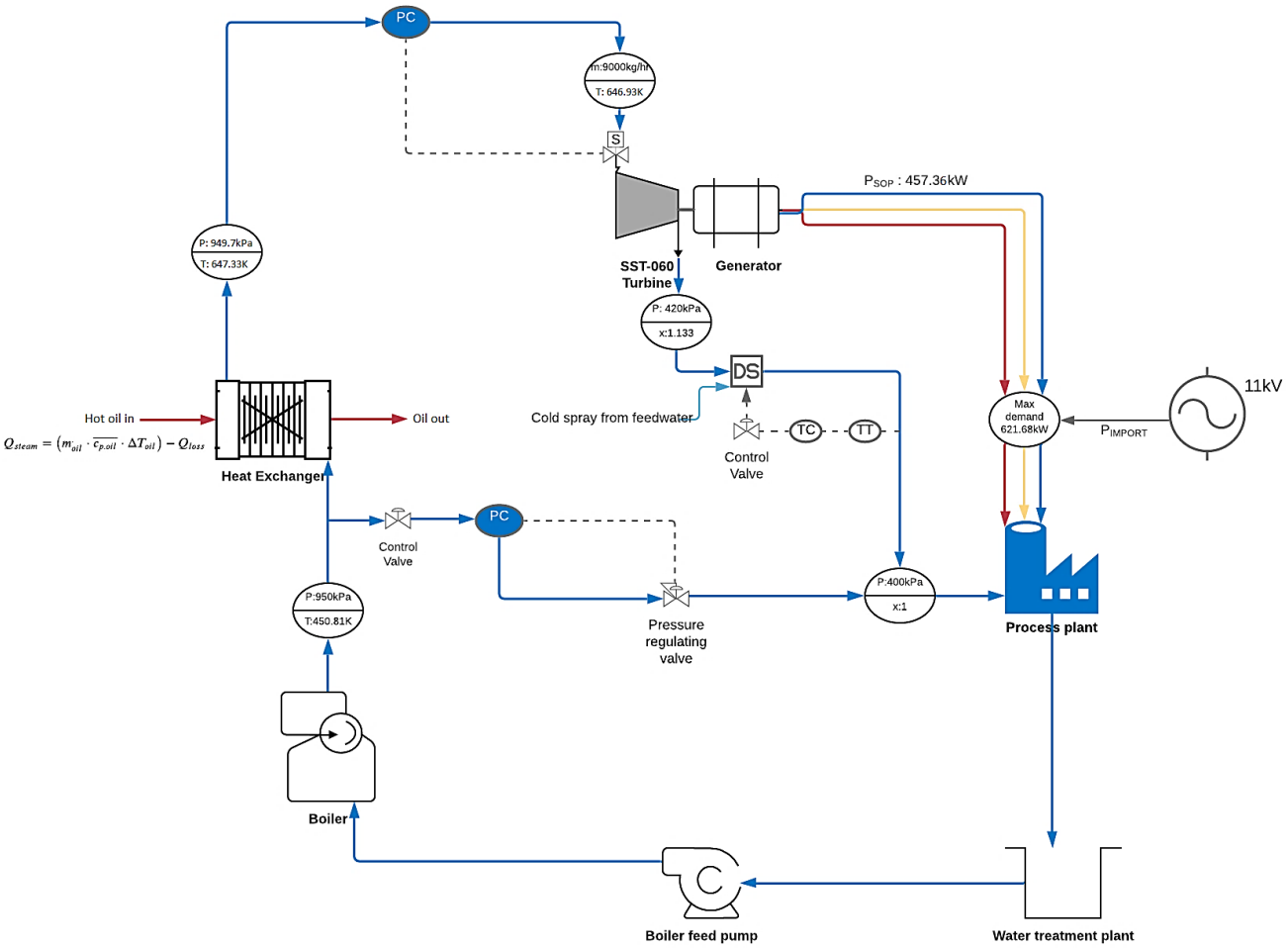

Figure 29: Proposed steam plant process flow diagram

The above P&ID diagram was developed to show the new steam and condensate flow if the steam turbine topping cycle is retrofitted into the existing process steam plant. Steam leaves the boiler, dry saturated at 950kPa, and is piped to the heat exchanger shell side, where it is superheated by hot oil from the solar field, which flows in the tube side of the heat exchanger. The superheated steam is expanded in the turbine, which exhausts at a pressure which is sufficient to ensure the process steam thermal requirements are met. The generator is synchronized with the plant's main bus bar and feeds the generated electricity to the plant. There is a T-junction after the boiler, which allows for by-passing the power block and feeding straight to the process steam plant in the case of emergencies or low solar insolation when the power cycle is offline.

The following sections discuss the general system parameters and results from the analysis models in Appendix B and C.

4.2 Physical system parameters

Heat exchanger: Type BEM, Size 39 – 360 (991 – 9144) (base assumptions case)

Coal fired boiler output (steam inlet to the heat-exchanger)

- Mass flow: 2.5kg/s,
- Pressure: 950kPa,
- Temperature: 177.67 ˚C,
- Quality: dry saturated.

HTF to inlet conditions (hot fluid inlet into heat exchanger)

- HTF: Therminol VP-1,
- Mass flow: 20kg/s,
- Temperature: 400 ˚C.

Heat exchanger model outputs

- Shell diameter: 39” (990.6mm),
- Tubes length: 15 – 60ft. Based on the initial sizing, the first length chosen was 30 ft, and this will be referred to as the Base case,
- Total heat transfer area: 158 – 637m^2,
- Steam heat addition: 0.8 – 1.17MW,
- Heat exchanger effectiveness: 66.8 – 98.5%,
- Steam outlet temperature: 325.7 – 395.8 ˚C,
- Heat exchanger cost: mR0.64 – mR2.4[6].

Figure 30 below shows the steam heat addition requirement, versus the tube length.

[6] mR0.64 means 0.64 million rands

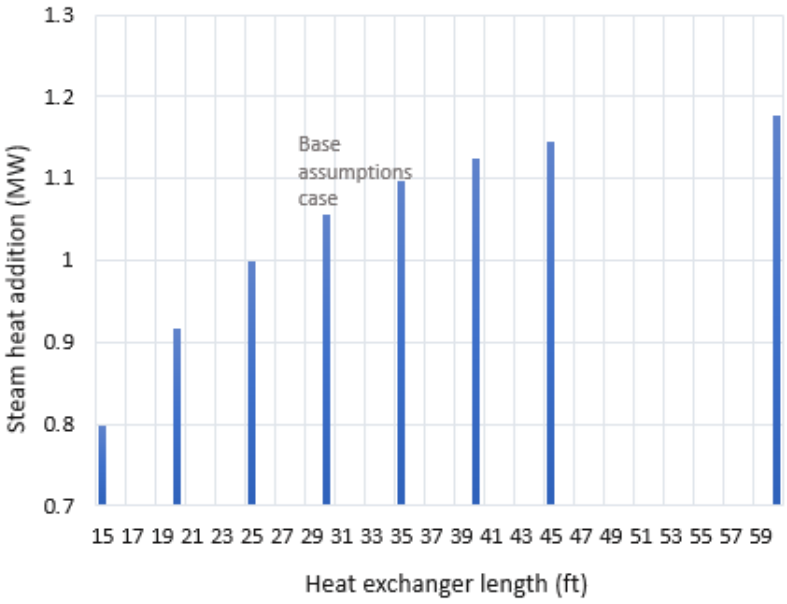

Figure 30: Steam heat addition vs heat exchanger length

Solar field size required to heat HTF to max temperature

- Technology: Default SAM NREL collectors and receivers (SkyFuel SkyTrough collector and Schott PTR80 receiver).
- Required aperture reflective area: 1250 – 1844 m^2.
- System capital cost: US$ 448,000.00 – 660,800.00.

Turbine model output

- Turbine: Siemens SST-060.
- Turbine capital cost: €630,000.00.
- Sent out power: 418.2 – 472.4kW.
- Auxiliary oil pump power: 12.1kW.
- Imported power: 245.3 – 292.6kW.
- Turbine exhaust steam exit temperature: 278.67 ˚C.

4.3 Energy output

4.3.1 Heat map

The solar resource is intermittent; thus the steam plant will only be operated when the solar resource is available. Figure 31 below shows the annual average heat map from the solar field.

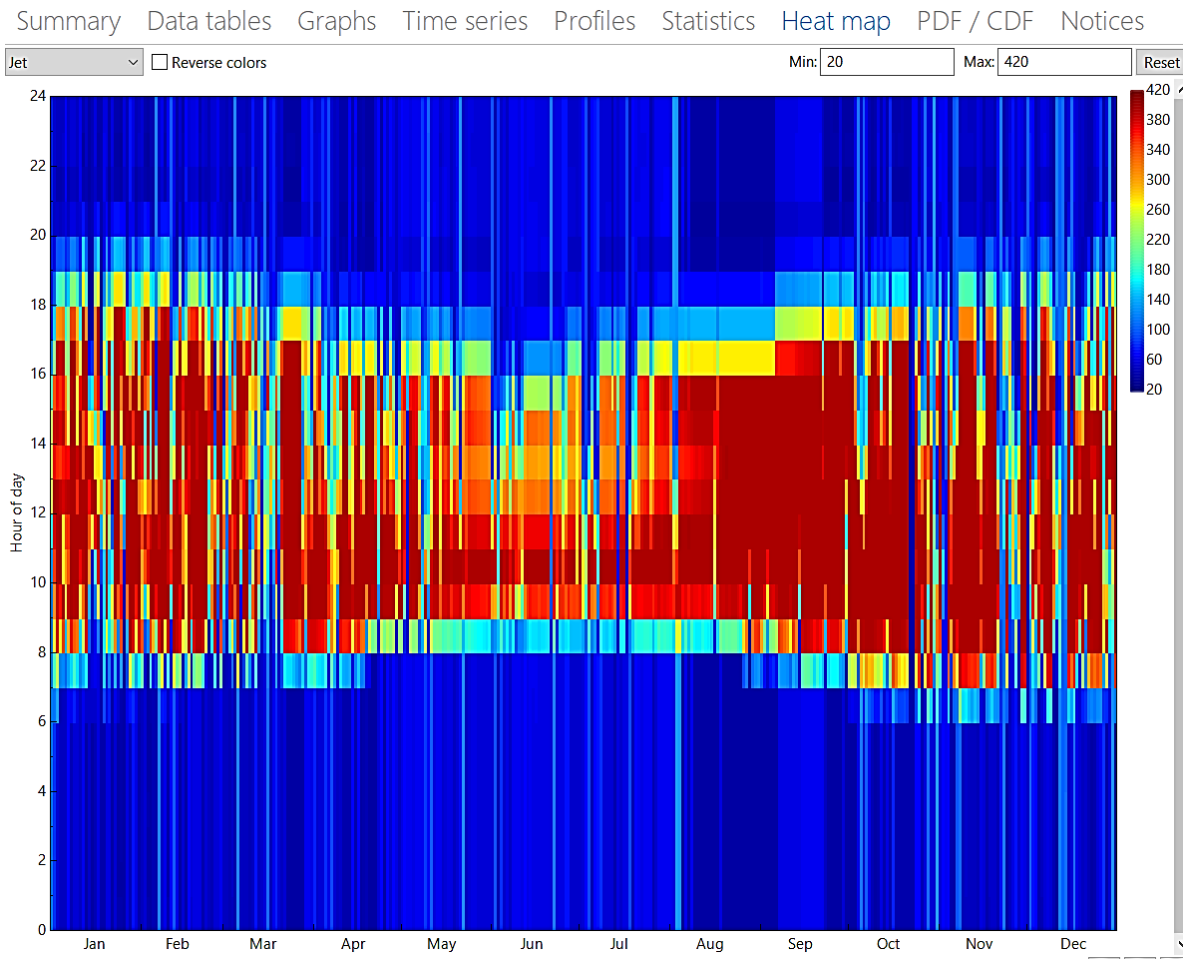

Figure 31: Timestep- averaged system outlet temperature

As expected, the solar collector performs better in the summer months, from mid-August to October when the DNI is high. The system peaks to maximum outlet temperatures as early as 8am in the morning and has very high outlet temperatures throughout the day in these months. From November to May, the heat output oscillates between high and low in between days as this is usually the rainy season in Zimbabwe, with the most rains falling around March which experiences the lowest values of thermal energy output. This is because on rainy days, there is mostly cloudy conditions reducing the incident beam radiation. From April to May the weather transitions to winter, with winter falling between June and July. In winter there is also a lot of cloud cover which will see some days not receiving beam radiation on thick cloud days.

4.3.2 Daily hourly average thermal energy

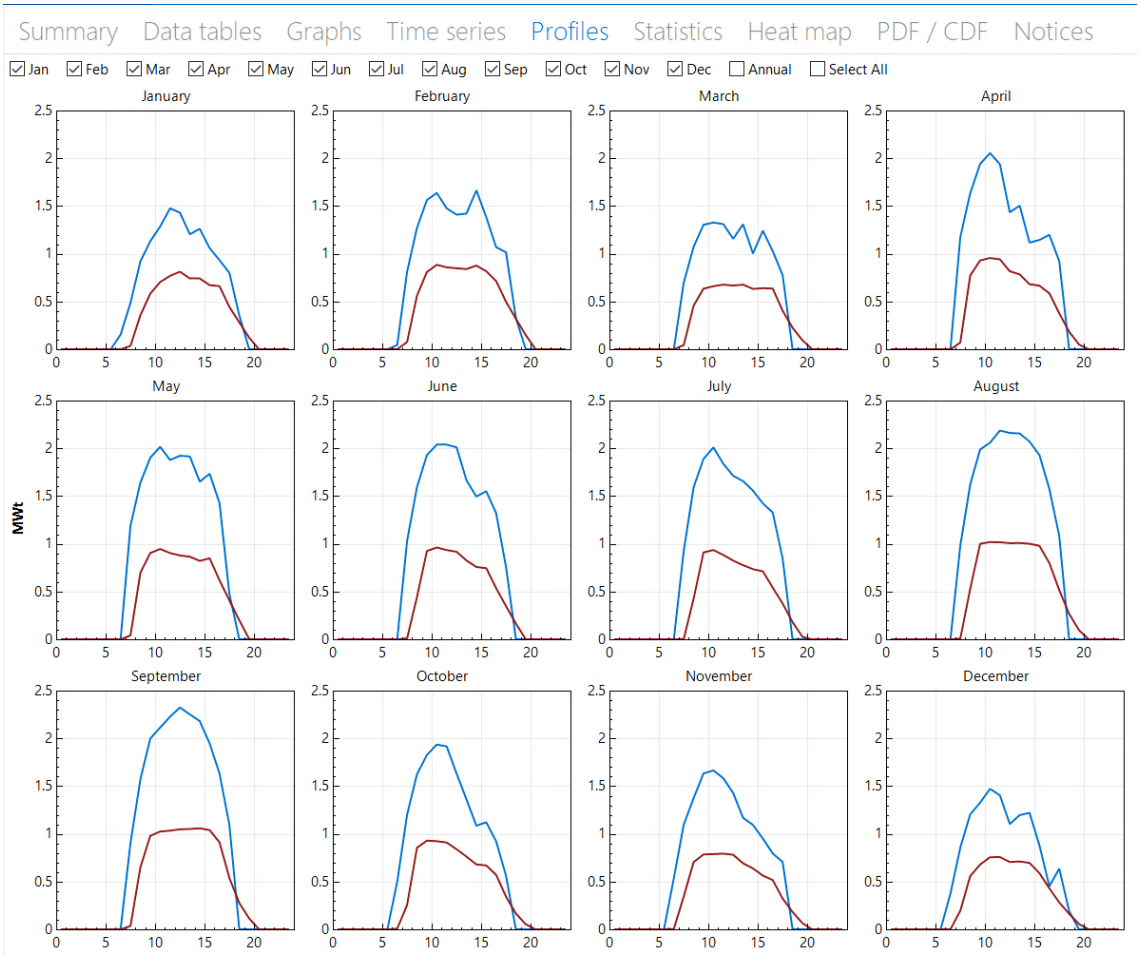

Figure 32: Typical daily hourly average thermal energy variation per month for a 1.06 MW (base case) design heat sink power

Figure 32 above shows the daily hourly average incident thermal power on the collector (in blue), and the outlet thermal energy delivered by the HTF to the heat sink from January to December (in red) for the base case heat exchanger. One can see that the required 1.06MW of thermal energy is essentially the maximum heat sink power the field can supply and occurs only in September. Since the peak is achieved quite soon after sunrise, it is assumed that the required heat is available from 8:00 to 16:00 (8 hours) during the peak month. In subsequent solar field results, this will be termed "Normal solar output".

March, as shown in Figure 32 above, is the lowest output month with the system only delivering slightly above half of the required thermal energy throughout the productive solar hours of the day.

To ensure that the heat exchanger heat load requirement is met throughout the year, the solar field needs to be oversized. It was found that the solar field had to be scaled up by a factor of 1.65 to ensure a theoretical constant maximum output during operation from 08:00 – 16:00 for the whole

year (see Figure 33). This factor was then used to scale up the heat sink for different heat exchanger lengths and the total investment, cash savings and subsequent payback period calculated. This will be termed “Maximum solar output”.

The drawback with oversizing the solar field, is that excess energy during the peak months cannot be used, and some portions of the collector must be shut to avoid overheating. It does however enable maximum electricity production throughout the year, which may be financially more beneficial compared to the extra capital investment.

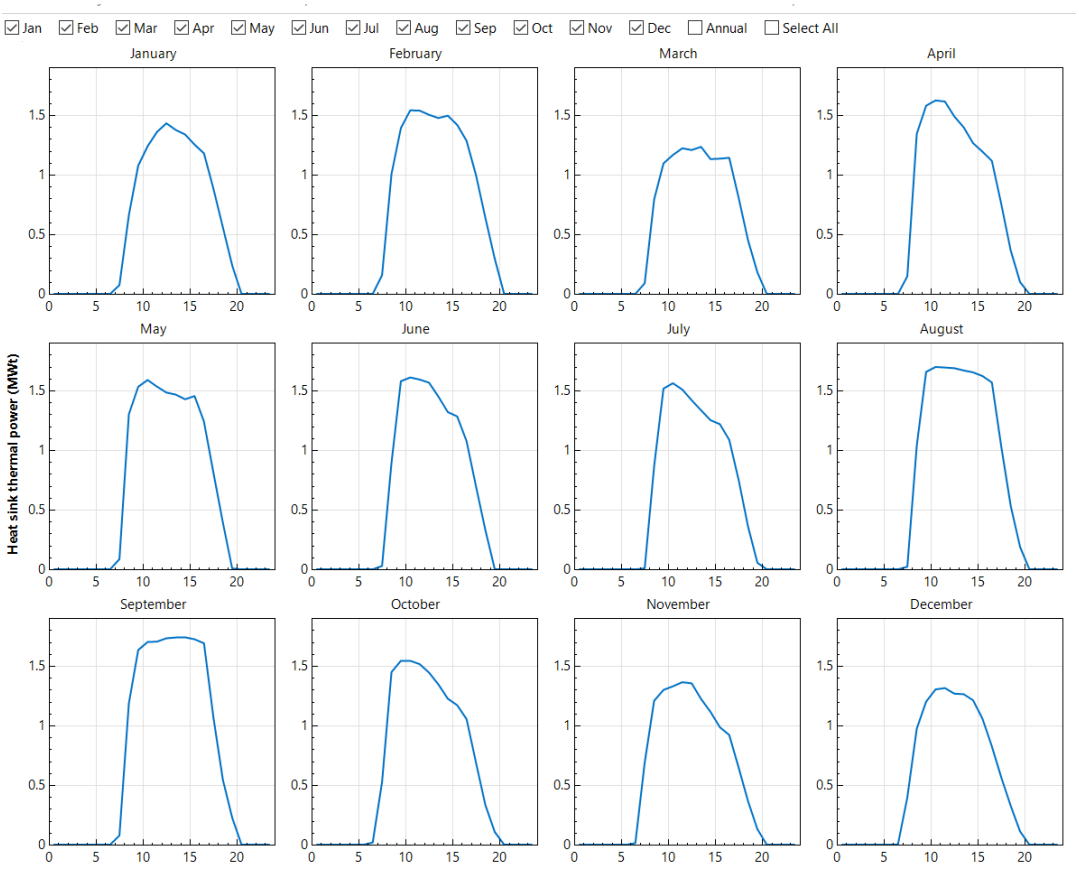

Figure 33: Annual daily hourly average output required for solar output throughout the year.

4.3.3 Annual electricity production

For every 1.06MW input of thermal energy into the heat exchanger, the power cycle sends out 457.79kW of electrical power to the main busbar. The SAM model provided the net annual thermal energy delivered to the heat sink, and using direct proportion, the annual energy production was calculated. The table below shows the annual thermal energy output from the normal solar field output, for all scenarios analysed, including maximum and minimum values.

Table 7: Annual thermal and electrical energy output for a Normal solar field

Heat exchanger length (ft)	Q_heatsink_design (MWt)	Annual_energy_heat sink (kWt-hr)	Max monthly output (MWt-hr)	Min monthly output (MWt-hr)
15	0.8	2.26E+06	243.93	172.95
20	0.9	2.48E+06	263.38	185.97
25	1.0	2.61E+06	280.97	194.32
30	1.06	2.71E+06	293.37	200.34
35	1.10	2.77E+06	301.53	204.22
40	1.13	2.81E+06	307.61	207.09
45	1.15	2.84E+06	311.68	209.03
60	1.18	2.88E+06	317.63	211.71

The net annual energy outputs for both the normal and maximum solar field outputs were obtained by running a parametric simulation and using the heat sink power as input, and selecting the gross and net annual thermal energy production as the output as shown in the figure below:

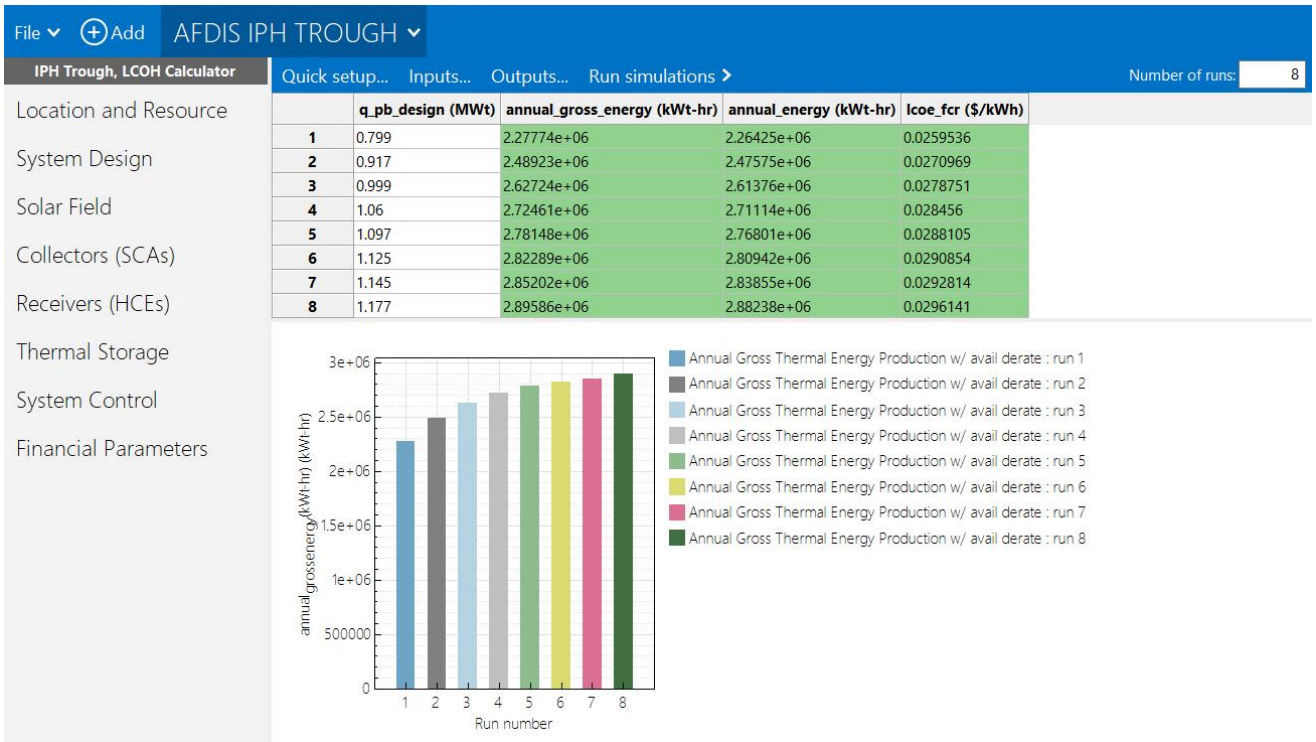

Figure 34: Annual thermal energy output for normal solar field

The maximum and minimum monthly values were obtained from the Statistics tab in SAM *[18]*

Table 8: Annual thermal and electrical energy output for a Maximum solar field

Heat exchanger length (ft)	Q_heatsink_design (MWt)	Annual_energy_heat sink (kWt-hr)	Max monthly output (MWt-hr)	Min monthly output (MWt-hr)
15	1.32	3.04E+06	344.11	223.18
20	1.51	3.17E+06	368.39	235.20
25	1.65	3.21E+06	372.42	236.77
30	1.75	4.80E+06	505.61	362.38
35	1.81	4.91E+06	519.97	368.89
40	1.86	4.99E+06	531.51	374.10
45	1.89	5.05E+06	538.34	377.29
60	1.94	5.14E+06	549.36	382.52

The maximum solar field heat sink power was calculated as explained in section 4.3.2, annual net thermal energy obtained from the parametric simulation.

4.4 System outputs

Table 9: System outputs

Shell & Tube Heat Exchanger, Type BEM									
Item Description	*Units*	**1**	**2**	**3**	**4**	**5**	**6**	**7**	**8**
Shell inner diameter	*in*	39.0	39.0	39.0	39.0	39.0	39.0	39.0	39.0
Tube length	*ft*	15.0	20.0	25.0	30.0	35.0	40.0	45.0	60.0
Steam outlet temperature	*°C*	325.7	347.6	362.8	374.2	381.0	386.2	390.0	395.8
Heat input to steam	*MW*	0.8	0.9	1.0	1.1	1.1	1.1	1.1	1.2
Heat transfer area	m^2	158.3	211.5	264.6	317.8	371.0	424.2	477.4	637.0
Effectiveness	*%*	66.9	76.8	83.7	88.4	91.9	94.2	95.9	98.5
Heat exchanger cost	*ZAR*	640191.5	834786.0	1029380.5	1224192.8	1418569.6	1613164.1	1807758.6	2391542.2
External Solar Field Inputs									
Normal solar field size									
Total required aperture reflective area	m^2	1,250.0	1,438.0	1,563.0	1,656.0	1,719.0	1,766.0	1,797.0	1,844.0
Capital costs	*USD*	448,000.0	515,200.0	560,000.0	593,600.0	616,000.0	632,800.0	644,000.0	660,800.0
Operational costs	*USD*	6,400.0	7,360.0	8,000.0	8,480.0	8,800.0	9,040.0	9,200.0	9,440.0
Maximum solar output									
Total required aperture reflective area	m^2	2,063.0	2,359.0	2,578.0	2,719.0	2,828.0	2,906.0	2,953.0	3,031.0
Capital costs	*USD*	739,200.0	845,600.0	924,000.0	974,400.0	1,013,600.0	1,041,600.0	1,058,400.0	1,086,400.0
Operational costs	*USD*	10,560.0	12,080.0	13,200.0	13,920.0	14,480.0	14,880.0	15,120.0	15,520.0
Turbine Output									
Turbine SOP	*kW*	418	435	447	458	461	465	468	472
Import power	*kW*	293	275	264	255	250	246	243	238
Turbine capital cost	*Euro*	630,000 €	630,000 €	630,000 €	630,000 €	630,000 €	630,000 €	630,000 €	630,000 €

The created heat exchanger and turbine analysis models, together with the SAM solar simulation package were used to analyse the system's output, while varying the heat exchanger length. Heat exchanger effectiveness, steam outlet temperature, turbine sent out and imported power and equipment capital costs (shown in Table 9 above) were amongst the key output parameters. The results were used for the financial analysis.

4.5 Performance Evaluation

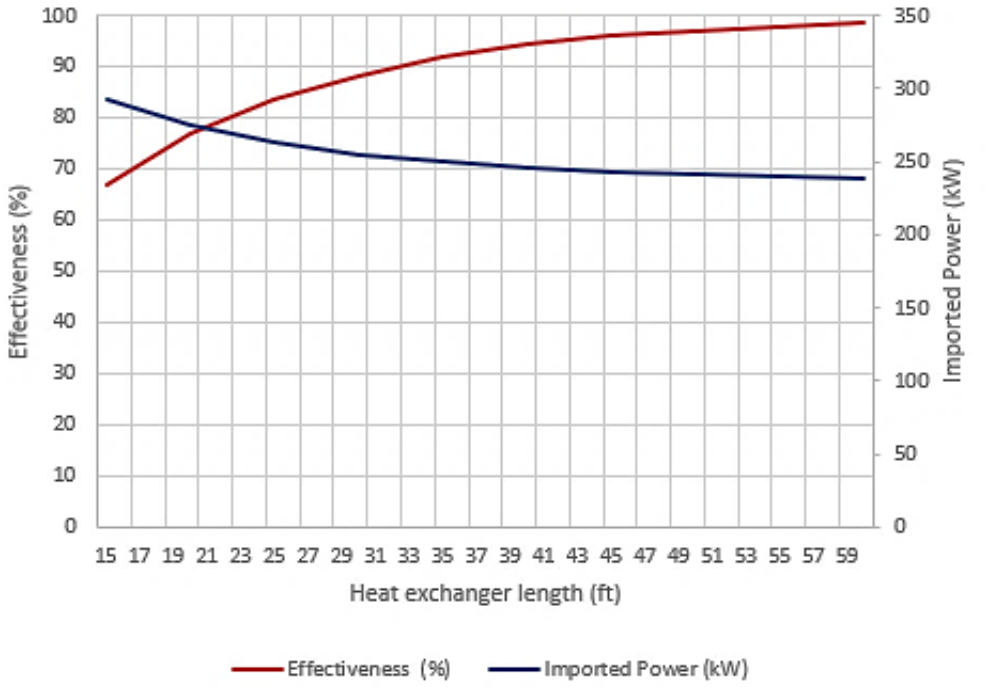

Figure 35: Variation of heat exchanger effectiveness and imported power with the heat exchanger length

As expected, the heat exchanger effectiveness increases with an increase in heat exchanger length. This is because as the heat exchanger length increases, the greater the area available for heat transfer and the closer the steam outlet temperature gets to the oil inlet temperature. However, there are diminishing returns as the length increases, hence an excessively large heater would not be financially viable. At 30ft length, the steam outlet temperature is 374.2˚C, and doubling the size of the heat exchanger gives a steam outlet temperature of 396˚C, which is only 4.3˚C below the oil inlet temperature. However, halving the length to 15 ft results in a steam outlet temperature of 325°C, which is 75°C below the achievable oil temperature.

From the project objectives, the designed system should meet the plant electrical maximum demand of 621.68kW while still producing steam to the process at 400 kPa. This high exhaust pressure means the steam is still superheated at the turbine outlet and will require de-superheating spray to meet the 100°C temperature conditions. The downside of exhausting at such a high backpressure is that the power cycle cannot meet the process plant electrical energy requirements, and the deficit has to be imported from the grid supply. In all eight instances under investigation, even at 98.5% heat exchanger effectiveness, the system did not produce enough electrical energy to meet the process plant demand and the deficit must be imported from the grid. However, it was noted that as the turbine output power increases the deficit reduces, decreasing the amount of

power imported from the grid, as shown by the blue line in Figure 35. To get to the 621.68kW sent out power from the generator, the following could be done:

- Increase mass flow,
- Increase the thermal state at turbine inlet,
- Reduce turbine exhaust pressure.

Option 1: Increase mass flow.

The power output is directly proportional to the steam mass flow. The mass flow of steam can be increased by increasing the size of the boiler to 13.91tph, a 55% increase in the steam flow rate. This implies purchasing a bigger size boiler which is not feasible as the additional steam which is not used in the process must be condensed, increasing the system components, which escalates both capital and operational costs. This also reduces the net thermal efficiency of the cycle as heat added in the boiler and superheater section is lost in the condenser without doing any useful work.

Option 2: Increase thermal state at turbine inlet.

The thermal state at turbine inlet can be increased by either increasing the inlet pressure or inlet temperature. Increasing the pressure is not an option as the boiler pressure cannot be altered without changing the boiler itself. Increasing the temperature can be done by using a heat transfer fluid which can be heated to more than the current HTF limit of 400˚C for Therminol VP-1. An option will be using Hi-tec salt which can go as high up as 593˚C. Hi-Tec is not yet popular in practical CSP applications due to its high freeze temperature of 235˚C. This freeze temperature is too high, for a site like AFDIS with an average annual ambient temperature of 18.5˚C and no thermal storage. To ensure the HTF flows through the system, a freeze protection system must be installed, which not only increases the CAPEX and OPEX requirement, but poses a threat of operational challenges like pipe blockages and need for more auxiliary power to keep the freeze protection system running.

Option 3: Reducing turbine exhaust pressure.

At 289kPa turbine exhaust pressure (28% reduction in exhaust pressure), using the base assumptions, the sent-out power is 625.17kW. This reduction in turbine exhaust pressure increases turbine output but goes against the original objective of providing power without altering the original process thermal needs. To ensure that the process plant steam meets its boundary conditions requirements (at 289kPa turbine exhaust pressure), it will thus be necessary to pressurize the condensate to process steam pressure which is not technically feasible as the exhaust will still

be in gas form and cannot be compressed with a pump. The gas could be compressed using a gas compressor but the moisture content in the exhaust steam is too high for a gas compressor. This could also increase the auxiliary power requirement thus it is better to have a backpressure which corresponds to the process steam requirement and import the deficit electrical power from the National grid.

4.6 System capital costs

The initial project costing was done with the BEM 39 – 360 (991 – 9144) heat exchanger. Base assumptions for the loan interest rate (5%), exchange rate (Euro: US$ of €1: $1.13 and US$: ZAR of $1: R17.58) and electricity tariff of R1.50/ kWhr were used to calculate the total capital investment and payback period using equations developed in section 2.8.4.

Table 10: Total system costs

Hx size (ft)	**15**	**20**	**25**	**30**	**35**	**40**	**45**	**60**
Imported Power (kW)	292.6	275.5	263.7	255.2	249.7	245.6	242.8	238.3
Imported power gain (kW)	-37.1	-20.0	-8.2	0.0	5.8	9.8	12.7	17.2
Effectiveness (%)	66.9	76.8	83.7	88.4	91.9	94.2	95.9	98.5
Turbine capital cost	R12,515,202	R12,515,202	R12,515,202	R12,515,202	R12,515,202	R12,515,202	R12,515,202	R 12,515,202
Hx capital cost	R 640,192	R 834,786	R 1,029,381	R 1,224,193	R 1,418,570	R 1,613,164	R 1,807,759	R 2,391,542
Total Investment required (normal solar output)								
Solar capital cost	R 7,875,840	R 9,057,216	R 9,844,800	R10,435,488	R10,829,280	R11,124,624	R11,321,520	R 11,616,864
Total CAPEX required	R21,031,234	R22,407,204	R23,389,383	R24,174,665	R24,763,052	R25,252,990	R25,644,481	R 26,523,608
Annual OPEX (ZAR)	R 309,843	R 329,639	R 343,809	R 355,166	R 363,711	R 370,849	R 376,580	R 389,556
Total Investment required (max solar output)								
Solar capital cost	R12,995,136	R14,865,648	R16,243,920	R17,129,952	R17,819,088	R18,311,328	R18,606,672	R 19,098,912
Total CAPEX required	R26,150,530	R28,215,636	R29,788,503	R30,869,129	R17,819,088	R32,439,694	R32,929,633	R 34,005,656
Annual OPEX (ZAR)	R 382,976	R 412,616	R 435,225	R 450,801	R 463,565	R 473,516	R 480,654	R 496,443

Table 10 above shows the total project cost for all the heat exchanger lengths under investigation, focusing on two solar field design scenarios, namely:

- Normal solar output: which achieves the desired heat only on the peak month.
- Maximum solar output: which achieves the desired heat throughout the year.

The chart below shows the distribution of the system capital costs, for three heat exchanger size options.

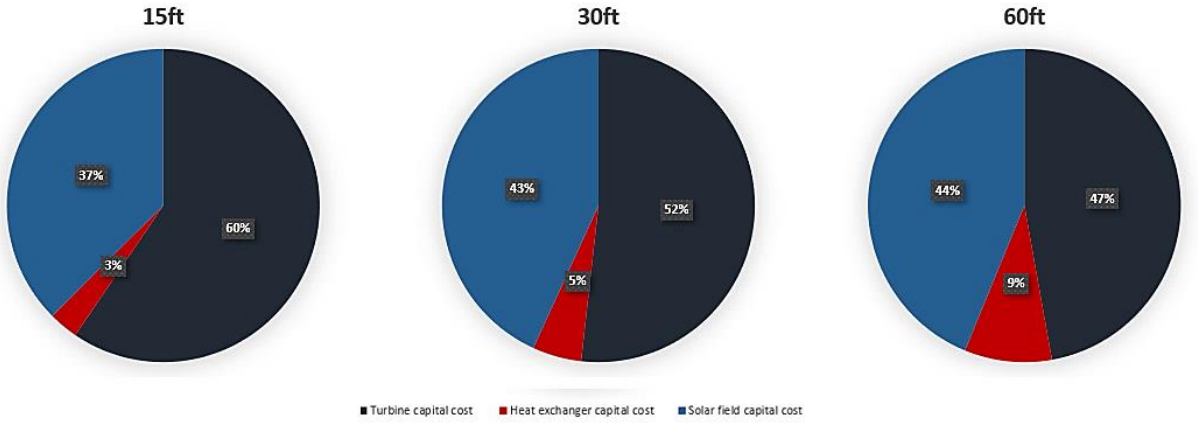

Figure 36: System capital costs breakdown

Figure 36 above shows the capital cost breakdown for the 15ft, 30ft and 60ft heat exchanger. The turbo-alternator capital costs contribution to the CAPEX decreased with increase in HX length although it was the most capital-intensive item in all the systems. Solar thermal field capital costs were the next capital-intensive variable, increasing with increase in HX length. Although the heat exchanger costs appear insignificant compared to the other two cost drivers, it is important to note that there is direct proportionality between heat exchanger size and solar field capital costs as the amount of thermal heat input determines the solar field size. Despite using the same turbo-alternator in all three instances, the smaller HX lengths had the lowest heat transfer area, which translated to the lowest HX capital costs. This in turn made the contribution of the turbo-alternator costs to the CAPEX decrease with increase in HX costs.

4.7 Payback period and optimal length

4.7.1 Normal solar output

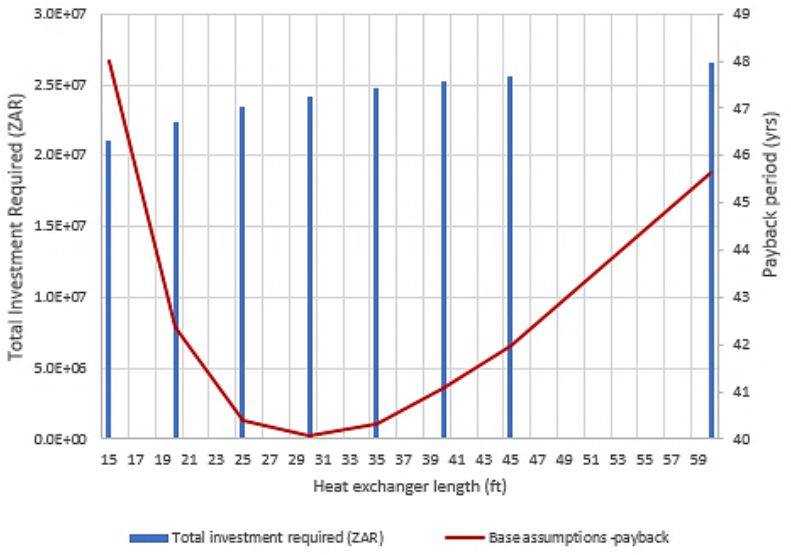

Figure 37: Total investment required and payback period vs heat exchanger length for normal solar output

It is evident that there appears to be an optimum point (about 30 ft) where the payback period is a minimum for a given heat exchanger length. For smaller lengths, the cash savings due to electricity production are too low compared to the CAPEX requirement. Larger heat exchanger lengths do not give enough cash saving benefit to outweigh the CAPEX increase. The payback period is in the range of 40 -50 years for all scenarios under investigation. This is not economically viable as the technical lifespan of most solar thermal plants is at most 25 years.

4.7.2 Maximum solar output

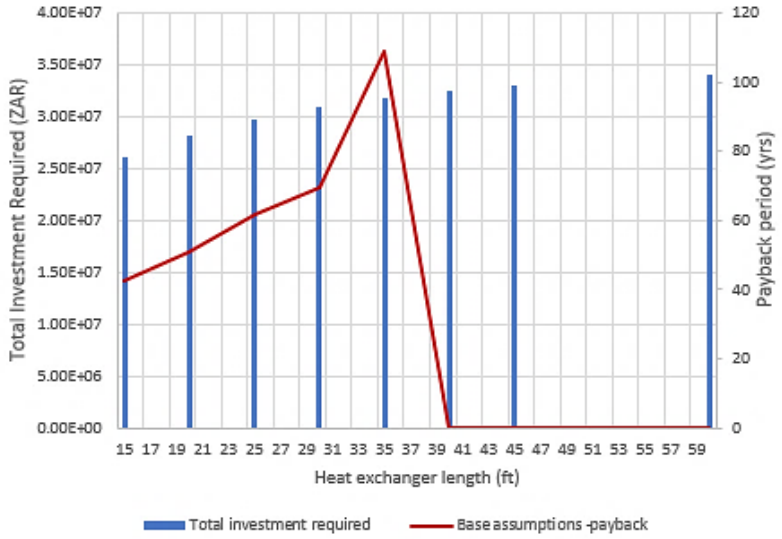

Figure 38: : Total investment required and payback period vs heat exchanger length for maximum solar output

In the case where the solar field is oversized to always produce the required heat, a significant increase in payback period is noticeable. There also do not seem to be turning point, and in fact, above 35ft, the cash savings become too little to recoup the loan as well as cover the interest and there is no breakeven for the base assumptions case.

4.8 Sensitivity Analysis

From the initial cost analysis, it is clear that the current design does not pose a financially viable option. However, many of the terms which contribute to the payback period result contain rough assumptions. Verifying and improving on these assumptions is outside the scope of this project, so, instead a sensitivity analysis was performed on some of the main contributors. These were:

- loan interest rates,
- exchange rates,
- electricity tariff,
- solar resource,
- turbine capital costs.

Table 11 below shows the results of the various scenarios analysed. Its shows the different payback periods for the different heat exchanger sizes, when the different scenarios outlined above are considered. In addition to that, the variation in the total CAPEX required was also included for the different scenarios. It should be noted that the optimum heat exchanger length does vary due to some of the inputs.

Color based formatting was used to highlight and differentiate the payback periods for the different heat exchnager lengths, with the green colour scheme showing the lowest payback and thus optimum heater length for each scenario and red showing the largest payback period. Where the cell returns the #NUM! value, it means the cash saving is too low to recoup the capital investment[7].

[7] From equation (2.37), when the cash savings are too little, the term in the brackets becomes negative as the quotient becomes greater than one, thus the formula returns the #NUM! error as there is no natural logarithm for negative numbers.

Table 11: Sensitivity Analysis Results

Heat Exchanger size (ft)	**15**	**20**	**25**	**30**	**35**	**40**	**45**	**60**
Base assumptions case (interest rate 5%, tariff	48.68	42.86	40.81	40.48	40.74	41.54	42.45	46.23
Variation of Feed- in- Tariff								
Sell at the price you buy at from ESKOM)	48.68	42.86	40.81	40.48	40.74	41.54	42.45	46.23
With NERSA Tariff	9.65	9.30	9.15	9.12	9.14	9.20	9.27	9.51
Variation of USD/ ZAR & Euro/USD exchange rate								
5 year average (US$1: R14.21; US$1: 1.13€)								
Total investment required (ZAR million)	*17.1*	*18.3*	*19.1*	*19.8*	*20.3*	*20.7*	*21.1*	*21.9*
Sell at the price you buy at from ESKOM)	*24.61*	*23.25*	*22.74*	*22.72*	*22.87*	*23.20*	*23.55*	*24.85*
With NERSA Tariff	7.28	7.05	6.96	6.96	6.99	7.05	7.11	7.32
10 year average (US$1: R11.66; US$1: 1.217€)								
Total investment required (ZAR million)	*14.8*	*15.8*	*16.5*	*17.1*	*17.5*	*17.9*	*18.3*	*19.0*
Sell at the price you buy at from ESKOM)	*18.10*	*17.25*	*16.94*	*16.94*	*17.06*	*17.28*	*17.53*	*18.44*
With NERSA Tariff	6.04	5.85	5.78	5.78	5.81	5.86	5.92	6.12
Variation of Interest rate								
Interest at 7%	#NUM!	#NUM!	#NUM!	#NUM!	#NUM!	#NUM!	#NUM!	#NUM!
Interest at 2.5%	24.37	23.29	22.84	22.77	22.83	23.01	23.21	23.95
With NERSA Tariff and 2.5% interest rate	8.46	8.19	8.08	8.06	8.07	8.12	8.17	8.36
Variation of solar resource								
Design for highest insolation month (September)								
Annual electrical energy produced ($MWhr_{peak}$)	*1260.88*	*1361.46*	*1452.35*	*1516.44*	*1558.62*	*1590.04*	*1611.12*	*1641.85*
Payback period (years)	21.91	21.28	20.33	19.91	19.77	19.76	19.85	20.46
Design for lowest insolation month (March)								
Annual electrical energy produced ($MWhr_{peak}$)	*893.98*	*961.31*	*1004.47*	*1035.59*	*1055.63*	*1070.48*	*1080.50*	*1094.34*
Payback period (years)	#NUM!	#NUM!	#NUM!	#NUM!	#NUM!	#NUM!	#NUM!	#NUM!
Variation of turbine capital costs								
Turbine CAPEX less by 15%								
Total investment required (ZAR million)	*19.2*	*20.5*	*21.5*	*22.3*	*22.9*	*23.4*	*23.8*	*24.6*
Payback period (years)	33.36	31.35	30.65	30.73	31.05	31.63	32.24	34.48
Turbine CAPEX less by 25%								
Total investment required (ZAR million)	*17.9*	*19.3*	*20.3*	*21.0*	*21.6*	*22.1*	*22.5*	*23.4*
Payback period (years)	27.46	26.38	26.08	26.28	26.62	27.13	27.65	29.43

Electricity tariff

The electricity tariff proved to be the deciding factor on the profitability of this project. Using the REFIT tariff, the payback period dropped from the range of 40 – 50 years in the base assumptions case to about 9 - 10 years, which is reasonable for such an investment. The payback period is even reduced further if the REFIT tariff is coupled with an interest rate lower than 5%.

Variation of the exchange rates (Euro/US$ and US$/ZAR)

The turbine capital cost was quoted in Euros and the solar field sizing was done using a software giving costs in US$. The effect of the exchange rate on the payback period was also analysed, given that the financial analysis was performed based on the South African rand. The five- and ten-year averages for the currencies were used to check the effect on the payback period. It was shown that for the 5-year averages, the project is not economically feasible, but using the ten-year average, payback period is below 20 years.

However, using the REFIT scheme, the payback period for both the five- and ten-year average exchange rates falls to a promising 6.96 and 5.78 years respectively. This shows that the project might be economically feasible in the future if the rand gains strength to the dollar and euro and the equipment capital costs decrease due to better technological advancement and competition in both the turbine manufacturing and CSP industries, similar to what happened to the solar photovoltaic energy capital costs in the past decade.

Loan interest rate

At high interest rates, greater than 5%, the project is not commercially viable as the cash savings are too low to recoup the initial investment. At an interest rate of 2.5%, the payback period almost halves to between 20 and 25 years, which is still not acceptable as it means the loan repayment will run through the course of the plant's technical lifespan.

Design for a worst- and best-case solar resource day

The best and worst resource months for the location were September and March. Options were analysed as-if the system will receive these outputs all year round for the Normal solar output case. It can be seen that for the best solar resource case, the payback period is almost half that of the

base assumptions case, but still too high considering the plant technical lifespan. For the worst solar resource scenario, the project is not economically viable.

Turbine capital costs

Turbine capital costs account for 52% of the system total CAPEX, based on a non-binding quote from 2016 of the Siemens SST-060 TG set. This quote may be inaccurate and does not include potential cost negotiations. However, even by reducing the turbine costs by 15% and 25%, the payback period was still longer than the technical lifespan of the plant.

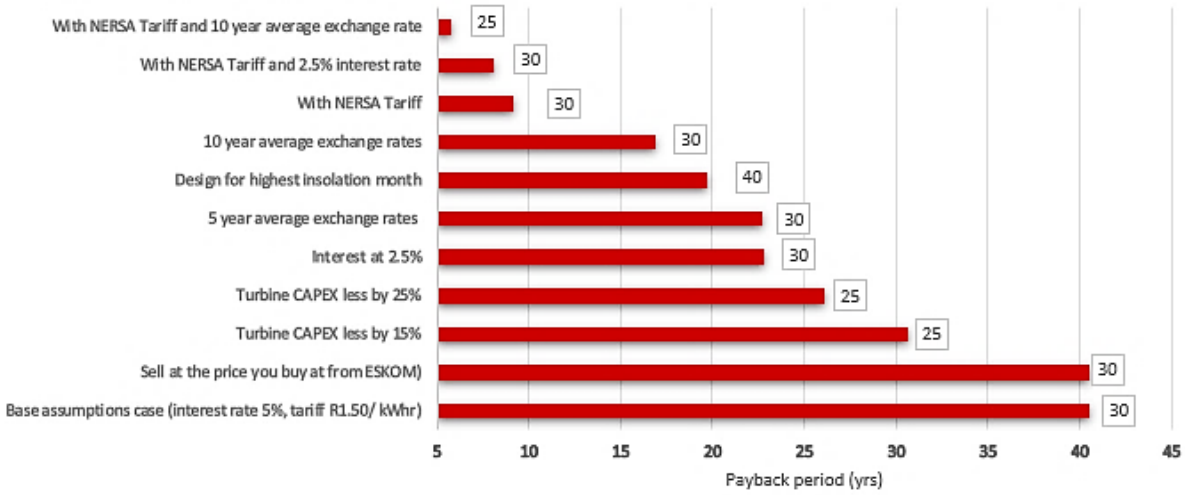

The figure shows a summary of cases where the minimum payback period is less than 40 years, along with the optimum heat exchanger length. From the figure, it is safe to conclude that the optimum heat exchanger length is generally 30ft. There are a few cases with a payback period less than 20 years, though these might be considered hypothetical. Most of the scenarios result in excessive paybacks, making the project economically unfeasible.

5. Conclusions and Recommendations

5.1 Conclusion

Chapter 1 gave a brief background to the research problem and objectives of the study. Literature pertinent to the study was discussed in Chapter 2, placing emphasis on what is already there and how the researcher would develop the system from existing models. In Chapter 3, the model was developed, beginning with analysis of the qualitative data obtained from site visits and merging it with the quantitative data gathered in the literature review. The results from the created models in Chapter 3 (including the performance evaluation and economic analysis) were discussed in Chapter 4, focusing on the base assumptions case.

From the above findings, it was concluded that although it is technically possible to convert an existing process steam plant into a combined heat and power plant using an external solar field without affecting the process thermal load requirements, the project is not yet economically viable on an independent investor financing model as it was established that the payback period is largely dependent on the tariff.

Although the NERSA REFIT for CSP projects without storage is R3.14/kWhr, which gives a positive reasonable payback period of 9.12 years for the optimum heat exchanger length, the tariff which is considered is the tariff the process plant buys its electricity from the power supply Authority not the feed in tariff. Unless the government offers an incentive of topping up the deficit of the REFIT to the process plant's savings to encourage the uptake of CSP projects, the project remains economically unviable until the CAPEX requirement for the solar and turbine technologies decreases.

However, it is also important to note that the need for this research came from the fact that most industries were losing uptime due to the rampant load shedding, affecting their revenue streams. Another downside of load-shedding is shorter equipment lifespans (particularly on electric motors which get damaged on start-ups and overload failures on shaft couplings and gearboxes on the drivetrains). During drive-train design of process plant equipment, the gearbox is sized for continuous operation and daily start-stops during load-shedding increase the possibilities of overload failure due to cyclic loading. By using the solar assisted power cycle to kick in just before power is switched off, the companies can keep their plants running during load-shedding and maintain their production volumes. This avoids revenue losses due to load-shedding, which if converted into monetary value can also add to the annual cash flows and decrease the payback period significantly.

The downside of switching the power cycle on and off however is the introduction of thermal cycles in the system, which deteriorates the heat exchanger and piping system material. With that said, tube leaks in the heat exchanger will be expected in 5 years, and piping bends should be replaced within 10 years.

5.2 Recommendations

Recommendations for further research

- Given a chosen heat exchanger size, it would be beneficial to develop a comprehensive process model that links the solar field actual heat uptake with the power block, thereby enabling more accurate annual savings calculations.
- A more detailed cost model can be employed particularly in the heat exchanger manufacturing costs using the generic model developed by Caputo et al [42], as well as other system costs that may have been overlooked.
- Solar system optimization by exploring the benefit of employing thermal storage, particularly in this era when there is more research on the use of molten salts as HTFs which can attain temperatures as high as +500˚C.
- A thorough cost benefit analysis should be done considering the monetary value of intangible benefits like maintaining the plant availability in the event of load shedding.
- Use of other profitability indicators like Net Present Value and Internal Rate of Return to check the economic viability of the project.

Recommendations for process steam plants

The energy sector is already experiencing massive shifts to renewable energy sources in a bid to curb the effects of climate change caused by greenhouse gas emissions. It would be a noble development to do a thorough feasibility assessment to evaluate profitability of such a project.

The benefits of cogeneration cannot be overemphasized again in this section as it is evident that cogeneration not only reduces the carbon footprint of a coal fired process steam plant, but also offers a reliable power source. In this era where most African power utilities are struggling to meet rise in demand and opting for load-shedding during peak demand, cogeneration will go a long way in minimizing revenue losses being experienced by most companies during load shedding.

Recommendations for energy regulatory bodies

It is time more lucrative incentives are put in place to ensure that independent investors can invest in the supply of renewable energies in Africa. European and Asian energy policies are already shifting to renewables due to the adverse effects on the climate of brown power generation. China, the largest producer of electricity in the world and also the largest emitter is already taking strides to phase out less efficient systems in its High Efficiency Low Emissions (HELE) blueprint [51], and if Africa adopts energy efficiency centred policies to merge the renewables and brown technologies, it can both reduce its energy poverty and boost productivity.

The government should provide additional incentives, other than renewable energy feed-in tariffs like equity or debt based financial instruments to encourage the uptake of solar thermal projects at private investor levels. One way of offering such incentives is topping up the cost savings for the process plant, by adding the deficit ESKOM will not pay to the investor (difference between NERSA REFIT and the price the process plant buys the electricity from ESKOM) either in cash or as an investment tax credit.

Retrofitment of process steam plants to enable cogeneration, after a thorough financial feasibility study is a noble idea. However, the question to go to SAPG or just traditional steam cogeneration plants still relies on the competitiveness of solar thermal technology, whose costs have remained quite high compared to solar photovoltaic systems in the past decade. Most SAPG projects have failed to take off due to high technology costs.

6. Bibliography

[1] C. Trimble, M. Kojima, I. P. Arroyo and M. Farah, “Financial Viability of Electricity Sectors in Sub-Saharan Africa: Quasi-Fiscal Deficits and Hiddne Costs,” World Bank Group: Energy and Extractives Global Practice Group, 2016.

[2] T. D. Eastop and A. McConkey, Applied Thermodynamics for Engineering Technologists, Delhi: Dorling Kindersley (India) Pvt. Ltd, 2009.

[3] Y. M. A. B and C. A, Thermodyanmics: An Engineering Approach, 5th Edition, Boston: McGraw-Hill College, 2006.

[4] J. Veerapa and M. Beerepoot, “Cogeneration and Renewables: Solutions for a low carbon energy future,” International Energy Agency, Paris, 2011.

[5] B. F. Kolanowski, Small Scale Cogeneration Handbook Second Edition, Georgia: The Fairmont Press, Inc, 2003.

[6] J. A. Duffie and W. A. Beckman, Solar Engineering of Thermal Processes, Fourth Edition, John Wiley & Sons, Inc, 2013.

[7] National Renewable Energy Laboratory, “SkyFuel Parabolic Trough Optical Efficiency Testing: Cooperative Research and Development Final Report,” U.S. Department of Energy, Oak Ridge, 2010.

[8] W. T. Pierce, “Solar Assisted Power Generation (SAPG): Investigation of Solar Preheating of Feedwater,” Stellenbosch University http://scholar.sun.ac.za, Stellenbosch, 2013.

[9] M. Petrov, M. Popa and T. Fransson, “Solar Augmentation of conventional steam plants: From system studies to reality,” in *Proceedings of WREF 2012*, Denver, 2012.

[10] Y. Yang, Q. Yan, R. Zhai, A. Kouzani and E. Hu, “An efficient way to use medium or low temperature solar heat for power generation - integration into conventional power plant,” *Applied Thermal Engineering,* no. 31, pp. 157-162, 2011.

[11] E. Hu, Y. Yang, A. Nishimura, F. Yilmaz and A. Kouzani, “Solar Thermal Aided Power Generation,” *Applied Energy,* no. 87, pp. 2881-2885, 2010.

[12] J. Gottshe and T. Hove, “Mapping global, diffuse and beam solar radiation in Zimbabwe,” *Renewable Energy an International Journal,* pp. 3-7, 1998.

[13] M. P. Petrov, M. Salomon Popa and T. H. Fransson, “Solar Augmentation of conventional steam plants,” in *World Renewable Energy Forum, WREF 2012*, Colorado, 2012.

[14] S. Mills, “Combining solar power with coal fired power plants, or co-firing natural gas,” *Clean Energy,* vol. 2, no. 1, pp. 1-9, 2018.

[15] Google Inc, “Google Images,” [Online]. Available: https://www.google.com/search?safe=active&tbs=simg:CAESlwIJmhwclhKV_1k8aiwILELCMpwgaYQpfCAMSJ9IUnQuBFtMU5wLWFUumA5Ie0xXuOKoqlyuEP7oq0TjNOPcijDmwKhowbdu3wvZdpKmBmQ_1xNu9qaMK3OO7w8h6--iPlhaPcp0sY0mGwxJTcQSTeIC2Otg1sIAQMCxCOrv4IGgoKCAgBEgS63XJODAsQne3BCRqEAQ. [Accessed 4 October 2020].

[16] AUSTELA, “Australian Solar Thermal Energy Association,” 2020. [Online]. Available: http://www.austela.net.au/newsletter/122-solar-boost-at-liddell-hunter-valley. [Accessed 2020].

[17] CS Energy, “Solar Boost Project: End of project report on the Kogan Creek Power Station,” ARENA, Queensland, 2016.

[18] Alliance for Sustainable Energy, LLC, *System Advisor Model Help.*

[19] G. F. Hewitt and S. J. Pugh, “Approximate Design and Costing Methods for Heat Exchangers,” *Heat Transfer Engineering,* vol. 28, no. 2, pp. 76-86, 2007.

[20] Alfa Laval, “Alfa Laval - Plate Technology,” 2020. [Online]. Available: https://www.alfalaval.com/globalassets/documents/industries/chemicals/petrochemicals/brochure_alfa_laval_plate_technology_ppm00063en.pdf. [Accessed February 2020].

[21] Tubular Exchanger Manufacturers Association, Standards of the Tubular Exchanger Manufacturers Association, Ninth Edition, New York: Tubular Exchanger Manufacturers Association, Inc, 2007.

[22] J. E. Edwards, “Design and Rating Shell and Tube Heat Exchangers,” *MNL 032A,* pp. 1-30, 29 August 2008.

[23] T. Kuppan, Heat Exchanger Design Handbook, New York: Marcel Dekker, Inc, 2000.

[24] F. P. Incropera, D. P. Dewitt, T. L. Bergman and A. S. Lavine, Fundamentals of Heat and Mass Transfer, Sixth Edition, New Jersey: John Wiley & Sons, Inc, 2007.

[25] A. N. Caglayan and P. Buthod, “Factors to correct air cooler and shell and tube exchanger LMTD,” *Oil and Gas Journal,* vol. 6, pp. 91-94, 1976.

[26] J. Ball, “Construction Basics of Shell and Tube Heat Exchangers,” *API Heat Transfer,* 1 March 2000.

[27] Enerquip Administrator, “Enerquip: The Helpful Heat Exchanger Experts,” 26 March 2018. [Online]. Available: https://www.enerquip.com/2018/03/26/7-shell-configurations-what-you-need-to-know-when-designing-a-shell-and-tube-heat-exchanger/. [Accessed 16 February 2020].

[28] Enerquip administrator, “Enerquip: The Helping Heat Exchanger Experts,” 26 March 2018. [Online]. Available: https://www.enerquip.com/2018/03/26/tubeside-or-shellside-comparing-fluid-allocation-options-for-your-shell-and-tube-heat-exchanger/. [Accessed 16 February 2020].

[29] D. Q. Kern, Process Heat Transfer, Tokyo: Mc-Graw Hill Book Company, Inc, 1965.

[30] Chemstations, Inc, *CHEMCAD THERM Version 5.1 User Guide.*

[31] Eastman Therminol, “Therminol - Heat Transfer Fluids by Therminol,” 2019. [Online]. Available: https://info.therminol.com/WF_2019_HTF_Calculator_Download-2.html#_ga=2.139334070.44303310.1592303265-1194112209.1592303265. [Accessed 31 October 2019].

[32] Wolverine Tube, Inc, “Single-Phase Shell-Side Flows and Heat Transfer,” in *Engineering Data Book III*, pp. 3-1 - 3-20.

[33] P. Subbarao, “Indian Institute of Technology, Delhi,” 14 February 2006. [Online]. Available: http://web.iitd.ac.in/~pmvs/courses/mel709/SHTE.pdf. [Accessed 23 March 2020].

[34] F. C. Magazoni, L. Cabezas-Gomez, P. F. Alvarino and J. M. Saiz-Jabardo, “Thermal Performance of One-Pass Shell and Tube Heat Exchangers in Counter-Flow,” *Brazilian Journal of Chemical Engineering,* vol. 36, no. 02, pp. 869-883, 2019.

[35] T. N. Raval and R. Patel, “Optimization of Auxiliary Power Consumption of Combined Cycle Power Plant,” *Procedia Engineering,* pp. 751-757, December 2013.

[36] S. Teir, Steam Boiler Technology, Second Edition, Helsinki: Helsinki University of Technology Department of Mechanical Engineering, Enenrgy Engineering and Environmental Protection Publications, 2003.

[37] E. F. Church, Steam Turbines, First Edition, New York: McGraw-Hill Book Company Inc, 1928.

[38] Howden Group, “Howden Group Products,” [Online]. Available: https://www.howden.com/en-gb/products/steam-turbines. [Accessed 23 March 2020].

[39] Siemens Turbomachinery Equipment (STE) GmbH, “IEA BioEnergy Task 32/33: Workshop on State-of-the-art technologies for small biomass co-generation, Copenhagen, Oct 7, 2010,” in *Steam turbines: What is the lower limits for feasibility, recent developments to reduce costs and increase efficiency on small steam turbine systems, Reiner Schenk, Siemens Frankenthal, Germany*, Copenhagen, 2010.

[40] P. Konstantin and M. Konstantin, Power and Energy Systems Engineering Economics: Best Practice Manual, Burgstetten: Springer International Publishing, AG, 2017.

[41] H. B. Foumani, “Manufacturing Cost Optimization of A Shell & Tube Heat Exchanger using the Differential Evolution Algorithm,” Lappeenranta University of Technology, Lappeenranta, Finland, 2018.

[42] A. Caputo, P. M. Pelagagge and P. Salini, “Manufacturing cost model for heat exchangers optimization,” *Applied Thermal Engineering,* no. 94, pp. 513 - 533, 2016.

[43] “European Commision Photovoltaic Geographical Information System,” [Online]. Available: https://re.jrc.ec.europa.eu/pvg_tools/en/tools.html#TMY.

[44] “sam.nrel.gov”.

[45] Coastal Chemical Co, L.L.C., “HITEC Heat Transfer Salt,” Brenntag Company, Texas.

[46] The International Association for the Properties of Water and Steam, “Revised Release on the IAPWS Industrial Formulation 1997 for the Thermodynamic Properties of Water and Steam,” The International Association for the Properties of Water and Steam, Lucerne, 2007.

[47] R. K. Sinnott, Coulson & Richardsons Chemical Engineering: Chemical Engineering Design, Volume 6, Fourth Edition, Oxford: Elsevier Butterworth-Heinemann, 2005.

[48] Aveng Trident Steel, “Aveng Trident Steel Product Catalogue,” 2020. [Online]. Available: http://www.aveng.co.za. [Accessed 10 March 2020].

[49] National Renewable Energy Laboratory, *System Advisor Model Industrial Process Heat,* 2020.

[50] P. Gilman, “Using parabolic trough field collector DNI for tower (salt),” 08 February 2017. [Online]. Available: sam.nrel.gov/forum/forum-general/1658-using-parabolic-trough-field-collector-dni-for-tower-salt.html. [Accessed 2020].

[51] I. C. C. Centre, Composer, *China - Policies, HELE technologies and CO2 reductions.* [Sound Recording]. International Energy Agency Clean coal centre. 2016.

[52] J. P. Laudon and K. C. Laudon, Essentials of Management Information Systems, New Jersey: Prentice Hall international editions, 2003.

[53] J. A. Duffie and W. A. Beckman, Solar Engineering of Thermal Processes, New Jersey: John Wiley & Sons,Inc, 2013.

[54] "Energypedia," [Online]. Available: https://energypedia.info/wiki/South_African_Renewable_Energy_Feed-in_Tariff. [Accessed 19 August 2020].

[55] Verein Deutscher Ingenieure, VDI- Gesellschaft Verfahrenstechnik und Chemieingenieurwesen GVC, VDI Heat Atlas, Second Edition, Dusseldorf: Springer, 2010.

Appendix A. Heat exchanger approximate sizing

Reference:C:\Research\Water-Steam IAPWS-IF97 rev 1.2.xmcd

HEATER APPROXIMATE SIZING

Steam mass flow: $m'_s := 9000\ \frac{kg}{hr} = 2.5\ \frac{kg}{s}$

Steam inlet conditions: $P_{s.i} := 950 \cdot kPa$ $x := 1$

$cp_s := Cp_{steam}(P_{s.i}, "", "", x, "", "") = 2.688 \cdot \frac{kJ}{kg \cdot K}$

$T_{s.i} := T_{steam}(P_{s.i}, "", "", "") = 177.669 \cdot °C$

$\mu_s := \mu_{steam}(P_{s.i}, "", "", x, "", "") = 14.906 \times 10^{-6}\ s \cdot Pa$

$k_s := \lambda_{steam}(P_{s.i}, "", "", x, "", "") = 0.035 \cdot \frac{W}{m \cdot K}$

$\rho_s := \rho_{steam}(P_{s.i}, "", x, "", "") = 4.9\ \frac{kg}{m^3}$

Oil inlet conditions: $T_{o.i} := 400\ °C$ $\rho_o := 695.7\ \frac{kg}{m^3}$

$cp_o := 2.624\ \frac{kJ}{kg \cdot K}$ $\mu_o := 1.469 \cdot 10^{-4} \cdot Pa \cdot s$

Assume oil flow: $m'_o := 8 \cdot m'_s = 20\ \frac{kg}{s}$

Target heater outlet TTD: $TTD := 5 \cdot \Delta°C$

Steam outlet: $T_{s.e} := T_{o.i} - TTD = 395 \cdot °C$

Heat transfer: $Q := m'_s \cdot \left(h_{steam}(P_{s.i}, T_{s.e}, "", "", "") - h_{steam}(P_{s.i}, "", "", x, "")\right) = 1.199 \cdot MW$

Oil outlet: $T_{o.e} := T_{o.i} - \frac{Q}{m'_o \cdot cp_o} = 377.162 \cdot °C$

LMTD: $\Delta T_{LMTD} := \frac{(T_{o.i} - T_{s.e}) - (T_{o.e} - T_{s.i})}{\ln\left[\frac{(T_{o.i} - T_{s.e})}{(T_{o.e} - T_{s.i})}\right]} = 52.761\ K$

Desired heater UA: $UA := \frac{Q}{\Delta T_{LMTD}} = 22.716 \cdot \frac{kW}{K}$

Assume typical tube diameter: $D := \frac{3}{4} \cdot in = 19.05 \cdot mm$

Assume typical fluid velocity: $v_s := 20 \cdot \frac{m}{s}$

$v_o := 1 \cdot \frac{m}{s}$

Steam side heat transfer:

$$Pr_s := \frac{cp_s \cdot \mu_s}{k_s} = 1.144 \qquad Re_s := \frac{\rho_s \cdot v_s \cdot D}{\mu_s} = 125240.512$$

$$Nu_s := 0.36 \cdot Re_s^{0.55} \cdot Pr_s^{0.33} = 239.529$$

$$h_s := \frac{Nu_s \cdot k_s}{D} = 440.311 \cdot \frac{W}{m^2 \cdot K}$$

Oil side heat transfer:

$$Pr_o := \frac{cp_o \cdot \mu_o}{k_o} = 5.083 \qquad Re_o := \frac{\rho_o \cdot v_o \cdot D}{\mu_o} = 90218.414$$

$$Nu_o := 0.027 \cdot Re_s^{0.8} \cdot Pr_s^{0.33} = 337.952$$

$$h_o := \frac{Nu_o \cdot k_o}{D} = 1345.421 \cdot \frac{W}{m^2 \cdot K}$$

Overall heat transfer:

$$U := \left(\frac{1}{h_s} + \frac{1}{h_o} \right)^{-1} = 331.743 \cdot \frac{W}{m^2 \cdot K}$$

Required heater area:

$$A_{HT} := \frac{UA}{U} = 68.405\ m^2$$

Number of tubes in parallel:

$$n_t := \frac{m'_o}{\rho_o \cdot v_o \cdot \frac{1}{4} \cdot \pi \cdot D^2} = 100.862$$

Total length of a single tube:

$$L_t := \frac{A_{HT}}{n_t \cdot \pi \cdot D} = 37.179 \cdot ft$$

Shell outer diameter:

$L_{tp} := 1.25 \cdot D$ $\quad CL := 1$ $\quad CTP := 0.90$

$$D_{ctl} := \sqrt{\frac{4 \cdot n_t \cdot CL \cdot L_{tp}^2}{\pi \cdot CTP}} = 11.199 \cdot in$$

Clearance:

$L_{bb} := 12.7mm$ $\quad$ *300mm< D_S < 1000mm, clearance = 0.5in*

Outer tube limit diameter:

$$D_{otl} := D_{ctl} + D = 0.303\ m$$

Shell diameter:

$$D_S := D_{otl} + L_{bb} = 12.449\ in$$

Appendix B. Heat exchanger program code

Reference:C:\Research\Water-Steam IAPWS-IF97 rev 1.2.xmcd

1. SYSTEM INPUTS

1.1 Problem specification: Heat exchanger inlet and exit conditions for steam

NB: Boiler exit & turbine inlet are heat exchanger inlet & exit respectively, assuming constant mass flow

Boiler exit: $m'_{steam.outlet} := 9000 \frac{kg}{hr}$

$P_{steam.outlet} := 950 kPa$

$T_{steam.out} := T_{steam}(P_{steam.outlet}, "", "", "") = 450.819 K$

Turbine inlet: $m'_{in} := 9000 \frac{kg}{hr}$

$p_{in} := 900 kPa$

1.2 Fluid properties and flow arrangements

Shell side: Steam

Mass flow: $m'_s := m'_{steam.outle}$

Inlet conditions: $P_{si} := P_{steam.outle}$ $x := 1$

$c_{p.si} := Cp_{steam}(P_{si}, "", "", x, "", "") = 2.688 \cdot \frac{kJ}{kg \cdot K}$

$T_{si} := T_{steam}(P_{si}, "", "", "") = 450.819 K$

Tube side: Therminol VP 1 oil from external solar source

Inlet conditions: $T_{hi} := 400 °C$ $\mu_{oil} := 1.469 \cdot 10^{-4} Pa \cdot s$

$c_{p.oil} := 2.624 \frac{kJ}{kg \cdot K}$ $\rho_{oil} := 695.7 \frac{kg}{m^3}$

Fluid properties sourced from Therminol Fluid Properties calculator:

https://info.therminol.com/WF_2019_HTF_Calculator_Download-2.html#_ga=2.139334070.44303310.1592303265-1194112209.1592303265

1.3 Heat Exchanger Schematic

Selected Model: Shell & Tube Heat Exchanger with a single shell, baffles and single tube pass

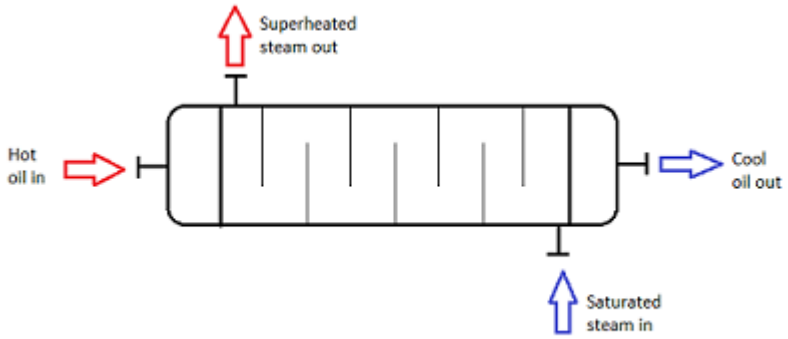

Fig 1: Shell schematic, showing fluid inlets and outlets and baffle arrangement

1.4 Chosen variable inputs

Shell diameter: $D_S := 39\,in$

Tube length: $L_t := 30\cdot ft$

Oil scale factor: $S_{m'.oil} := 8$ *Chosen value to meet HTF flow requirements*

1.5 Assumptions

i. Overall heat transfer coefficient is constant throughout the heat exchanger
ii. Mass flow rate of both shell side and tube side fluid is constant
iii. Each pass has the same heat transfer area
iv. System heat losses are negligible
v. Specific heat capacity of cold and hot fluid is constant and independent of temperature
vi. The flow rates of both fluid streams are steady, and flow is evenly distributed

2. SHELL & TUBE GEOMETRY

Tube side

Assuming SS tube (3/8"nominal pipe size) with schedule 40 and a square pitch of 1.25"

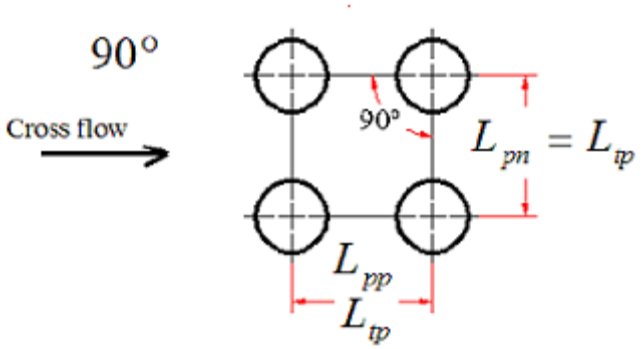

Fig 2: Tube arrangement adapted from Wolverine Tube, Inc Engineering Data Book III

Tube thermal conductivity $k_{steel} := 14.4\frac{W}{m\cdot K}$

Tube diameter : $D_o := 0.675in$ $t := 0.091in$ *Dimensions of welded and seamless pipes Table D-1 TEMA - taken from ANSI 836.10 - for NPS 3/8*

Tube inner diameter $D_i := D_o - 2 \cdot t = 0.013\,m$

Tube pitch $L_{tp} := 1.25in$ $L_{pp} := L_{tp}$ $L_{pn} := L_{tp}$

Tube length: $L_t = 9.144m$

Tube hole diameter: $D_{th} := 0.679in$ *Standard fit: Table RCB-7.21 TEMA tube hole diameters & standard tolerances*

Clearance $L_{tb} := D_{th} - D_o = 1.016 \times 10^{-4}\,m$

Shell side

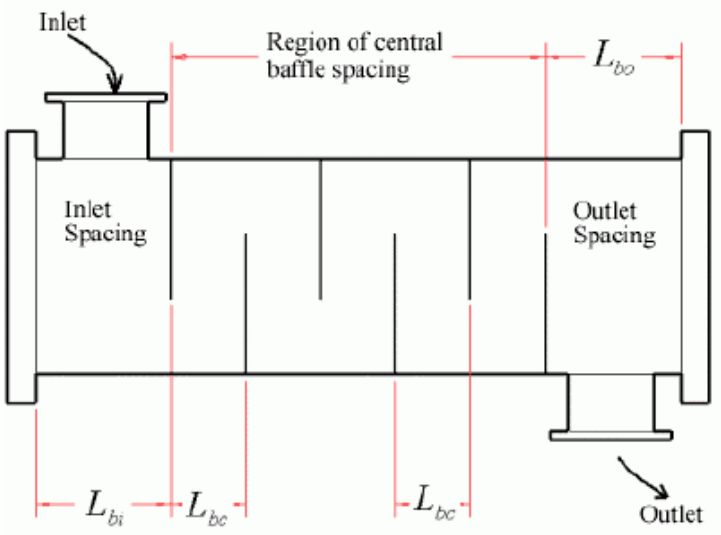

Fig 3: Shell baffle spacing adapted from Wolverine Tube, Inc Engineering Data Book III

Shell diameter $D_S = 0.991m$

Min shell wall thickness: $t_s := 14.3mm$ *Min shell thickness = 11.1mm +3.2mm corrosion allowance for all pressure parts RCB1.51*

Shell outside diameter: $D_{SO} := D_S + 2 \cdot t_s = 1.019m$

Equivalent shell diameter $D_e := \dfrac{4 \cdot \left(L_{tp}^{\,2} - \frac{\pi}{4} \cdot D_o^{\,2} \right)}{\pi \cdot D_o} = 0.058m$

Tube clearance $C_t := L_{tp} - D_o = 14.605\,mm$

Assuming 25% cut segmented baffles, with spacing equal to half the shell diameter

Baffle cut $B_c := 25\%$

Baffle cut height $L_{bch} := B_c \cdot D_S = 0.248\,m$

Center baffle spacing $L_{bc} := 0.5 \cdot D_S = 0.495\,m$ *0.3 D_S < Baffle spacing < 0.5 D_S for optimum spacing*

Inlet baffle spacing $L_{bi} := L_{bc}$

Outlet baffle spacing $L_{bo} := L_{bc}$

Clearance between baffle and shell inner diameter $L_{sb} := 1.6mm + 0.004 D_S = 5.562\,mm$

Number of baffles: $n_b := ceil\left(\frac{L_t}{L_{bc}}\right) = 19$

Assume shell inner diameter and outer tube limit diameter clearance, L_{bb}

Clearance $L_{bb} := 12.7mm$ *300mm< D_S < 1000mm, clearance = 0.5in*

Outer tube limit diameter $D_{otl} := D_S - L_{bb} = 0.978\,m$

Centre line tube limit diameter $D_{ctl} := D_{otl} - D_o = 0.961\,m$

2.1 TUBE COUNT CALCULATION

Guess tube wall temperature $T_{wall.avg} := 658.084K$ $\mu_{wall} := 1.96e\text{-}4Pa \cdot s$

Number of tube passes: $n_p := 1$

Tube layout constant: $CL := 1$ *For square tube layout*

Tube pitch ratio $PR := \frac{L_{tp}}{D_o} = 1.852$

Tube pass constant: $CTP := 0.90$ *For single tube pass arrangement*

Number of tubes: $n_t := ceil\left(\frac{\pi \cdot CTP \cdot D_{ctl}^{\,2}}{4 \cdot CL \cdot PR^2 \cdot D_o^{\,2}}\right) = 648$ *Tube count within limits for given shell ID*

TABLE 9. TUBE-SHEET LAYOUTS (TUBE COUNTS)
Square Pitch

¾ in. OD tubes on 1-in. square pitch						1 in. OD tubes on 1¼-in. square pitch					
Shell ID, in.	1-P	2-P	4-P	6-P	8-P	Shell ID, in.	1-P	2-P	4-P	6-P	8-P
8	32	26	20	20		8	21	16	14		
10	52	52	40	36		10	32	32	26	24	
12	81	76	68	68	60	12	48	45	40	38	36
13¼	97	90	82	76	70	13¼	61	56	52	48	44
15¼	137	124	116	108	108	15¼	81	76	68	68	64
17¼	177	166	158	150	142	17¼	112	112	96	90	82
19¼	224	220	204	192	188	19¼	138	132	128	122	116
21¼	277	270	246	240	234	21¼	177	166	158	152	148
23¼	341	324	308	302	292	23¼	213	208	192	184	184
25	413	394	370	356	346	25	260	252	238	226	222
27	481	460	432	420	408	27	300	288	278	268	260
29	553	526	480	468	456	29	341	326	300	294	286
31	657	640	600	580	560	31	406	398	380	368	358
33	749	718	688	676	648	33	465	460	432	420	414
35	845	824	780	766	748	35	522	518	488	484	472
37	934	914	886	866	838	37	596	574	562	544	532
39	1049	1024	982	968	948	39	665	644	624	612	600

Assumed tube sheet thickness $t_{ts} := 18.802\,mm$

Min tube sheet thickness should be greater than 75% of tube outside diameter

Effective tube length: $L_{ta} := L_t - 2\cdot t_{ts} = 9.106m$

Heat transfer area $A_{HT} := \pi \cdot D_o \cdot L_{ta} \cdot n_t = 317.84m^2$

Shell leakage areas

Baffle cut angle $\theta_{ds} := 2\cdot acos\left(1 - 2\cdot B_c\right) = 120\cdot deg$

$\theta_{ds.deg} := 120$

Shell to baffle leakage area $S_{sb} := 0.00436\cdot D_S \cdot L_{sb} \cdot \left(360 - \theta_{ds.deg}\right) = 5.766\times 10^{-3} m^2$

Angle of baffle cut relative to H/E centerline $\theta_{ctl} := 2\cdot acos\left[\frac{D_S}{D_{ctl}}\cdot\left(1 - 2\cdot B_c\right)\right] = 117.934\cdot deg$

$\theta_{ctl.deg} := 116.48$

Fraction occupied by window $F_w := \frac{\theta_{ctl.deg}}{360} - \frac{\sin\left(\theta_{ctl.deg}\right)}{2\cdot\pi} = 0.362$

Tube-baffle hole leakage area $S_{tb} := \left[\frac{\pi}{4}\cdot\left[\left(D_o + L_{tb}\right)^2 - D_o^{\,2}\right]\right]\cdot n_t\cdot\left(1 - F_w\right) = 1.134\times 10^{-3} m^2$

Cross flow area at bundle centerline $S_m := L_{bc}\cdot\left[L_{bb} + \frac{D_{ctl}}{L_{tp}}\cdot\left(L_{tp} - D_o\right)\right] = 0.225m^2$

Fraction in crossflow $F_c := 1 - 2\cdot F_w = 0.275$

2.2 SHELL-SIDE: STEAM CONVECTIVE HEAT TRANSFER COEFFICIENT CALCULATION

Guess mean bulk fluid temperature: $T_{steam.avg} := 546.29K$

Shell side cross flow area $A_s := \frac{C_t\cdot L_{bc}\cdot D_S}{L_{tp}} = 0.226m^2$

Shell side mass velocity $G_{steam} := \frac{m'_s}{S_m} = 11.102\frac{kg}{m^2\cdot s}$

Density $\rho_{steam.avg} := \rho_{steam}\left(P_{si}, T_{steam.avg}, "", "", ""\right) = 3.879\frac{kg}{m^3}$

Kinematic viscosity

$$\mu_{steam.avg} := \mu_{steam}\left(P_{si}, T_{steam.avg}, "", "", "", ""\right) = 1.906 \times 10^{-5} \frac{kg}{m \cdot s}$$

$$\mu_{steam.wall} := \mu_{steam}\left(P_{si}, T_{wall.avg}, "", "", "", ""\right) = 2.38 \times 10^{-5} \frac{kg}{m \cdot s}$$

Reynolds number

$$Re_S := \frac{G_{steam} \cdot D_e}{\mu_{steam.avg}} = 3.361 \times 10^4$$

Maximum inter-tube velocity

$$v_{max} := \frac{m'_s}{\rho_{steam.avg} \cdot S_m} = 2.862 \frac{m}{s}$$

Specific heat capacity

$$c_{p.steam.avg} := Cp_{steam}\left(P_{si}, T_{steam.avg}, "", "", "", ""\right) = 2.158 \cdot \frac{kJ}{kg \cdot K}$$

Prandtl number

$$Pr_{steam.avg} := Pr_{steam}\left(P_{si}, T_{steam.avg}, ""\right) = 0.986$$

Thermal conductivity

$$k_{steam.avg} := \lambda_{steam}\left(P_{si}, T_{steam.avg}, "", "", "", ""\right) = 0.042 \frac{m \cdot kg}{K \cdot s^3}$$

Nusselt number

$$Nu_{steam} := 0.36 \cdot Re_S^{0.55} \cdot Pr_{steam.avg}^{\frac{1}{3}} \cdot \left(\frac{\mu_{steam.avg}}{\mu_{steam.wall}}\right)^{0.14} = 107.217$$

Ideal shell side heat transfer coefficient

$$\alpha_I := \frac{Nu_{steam} \cdot k_{steam.avg}}{D_e} = 77.55 \frac{kg}{K \cdot s^3}$$

Baffle cut correction factor

Baffle cut correction factor

$$J_C := 0.55 + 0.72 \cdot \left(1 - 2 \cdot F_w\right) = 0.748$$

Baffle leakage correction factor

Coefficients

$$r_{lm} := \frac{S_{sb} + S_{tb}}{S_m} = 0.031 \qquad r_s := \frac{S_{sb}}{S_{sb} + S_{tb}} = 0.836$$

Baffle leakage correction factor

$$J_L := 0.44 \cdot \left(1 - r_s\right) + \left[1 - 0.44 \cdot \left(1 - r_s\right)\right] \cdot e^{-2.2 \cdot r_{lm}} = 0.94$$

Bundle by-pass, Laminar flow and unequal baffle spacing correction factors

Bundle by-pass correction factor

$$J_B := 1$$ *No flow leakages through pass partition*

Unequal spacing correction factor

$$J_S := 1$$ *Baffle spacing is equal*

Laminar flow correction factor

$$J_R := 1$$ *Flow in turbulent regime*

Actual shell side heat transfer coefficient

$$h_{steam.corrected} := \alpha_I \cdot J_B \cdot J_R \cdot J_S \cdot J_L \cdot J_C = 54.5 \frac{kg}{K \cdot s^3}$$

2.3 TUBE-SIDE: OIL CONVECTIVE HEAT TRANSFER COEFFICIENT CALCULATION

Oil flow rate: $m'_{oil} := S_{m'.oil} \cdot m'_s = 20 \frac{kg}{s}$

Tube side Reynold's #: $Re_{oil} := \frac{4 \cdot m'_{oil} \cdot \frac{n_p}{n_t}}{\pi \cdot D_i \cdot \mu_{oil}} = 21363.021$ *Flow in turbulent regime*

Oil velocity: $v_{oil} := \frac{Re_{oil} \cdot \mu_{oil}}{\rho_{oil} \cdot D_i} = 0.36 \cdot \frac{m}{s}$ *0.36 < $v_{Therminol}$ < 4.97m/s, min to avoid fouling, max to prevent tube erosion*
Source: SAM NREL IPH Model

Prandtl number $Pr_{oil} := \frac{c_{p.oil} \cdot \mu_{oil}}{k_{oil}} = 5.083$

Nusselt number $Nu_{oil} := 0.027 \cdot Re_{oil}^{0.8} \cdot Pr_{oil}^{0.33} \cdot \left(\frac{\mu_{oil}}{\mu_{wall}} \right)^{0.14} = 128.994$

Oil side heat transfer coefficient $h_{oil} := \frac{Nu_{oil} \cdot k_{oil}}{D_i} = 781.246 \cdot \frac{W}{m^2 \cdot K}$

2.4 OVERALL HEAT TRANSFER COEFFICIENT

Overall heat transfer coefficient: $U := \left(\frac{1}{h_{steam.corrected}} + \frac{1}{h_{oil}} \cdot \frac{D_o}{D_i} + \frac{D_o \cdot \ln\left(\frac{D_o}{D_i} \right)}{2 k_{steel}} \right)^{-1} = 49.29 \frac{kg}{K \cdot s^3}$

2.5 HEATER OUTLET TEMPERATURES

Desired heater UA: $UA := U \cdot A_{HT} = 1.567 \times 10^4 \cdot \frac{W}{K}$

Number of transfer units: $NTU := \frac{UA}{m'_s \cdot c_{p.si}} = 2.331$

Specific heat ratio $C_R := \frac{m'_s \cdot c_{p.si}}{m'_{oil} \cdot c_{p.oil}} = 0.128$

Heat exchanger effectiveness: $\varepsilon_{HE} := \frac{1 - e^{-NTU \cdot (1 - C_R)}}{1 - C_R \cdot e^{-NTU \cdot (1 - C_R)}} = 0.884$ *Assume pure counterflow since number of baffles is greater than 6*
Source: Cayglan and Buthod (1976)

Steam outlet temperature: $T_{so} := \varepsilon_{HE} \cdot (T_{hi} - T_{si}) + T_{si} = 374.179\,°C$

Shell-side fluid mean temperature convergence check

Given

$$T_{steam.avg} - \left(\frac{T_{so} + T_{si}}{2}\right) = 0$$

$$T_{steam.calc} := T_{steam.avg} \rightarrow 546.29\,K$$

$$Accuracy_{steam.temp} := \frac{T_{steam.calc} - \left|T_{steam.calc} - T_{steam.avg}\right|}{T_{steam.calc}} = 100\cdot\%$$

True temperature difference

Heat added to the steam $Q_{HE} := m'_s \cdot c_{p.steam.avg}\left(T_{so} - T_{si}\right) = 1.06\,MW$

True temperature difference $\Delta T_{true} := \frac{T_{so} - T_{si}}{\frac{UA}{m'_s \cdot c_{p.steam.avg}}} = 67.678\,K$

Oil outlet temperature $T_{ho} := T_{hi} - \frac{\Delta T_{true} \cdot UA}{m'_{oil} \cdot c_{p.oil}} = 379.797\cdot°C$

Tube wall temperature convergence check

Calculated HE heat transfer rate $Q_{HE.calc} := U \cdot A_{HT} \cdot \Delta T_{true} = 1.06\,MW$

Wall temperature convergence check $T_{oil.avg} := \frac{T_{ho} + T_{hi}}{2} = 389.898\cdot°C$

Given

$$T_{wall.avg} - \left(T_{oil.avg} - Q_{HE.calc} \cdot \frac{1}{h_{oil} \cdot A_{HT}}\right) = 0$$

$$T_{wall.calc} := T_{wall.avg} \rightarrow 658.084\,K$$

$$Accuracy_{wall.temp} := \frac{T_{wall.calc} - \left|T_{wall.calc} - T_{wall.avg}\right|}{T_{wall.calc}} = 100\cdot\%$$

3. SHELL & TUBE PRESSURE DROP CALCULATIONS

3.1 TUBE-SIDE: PRESSURE DROP CALCULATION

Isothermal friction factor $f_{isotherm} := 0.02$

$\rho_{H2O} := 1000\,\frac{kg}{m^3}$

Corrected friction factor $f_{corrected} := \frac{f_{isotherm}}{\left(\frac{\mu_{oil}}{\mu_{wall}}\right)^{0.14}} = 0.026$

Tube flow area: $A_{tube} := \frac{n_t \cdot 0.25 \cdot \pi \cdot D_i^{\,2}}{n_p} = 0.08\,m^2$

Tube side mass velocity: $G_{tube} := \frac{m'_{oil}}{A_{tube}} = 250.613\,\frac{kg}{m^2 \cdot s}$

Specific gravity of oil: $s_{g.oil} := \frac{\rho_{oil}}{\rho_{H2O}} = 0.696$

Tube head loss: $\Delta p_t := \frac{f_{corrected} \cdot v_{oil}^{\,2} \cdot L_t}{D_i \cdot 2 \cdot g} = 0.126\,m$

Return loss: $\Delta p_{tr} := \frac{4 \cdot n_p \cdot v_{oil}^{\,2}}{s_{g.oil} \cdot 2 \cdot g} = 0.038\,m$

Total tube side pressure drop $\Delta p_{tube.tot} := \left(\Delta p_{tr} + \Delta p_t\right) \cdot g \cdot \rho_{oil} = 1.118\,kPa$

3.2 OIL PUMP DUTY CHECK

Type: Seal less centrifugal pump (magnetic pump)

Specification: Klaus SLM NHO 065-040-315

Pump volumetric flowrate: $V'_{oil.pump} := \frac{m'_{oil}}{\rho_{oil}} = 103.493 \cdot \frac{m^3}{hr}$

Suction head: $h_s := 30m$ *Tank height adapted from SAM NREL IPH thermal fluid reservoir dimensions*

Total pump head: $H_s := h_s + \left(\Delta p_{tr} + \Delta p_t\right) = 30.164m$

Pump efficiency: $\eta_{pump} := 60\%$

Pump power: $P_{aux.oil.pump} := \frac{\rho_{oil} \cdot g \cdot H_s \cdot V'_{oil.pump}}{\eta_{pump}} = 9.86 \cdot kW$

3.3 SHELL-SIDE: PRESSURE DROP CALCULATION

Assume that the inlet and outlet nozzle pressure drop = 2 velocity heads each

Ideal shell pressure drop

Shell side friction factor: $f_S := 0.001$

Corrected friction factor $f_{S.corrected} := \frac{f_S}{\left(\frac{\mu_{steam.avg}}{\mu_{steam.wall}}\right)^{0.14}} = 1.238 \times 10^{-3}$

Shell side head loss: $\Delta p_{bl} := \frac{f_{S.corrected} \cdot G_{steam}^{2} \cdot D_S \cdot (n_b + 1)}{D_e \cdot 2 \cdot g \cdot \rho_{steam.avg}^{2}} \cdot g \cdot \rho_{steam.avg} = 6.752 \cdot Pa$

Crossflow pressure drop

Cross flow coefficient: $K_f := 0.267 + \frac{0.249 \cdot 10^{4}}{Re_S} - \frac{0.927 \cdot 10^{7}}{Re_S^{2}} + \frac{0.1 \cdot 10^{11}}{Re_S^{3}} = 0.333$

Number of cross flow rows: $N_c := \frac{D_S \cdot \left(1 - 2 \cdot \frac{L_{bch}}{D_S}\right)}{L_{tp}} = 15.6$

Crossflow pressure drop: $\Delta p_c := N_c \cdot K_f \cdot \left(\frac{1}{2} \cdot \rho_{steam.avg} \cdot v_{max}^{2}\right) = 0.083 \cdot kPa$

Window zone pressure drop

$\alpha := \frac{D_S - 2.L_{bch}}{D_S} = 0.5$

Window zone flow area: $S_w := \frac{D_S^{2}}{4} \cdot \left(\operatorname{acos}(\alpha) - \alpha \cdot \sqrt{1 - \alpha^{2}}\right) - \frac{n_t}{8} \cdot (1 - F_c) \cdot \pi \cdot D_o^{2} = 0.096 m^{2}$

Effective number of cross flow rows $N_{cw} := \frac{0.8 \cdot L_{bch}}{L_{tp}} = 6.24$

Window zone pressure drop: $\Delta p_w := \frac{(2 + 0.6 \cdot N_{cw}) \cdot m'_s{}^{2}}{2 \cdot S_m \cdot S_w \cdot \rho_{steam.avg}} = 0.213 \cdot kPa$

End zone pressure drop

Width of by-pass lane between tubes $L_{pl} := 0$ *No pass partition*

By-pass area $S_b := L_{bc} \cdot \left[\left(D_S - D_{otl}\right) + L_{pl}\right]$

Ratio of by-pass to cross flow area $F_{sbp} := \frac{S_b}{S_m} = 0.028$

By-pass correction factor:

$$r_{ss} := \left(\frac{\ln(J_B)}{-1.25 \cdot F_{sbp}} - 1 \right)^3$$

$$R_B := e^{-3.7 \cdot F_{sbp} \cdot \left(1 - \sqrt[3]{r_{ss}}\right)} = 0.813$$

$$p := -0.15 \cdot (1 + r_s) + 0.8 = 0.525$$

Leakage correction factor

$$R_L := e^{-1.33 \cdot (1 + r_s) \cdot r_{lm}^{\,p}} = 0.676$$

Unequal spacing correction factor

$$R_S := \left(\frac{L_{bc}}{L_{bo}} \right)^{2-0.2} + \left(\frac{L_{bc}}{L_{bi}} \right)^{2-0.2} = 2$$

Number of tubes crossed in the window area

$$N_{tcw} := \frac{0.8}{L_{pp}} \cdot \left(D_S \cdot B_c - \frac{D_S - D_{ctl}}{2} \right) = 5.864$$

Number of tubes crossed between baffle tips

$$N_{tcc} := \frac{D_S}{L_{pp}} \cdot (1 - 2.B_c) = 15.6$$

End zone pressure drop:

$$\Delta p_e := \Delta p_{bl} \cdot \left(1 + \frac{N_{tcw}}{N_{tcc}} \right) \cdot R_B \cdot R_S = 0.015 \cdot \text{kPa}$$

Inlet and outlet nozzle pressure drop:

$$\Delta p_{ie} := 2 \cdot \left(0.5 \cdot \rho_{steam.avg} \cdot v_{max}^{\,2} \right) = 0.032 \cdot \text{kPa}$$

Total shell side pressure drop

$$\Delta p_{shell} := \Delta p_w + \Delta p_e + \Delta p_c + \Delta p_{ie} = 0.343\,\text{kPa}$$

Steam exit pressure:

$$p_{hx.so} := P_{steam.outlet} - \Delta p_{shell} = 949.657\,\text{kPa}$$

Steam exit enthalpy:

$$h_{hx.so} := h_{steam}(p_{hx.so}, T_{so}, "", "", "") = 3.21 \times 10^3 \cdot \frac{\text{kJ}}{\text{kg}}$$

4. MATERIAL AND COST CALCULATIONS

4.1 TUBESHEET THICKNESS

4.1.1 Approximate tube sheet thickness

Appendix A TEMA pages A-11

Assumed material: A516 Grade 70 normalized carbon steel

$$\eta := 1 - \frac{0.785}{\left(\frac{L_{tp}}{D_o} \right)^2} = 0.771$$

Gasket diameter

$$G_{ts} := D_S = 0.991\text{m}$$

Factor for tube sheet support

$$F_{ts} := 1$$

Allowable stress in tension

$$S_{ts} := 380\text{MPa}$$

380 < Tensile strength < 510 MPa

Mean metal temperature $T_{mean} := \frac{T_{wall.calc} + T_{steam.avg}}{2} = 602.187\,K$

Assumed tube sheet thickness (bending): $T_{ts.bending} := \frac{F_{ts} \cdot G_{ts}}{3} \cdot \sqrt{\frac{P_{steam.outlet}}{\eta \cdot S_{ts}}} = 18.802 \cdot mm$

Assumed tube sheet thickness (shear): $T_{ts.shear} := \frac{0.31 \cdot D_e}{1 - \frac{D_o}{L_{tp}}} \cdot \frac{P_{steam.outlet}}{S_{ts}} = 0.097 \cdot mm$

Check if shear or bending is the controlling variable

Variable 1: $\frac{P_{steam.outlet}}{S_{ts}} = 2.5 \times 10^{-3}$

Variable 2: $1.6 \cdot \left(1 - \frac{D_o}{L_{tp}}\right) = 0.736$

Since $\frac{P_{steam.outlet}}{S_{ts}} << 1.6 \cdot \left(1 - \frac{D_o}{L_{tp}}\right)$ shear will not control, thus design for bending.

4.1.2 Design for bending

Equivalent differential expansion pressure

Elastic modulus:

$$E(T) := \left| \begin{array}{l} T \leftarrow T\ /°C \\ E \leftarrow \left(206 + -4.326 \cdot 10^{-2} \cdot T - 3.502 \cdot 10^{-5} \cdot T^2 \ldots \right. \\ \left. + -1 \cdot 6.592 \cdot 10^{-8} \cdot T^3 \right) \\ E \cdot GPa \end{array} \right.$$

Elastic modulus tube sheet $E_{ts} := E(T_{mean}) = 185.626\,GPa$

Elastic modulus shell $E_s := E(T_{steam.avg}) = 190.228\,GPa$

Elastic modulus of tubes $E_t := 193\,GPa$ *http://asm.matweb.com/search/SpecificMaterial.asp?bassnum=mq304a*

Coefficient of thermal expansion: $\alpha_t := 17.2 \frac{\mu m}{m \cdot K}$ $\alpha_s := 12 \frac{\mu m}{m \cdot K}$

Differential thermal growth between shell and tubes:

$$\Delta L := L_{ta} \cdot \left[\begin{array}{l} \alpha_s \cdot \left(T_{steam.avg} - 70\ °F \right) \ldots \\ + -1 \alpha_t \cdot \left(T_{oil.avg} - 70\ °F \right) \end{array} \right] = -30.222 \cdot mm$$

$J_{ts} := 1$ *Assume there are no shell expansion joints*

Coefficients: $K_{ts} := \frac{E_s \cdot t_s \cdot (D_{SO} - t_s)}{E_t \cdot t \cdot n_t \cdot (D_o - t)} = 0.637$

$$F_q := 0.25 + \left(F_{ts} - 0.6\right)\cdot\left[\frac{300\cdot t_s\cdot E_s}{K_{ts}\cdot L_{ta}\cdot E_{ts}}\cdot\left(\frac{G_{ts}}{T_{ts.bending}}\right)^3\right]^{\frac{1}{4}} = 7.547$$

Differential expansion pressure:

$$P_d := \frac{4\cdot E_s\cdot t_s\cdot\frac{\Delta L}{L_t}}{\left(D_{SO} - 3\cdot t_s\right)\cdot\left(1 + J_{ts}\cdot K_{ts}\cdot F_q\right)} = -6.339\times 10^3\cdot kPa$$

Effective shell side design pressure

Shell equivalent pressure:

$$P'_s := P_{steam.outlet}\cdot\left[\frac{0.4\cdot J_{ts}\cdot\left[1.5 + K_{ts}\cdot\left[1.5 + \left(1 - n_t\cdot\frac{D_o}{G_{ts}}\right)\right]\right]}{1 + J_{ts}\cdot K_{ts}\cdot F_q}\right]$$

Effective shell design pressure:

$$P_S := \frac{P'_s - P_d}{2} = 3.037\cdot MPa$$

Shell design pressure sufficient to withstand operating conditions

Effective tube side design pressure

Oil pressure:

$$P_{oil} := \rho_{oil}\cdot g\cdot H_s = 205.792\,kPa$$

Tube equivalent pressure:

$$P'_t := P_{oil}\cdot\left[\frac{1 + 0.4\cdot J_{ts}\cdot K_{ts}\cdot\left[1.5 + \left[1 - n_t\cdot\left(\frac{D_o - 2\cdot t}{G_{ts}}\right)^2\right]\right]}{1 + J_{ts}\cdot K_{ts}\cdot F_q}\right]$$

Effective tube design pressure:

$$P_t := P'_t - P'_s = 322.276\,kPa$$

Tube sheet thickness convergence check

Given

$$t_{ts} - \left(\frac{F_{ts}\cdot G_{ts}}{3}\cdot\sqrt{\frac{P_{steam.outlet}}{\eta\cdot S_{ts}}}\right) = 0$$

$$T_{ts.calc} := Find\left(t_{ts}\right) = 18.802\,mm$$

$$Accuracy_{ts.thickness} := \frac{T_{ts.calc} - \left|T_{ts.calc} - t_{ts}\right|}{T_{ts.calc}} = 99.998\cdot\%$$

Actual tube sheet standard thickness:

$$t_{ts.actual} := 20mm$$

4.2 DESIGN OF HEAT EXCHANGER INLET & OUTLET NOZZLE AND ENDS

Check if it is a thin/ thick cylinder: $\frac{D_S}{t_s} = 69.273$ *Since $^{d}/_{t}$ >> 20 the cylinder is a thick cylinder*

Design for a thick-walled cylinder, type E shell

External pressure: $P_2 := 1atm$

Internal pressure: $P_1 := 1.1 \cdot P_{steam.outle}$ *Effective design internal pressure = 110% of operating pressure (Richard & Coulson Vol.6)*

Internal radius: $R_1 := D_S \cdot 0.5 = 0.495m$

External radius: $R_2 := R_1 + t_s = 0.51m$

Lame's constants:

$A_{L.guess} := 5($ $B_{L.guess} := 1$

Given

$$A_{L.guess} - \frac{B_{L.guess}}{\left(\frac{R_1}{m}\right)^2} = \frac{-P_1}{Pa} \qquad A_{L.guess} - \frac{B_{L.guess}}{\left(\frac{R_2}{m}\right)^2} = \frac{-P_2}{Pa}$$

$$Constants := Find\left(A_{L.guess}, B_{L.guess}\right) = \begin{pmatrix} 1.601 \times 10^7 \\ 4.184 \times 10^6 \end{pmatrix}$$

Lame' constants:

$A_L := Constants_0 Pa = 16.009 MPa$

$B_L := Constants_1 N = 4.184 MN$

Longitudinal stress in shell: $\sigma_L := \frac{P_1 \cdot R_1^2 - P_2 \cdot R_2^2}{R_2^2 - R_1^2} = 16.009 \cdot MPa$

Mean shell radius: $r := 0.5 \cdot \left(R_1 + R_2\right) = 0.502m$

Radial stress in shell: $\sigma_r := A_L - \frac{B_L}{r^2} = -0.563 \cdot MPa$

Hoop stress in shell: $\sigma_H := A_L + \frac{B_L}{r^2} = 32.581 \cdot MPa$ *Select boiler steel for shell material A516 Grade 70 normalized steel*

4.2.1 Selection of heat exchanger ends

Cylindrical section plate thickness: $e_{design} := t_s = 14.3 mm$

Option 1: Torri spherical shape

Crown radius $R_c := D_S = 0.991\,m$

Knuckle radius: $R_k := 6\% \cdot R_c = 0.059\,m$

Stress concentration factor: $C_s := \frac{1}{4} \cdot \left(3 + \sqrt{\frac{R_c}{R_k}}\right) = 1.771$

Min thickness required: $e_{th} := \frac{P_1 \cdot R_c \cdot C_s}{2 \cdot \sigma_H + P_1 \cdot (C_s - 0.2)} = 27.438\,mm$

Option 2: Standard ellipsoidal head ratio 2:1 (major: minor axes)

Crown radius $R_{c.eh} := 0.90 D_S = 0.892\,m$ *ASME Section VIII Div. 1. UG -32(c) acceptable approximation*

Knuckle radius: $R_{k.eh} := 0.17 \cdot D_S = 0.168\,m$

Min thickness required: $e_{eh} := \frac{P_1 \cdot R_{c.eh}}{2 \cdot \sigma_H - 0.2 \cdot P_1} = 14.344\,mm$

Choice of end heads: Select ellipsoidal head of the same shell thickness

Actual shell plate thickness: $t_{s.actual} := 16\,mm$ *Next standard size of shell plate thickness*

Inside depth of dish $IDD := \frac{D_S}{4} = 0.248\,m$

Total head height: $H_{eh} := \frac{3\,IDD}{2} = 0.371\,m$ *Richard & Coulson Vol 6, Fig 13.15a pg 827*

Straight flange height: $h_{sf} := H_{eh} - IDD = 4.875\,in$

Major axis radius: $r_1 := \frac{D_S}{2} = 495.3\,mm$

Minor axis radius: $r_2 := 0.5 \cdot r_1 = 247.65\,mm$

Inner surface area of one head: $A_{eh} := 4\pi \cdot \left[\frac{(r_1 \cdot r_2)^{1.6} + (r_1 \cdot IDD)^{1.6} + (r_2 \cdot IDD)^{1.6}}{3}\right]^{\frac{1}{1.6}} + 2\pi \cdot r_1 \cdot h_{sf} \ldots = 1.701\,m^2$

4.2.2 Design of heat exchanger nozzles

Select 4-inch nozzle diameter with no impingement plate

Nozzle diameter: $D_n := 4\,in$

4.2.3 Baffle thickness and tie rods

Tie rod diameter: $D_t := 12.7mm$ *Table CB-4.71 TEMA 9th Edition*

Number of tie rods: $n_{tr} := 8$

Unsupported tube length between baffles: $L_{bu} := \frac{L_{ta}}{n_b} = 479.284 \cdot mm$

Baffle plate thickness: $t_{b.min} := 6.4mm$ *Table CB-4.41 TEMA 9th Edition*

Actual baffle thickness: $t_b := ceil\left(\frac{t_{b.min}}{mm}\right) \cdot mm = 7 \cdot mm$

4.3 MASS OF METAL REQUIRED

NB: All steel calculations were based on Aveng Trident Steel prices and specifications. Boiler steel was used for the shell and baffle plates and stainless-steel tubes.

4.3.1 Shell calculations: Including baffles

Density of boiler steel $\rho_{bs} := 7861 \frac{kg}{m^3}$

Multiplying factor: $MF := 7.85$

Cylindrical section:

Base perimeter $L_{PS} := \pi \cdot D_S = 3.112m$

Mass of cylinder: $m_{cylinder} := L_{PS} \cdot L_t \cdot t_s \cdot \rho_{bs} = 3.199 tonne$

Front and rear end heads:

Volume of each end: $V_{eh} := \frac{4}{3} \cdot \pi \cdot r_1 \cdot r_2 \cdot IDD + \pi \cdot r_1^2 \cdot h_{sf} = 222.675L$

Mass of steel: $m_{head} := \rho_{bs} \cdot V_{eh} = 1.75 \times 10^3 kg$

Total mass for front and rear ends: $m_{tot.head} := 2 \cdot m_{head} = 3.501 tonne$

Tube sheet:

Total volume required: $V_{ts} := \pi \cdot r_1^2 \cdot t_{ts.actual} 2 = 30.828L$

Total mass of steel: $m_{tubesheets} := \rho_{bs} \cdot V_{ts} = 242.34kg$

Actual thickness: $t_{ts.actual} = 20 \cdot mm$

Select standard width: $w_{plate.ts} := 1200mm$

Calculated length: $l_{plate} := 1.05 \frac{m_{tubesheets}}{w_{plate.ts} \cdot \rho_{bs} \cdot t_{ts.actual}} = 1.349m$ *Add 5% for cutting tolerance*

Baffles:

Total volume required: $V_b := (1 - B_c)\pi \cdot r_1^2 \cdot t_b \, n_b = 76.878\,L$

Total mass of steel: $m_{baffles} := \rho_{bs} \cdot V_b = 604.334\,kg$

Actual thickness: $t_{b.actual} := 8\,mm$

Select standard width: $w_{plate} := 2400\,mm$

Calculated length: $l_{plate.baffles} := 1.05 \dfrac{m_{baffles}}{w_{plate} \cdot \rho_{bs} \cdot t_{b.actual}} = 4.204\,m$

4.3.2 Tube bundle calculations

Tube material: ASTM A312 Stainless steel, schedule 40S, Grade TP304 fusion welded (dimensions based on ANSI B36.10)

Total number of tubes: $n_t = 648$

Tube length: $L_t = 30 \cdot ft$

Nominal pipe size: $NPS := \dfrac{3}{8} in$

Tube thickness: $t = 0.091 \cdot in$

Density of stainless steel: $\rho_{ss} := 8070 \dfrac{kg}{m^3}$

Total mass of steel: $m_{tubebundle} := n_t \cdot \pi \cdot D_i \cdot L_t \cdot t \cdot \rho_{ss} = 4.348\,tonne$

4.4 HEAT EXCHANGER MATERIAL COSTS

Cost per tonne:

Boiler steel: $C_{bs} := \dfrac{10000¤}{tonne}$ *Estimated Aveng Steel last known price*

Stainless steel: $C_{ss} := \dfrac{125¤}{m}$ *Confirmed Euro Steel price*

Total mass of steel

Boiler steel: $m_{tot.bs} := m_{baffles} + m_{tubesheets} + m_{tot.head} + m_{cylinder} = 7.546\,tonne$

Stainless steel: $m_{tot.ss} := m_{tubebundle} = 4.348\,tonne$

Total H/E steel cost: $Cost_{steel} := m_{tot.bs} \cdot C_{bs} + C_{ss} \cdot n_t \cdot L_t = 816128.54ZAR$

Total cost of H/E: $HE_{cost} := Cost_{steel} \cdot 1.5 = 1224192.81ZAR$

5.0 RESULTS

Heat exchanger spec: Type BEM Size 39 - 360 (991-9144)

Total heat transfer area: $A_{HT} = 317.84 m^2$

Steam heat addition: $Q_{HE} = 1.06 \cdot MW$

H/E effectiveness: $\varepsilon_{HE} = 88.386\,\%$

Cost of H/E: $HE_{cost} = 1224192.81 ZAR$

Steam outlet temperature: $T_{so} = 374.179\,°C$

Steam exit enthalpy: $h_{hx.so} = 3210.39 \cdot \frac{kJ}{kg}$

Appendix C. Turbine calculations program code

Reference:C:\Research\Water-Steam IAPWS-IF97 rev 1.2.xmcd

Reference:C:\Research\HEAT EXCHANGER DETAILED DESIGN.xmcd

1.TURBINE OUTPUT

Property data: Plant specifications

Plant capacity $P_{CAP} := 46 \cdot 10^6 \frac{L}{yr}$

Process steam requirements: $p_{plant} := 400 kPa$ $T_{plant} := 100 °C$

$h_{plant} := h_{steam}(p_{plant}, T_{plant}, "", "", "") = 419.32 \cdot \frac{kJ}{kg}$

Load rating: $P_{load} := 621.68 kW$ $\Phi_{PF} := 0.85$

Specification: Siemens SST -060 Turbine- Alternator set

1.1 GENERATOR INPUT SHAFT POWER: FULL LOAD REQUIREMENTS

Turbo-alternator efficiency $\eta_{ta} := 86\%$

Generator output apparent power $Q_{output} := \frac{P_{load}}{\Phi_{PF}} = 731388.24 V \cdot A$

Generator efficiency $\eta_{gen} := 95\%$

Generator input power $P_{in.gen} := \frac{P_{load}}{\eta_{gen}} = 654.4 \cdot kW$

1.2 TURBINE INLET STEAM CONDITIONS: FULL LOAD

Turbine efficiency $\eta_{turb} := \frac{\eta_{ta}}{\eta_{gen}} = 90.53 \cdot \%$

Turbine power $P_{turb.required} := \frac{P_{in.gen}}{\eta_{turb}} = 722.88 \cdot kW$

Assuming 5% pressure drop in the steam lines and governing valves:

Extraction line pressure drop $\Delta p_{loss} := 5\%$

Turbine exhaust pressure $p_{out} := p_{plant} \cdot ((1 + \Delta p_{loss})) = 420 \cdot kPa$

Steam header input to turbine

Boiler 1 & 2 exit pressure $p_{boiler} := 950 kPa$

Steam header pressure $p_{header} := p_{boiler} - \Delta p_{shell} = 949657.44\,Pa$

Turbine inlet pressure $p_{turb.in} := p_{header} \cdot \left(1 - \Delta p_{loss}\right) = 902174.57\,Pa$

1.3 TURBINE ACTUAL OUTPUT POWER

Assumed turbine inlet temp $T_{in} := T_{steam}\left(p_{turb.in}, "", h_{hx.so}, ""\right) = 646.93\,K$

Turbine inlet quality $x_{in} := x_{steam}\left(p_{turb.in}, T_{in}, "", "", ""\right) = 1.22$

Turbine inlet enthalpy $h_{in} := h_{steam}\left(p_{turb.in}, T_{in}, "", "", ""\right) = 3210.39 \cdot \frac{kJ}{kg}$

$s_{in} := s_{steam}\left(p_{turb.in}, T_{in}, "", "", ""\right) = 7.43 \cdot \frac{kJ}{kg \cdot K}$

$h_{ex.s} := h_{steam}\left(p_{out}, "", "", "", s_{in}\right)$

$h_{ex} := h_{in} - \eta_{turb} \cdot \left(h_{in} - h_{ex.s}\right) = 3023.33 \cdot \frac{kJ}{kg}$

$P_{turb} := m'_{in} \cdot \left(h_{in} - h_{ex}\right) = 467.65\,kW$

Turbine exit enthalpy $h_{exit} := h_{in} - \frac{P_{turb}}{m'_{in}} = 3023.33 \cdot \frac{kJ}{kg}$

Turbine exit temperature $T_{exit} := T_{steam}\left(p_{out}, "", h_{exit}, ""\right) = 278.92\,°C$

Turbine exit quality $x_{exit} := x_{steam}\left(p_{out}, "", "", h_{exit}, ""\right) = 1.13$

1.4 OIL PUMP AUXILLIARY POWER REQUIREMENTS & SOP

Pump power: $P_{aux.oil.pump} = 9.86\,kW$

Fraction of turbine output: $f_{aux} := \frac{P_{aux.oil.pump}}{P_{turb}} = 2.11 \cdot \%$

Sent out power $P_{SOP} := \left(1 - f_{aux}\right) \cdot P_{turb} = 457.79\,kW$

Imported power: $P_{import} := P_{turb.required} - P_{turb} = 255.24\,kW$

1.5 MASS FLOW REQUIRED TO MEET PLANT POWER REQUIREMENT

Turbine work: $w_{turb} := h_{in} - h_{exit} = 187.06 \frac{kJ}{kg}$

Mass flow required: $m'_{req} := \frac{P_{turb.required}}{w_{turb}} = 13.91 \frac{tonne}{hr}$

% increase in mass flow: $\%_{mf} := \frac{m'_{req} - m'_{in}}{m'_{in}} = 54.58\%$

Appendix D. Turbine Quote

Frey, Christoph <christoph.frey@siemens.com> Tue, Apr 12, 2016, 2:58 PM

to me

Dear Onekai,

a first rough calculation gives following result:

Pin: 8,5bara
Tin: 248,5°C
M: 7000kg/h
Pout: 1bara

Turbine Type. SST-060 (AFA4 G6A)
Est output: 465kWe

Est Price: 630.000EUR EXW Frankenthal Germany
Scope: turbine, gearbox, oil system, generator , control-/protection panels

Mit freundlichen Grüßen,
With best regards

Christoph Frey

NB: Efforts to get the current quote were unfruitful and the researcher used the last known price obtained in 2016 during the researcher's undergraduate research.